ADDIS ABABA UNIVERSITY

COLLEGE OF NATURAL AND COMPUTATIONAL SCIENCES

SCHOOL OF EARTH SCIENCES

3D JOINT INVERSION OF GRAVITY AND MAGNETICS DATA TO CHARACTERIZE THE GEOTHERMAL FIELD AND RESERVOIR GEOMETRY BENEATH THE TULU MOYE VOLCANIC COMPLEX, CENTRAL MAIN ETHIOPIAN RIFT

A THESIS SUBMITTED TO

THE SCHOOL OF GRADUATE STUDIES OF ADDIS ABABA UNIVERSITY IN PARTIAL FULFILLMENT OF THE REQUIREMENTS FOR THE DEGREE OF MASTER OF SCIENCE IN GEOPHYSICS (APPLIED GEOPHYSICS)

By:

Aklilu Hailu Tekka

ADDIS ABABA UNIVERSITY

ADDIS ABABA, ETHIOPIA

JUNE 2024

ADDIS ABABA UNIVERSITY

SCHOOL OF GRADUATE STUDIES

SCHOOL OF EARTH SCEINCES

This is to certify that the thesis prepared by **Aklilu HailuTekka**, entitled: **"3D Joint Inversion of Gravity and Magnetics Data to Characterize the Geothermal Field and Reservoir Geometry beneath the Tulu Moye Volcanic Complex, Central Main Ethiopian Rift"** and submitted in partial fulfillment of the requirements for the degree of Master of Science in Applied Geophysics complies with the regulations of the university and meets the accepted standards with respect to originality and quality.

Approved by examining committee:

Name	**Signature**	**Date**
Dr Bayisa Regassa (School head: Earth Science).	_____	_____
Dr Abera Alemu (Advisor)	_____	_____
Professor Tilahun Mamo (Examiner)	_____	_____
Professor Gezahegn Yirgu (Examiner)	_____	_____

DECLARATION

I, the undersigned, hereby declare that the thesis entitled with **"3D Joint Inversion of Gravity and Magnetics Data to Characterize the Geothermal Field and Reservoir Geometry beneath the Tulu Moye Volcanic Complex, Central Main Ethiopian Rift "** is my original work carried out under the supervision of Dr. Abera Alemu and has not presented to any university or institution for the award of any degree or diploma program and all sources of materials used for the thesis are duly acknowledged.

Name of the candidate **Signature** **Date**

Aklilu Hailu

This is to certify that the above declaration made by the candidate is correct to the best of my knowledge and it has been submitted for examination with my approval as university advisor.

Name of Advisor **Signature** **Date**

Dr Abera Alemu

(Advisor)

ABSTRACT

This study is conducted in the Central Main Ethiopian Rift (CMER) which is located 70km SE of Addis Ababa in Oromia Regional State East Arsi Zone. Geographically the area is bounded by 38.9^0-39.4^0 Longitude and 8.1^0-8.3^0 latitude. The study is meant to characterize the geothermal field and reservoir geometry beneath the Tulu Moye Volcanic Complex. Specifically, it is meant to define geothermal reservoir components like heat source, permeable zone, clay cap/ cap rock and recharge area of the geothermal system believed to exist in the study area. In the process the geometry and possible extent / volume of the geothermal system is also determined/ estimated.

Ground gravity and ground magnetics data, which are collected using Lacoste and Romberg and GSM 19T proton precession magnetometer, respectively are primarily used to reach the main and specific objectives of the study. In addition to the main data, other a priori geoinformations like microseisms and resistivity survey results in the area are used to complement the study methodologies, data processing steps and result analysis.

Microsoft products, Oasis montaj, Quantum GIS, and GRAVMAGINV3D applications and algorithms were deployed to organize, analyze, change discrete data to continuous surface, create derivative maps and generate 3D density and magnetic susceptibility models. The main methodology used in the study is 3D joint inversion of ground gravity and magnetics data to obtain 3D models of density and magnetic susceptibility. Both the 3D models obtained along with the a priori geo-information obtained from the area divulge presence of the anticipated main components (heat source, permeable zone/s, recharge area) of a typical geothermal system in the study area. Moreover, the study estimated the possible existent of the geothermal system believed to exist in the study area.

ACKNOWLEDGEMENTS

- I would like to express my heartfelt gratitude to all the members of the AAU Earth Science staff, with a special mention to **Dr. Abera, Prof. Tilahun, Prof. Tigistu, Prof. Gezahegn, Dr. Mebatseyon and Dr. Lev Chepigo**. Your unwavering support and guidance have been invaluable to me throughout my academic journey.

- I extend my special thanks to **Dr. Abera Alemu**, whose constant encouragement and advice have motivated me to work diligently and present my study results confidently. His mentorship has been instrumental in shaping my academic growth and success.

- I also would like to extend my special thanks to **Dr. Lev Chepigo** for his support in understanding how to use GMI (GravMagInv) 3D application and its mathematical background in addition to providing me the license with full working capability

- I have to convey my deepest gratitude to my dear wife **Tewedaj Alemu** and our five children. I am truly honored and humbled to acknowledge your unwavering patience, love, and support throughout my academic journey. Words cannot express my gratitude for the sacrifices you have made to help me achieve my academic goals. Your unwavering belief in me has been an endless source of motivation

- Once again, thank you to each member of the AAU Earth Science Staff for your continuous support and encouragement.

Table of Contents

LIST OF FIGURES

LIST OF ACRONYMS

Symbol / Abbreviations	Definition
μ_o	Vacuum permeability
μ_R	Medium permeability separating poles
B	Magnetic field strength
CMER	Central Main Ethiopian Rift
E	East
ER	Ethiopian Rift
EARS	East African Rift System
F	Gravitational/ Magnetic field force of attraction
G	Universal Gravitational constant
GNNS	Global Navigation Satellite System
GPS	Global positioning system
gu	gravity unit
H	magnetic force
IGRF	International Geomagnetic Reference Field
IGSN	International Gravity Standardization Network
J	induced magnetization
k	material magnetic susceptibility
M	magnetic moment
MER	Main Ethiopian Rift
mgal	milligal
N	North
NMER	North Main Ethiopian Rift
R	Earth's radius
RTK	Real Time Kinematics
S	south
SI	System International
SMER	South Main Ethiopian Rift
T	Tesla
TM	Tulu Moye
TRM	Thermo Remanent Magnetization
U	Gravitational Potential
UTM	Universal Transverse Mercator
V	Magnetic Potential
VRM	Viscous Remanent Magnetization
W	West
Wb	Weber
WFB	Wonji Fault Belt
δ	small change
Δg	difference in gravity measurement at a base station
Θ	Teta

CHAPTER I

I. Introduction

Geothermal Energy is an energy which can be abstracted from the earth's interior and be used for various purposes. Proper and relevant studies need to be carried out to assess the presence of this resource, its sustainability, (which is defined by various physical and geographical conditions), proper designing of accessing, utilizing, and monitoring it. The studies that are necessary to reach the target include Geophysics, Geology (Lithological and structural mapping), Geochemistry, Hydrogeology, and hydrology. Of course, there are various other methods applied remotely (like from satellites) which have considerable value in supporting interpretation of data collected from the mentioned methodologies. InSAR (Interferometric Synthetic Aperture Radar) is one of satellite-based sources of data for studying ground deformation & gives vital information which aids interpretation of various geophysical and geological data for geothermal resource potential identification.

The study area, Tulu Moye Geothermal, is in the Oromia Regional State 150km SE of Addis Ababa. The area is with in the Central Main Ethiopian Rift (CMER) where volcanic activities are believed to be active along the Wonji Fault Belt (WFB) corridor particularly the segment in the study area (Figure 1). There are various young volcanoes within the study area consisting of Tulu Moye, Bora, Berriccha, etc. The CMER is a segment of the Main Ethiopian Rift (MER) where 60 active volcanoes exist (Aspinall et al., 2011) many of which have vigorous hydrothermal systems fueled by magmatic heat sources, and some are deforming (e.g., Haledebi, Fentale, Kone, Aluto, Corbetti and Tulu Moye) (Albino et al., 2022). The MER's hydrothermal systems include geothermal energy resources with the potential to produce a considerable quantity of electricity (> 10,000 MW) from around 23 geothermal sites. (e.g., UNDP 1973; Kebede, 2016).

There are many geological features which have impacts on or relation with the occurrence of geothermal resource components. Listed below are some of the prominent geological features in the area.

i. Wonji Fault Belt (WFB): which is made of small-offset normal faults and fissures (Boccaletti et al., 1998) has three segments in Ethiopia and the most active is found in this study area. Its orientation is NNE-SSW.
ii. There are prominent volcanic features in the area among which most of them are young and still active. Specifically, volcanoes like Tulu Moye, Bora, Berriccha, Oda, Werdi, Giano Salen, (though found along / and believed to be the rift axis), Togea are few among many. Most of them are controlled by the volcano tectonic activities of the WFB.

iii. There is also an obsidian dome which covers 8.4 km^2 of the study area. This is also a prominent geological feature in the area.

Several geoscientific studies have been carried out to identify, characterize, and define possible zones of probable geothermal reservoir and works have been done to facilitate monitoring of the probable geothermal system under study. These include geophysical (Magnetotelluric, Transient Electromagnetic, Gravity, Magnetics, etc.), geological (lithological and structural mapping), geochemical (water and gas samples analysis), and drilling works. Though all these have been done, variations of different physical properties particularly density and magnetic susceptibility have never been seen in better detail based on 3D modelling. This study considers 3D joint inversion of ground magnetic and Gravity data would have vital role in understanding the resource conditions (particularly mode of occurrences) including their lateral and vertical boundaries. Producing a 3D model is preferred to the conventional techniques with the anticipation of showing variations of density and magnetic susceptibility in three dimensions to define the presence of the possible geothermal reservoir components of the study area with a better confidence.

For this study 3D joint inversion of gravity and magnetics data is basically proposed to characterize the geothermal sources in the study area. The existing geoscientific products compiled from the study area are employed as inputs in the process of inversion to constrain results. Moreover, the depth resolution of gravity method as compared to that of magnetic method is used as an advantage to constrain the magnetic data.

The rationale of this thesis is to employ ground gravity and magnetic data, generate 3D jointly inverted models and determine the characteristics of the geothermal sources believed to exist beneath the Tulu Moye volcanic complex and its vicinity. Characterizing the possible geothermal system includes identifying probable heat source areas, possible clay cap (Cap Rock) depths, permeable zones, and possible sources of recharge area. The possible recharge area could be inferred by incorporating the hydrogeological conditions and setting of the area and its surroundings. There are possibilities that the hydrogeological setting of the area and its vicinity could have positive and/or negative impacts on the geothermal resource (reservoir).

204 gravity and 21300 ground magnetic secondary data from both methods are used to produce this thesis. QGIS, Oasis montaj, Excel, and GravMagInv3D application software are mainly used in the process of organizing data, producing various 2D maps and 3D models.

I.I. Location and accessibility

The study area (Figure 1) is located 70km SW of Addis Ababa in Oromia Regional state Central Main Ethiopian Rift (CMER). Geographically it is bounded by 38.9^0-39.4^0 Longitude and 8.1^0-8.3^0 latitude, (or **UTM** 488982.8 - 544047.2m **E** and 895354.4 - 917485.8m **N**). The study area is accessible using dry weather roads from various directions. It covers 865 Km^2. As can be seen in Figure 1, the area can be accessed from the west and east using asphalt roads, then gravel road networks lead to the heart of the area (Tulu Moye Volcanic Complex) and give favorable conditions for data acquisition. The area is bound by the Eastern escarpment, the Western Escarpment, Ziway Lake to the south and Koka Lake to the north.

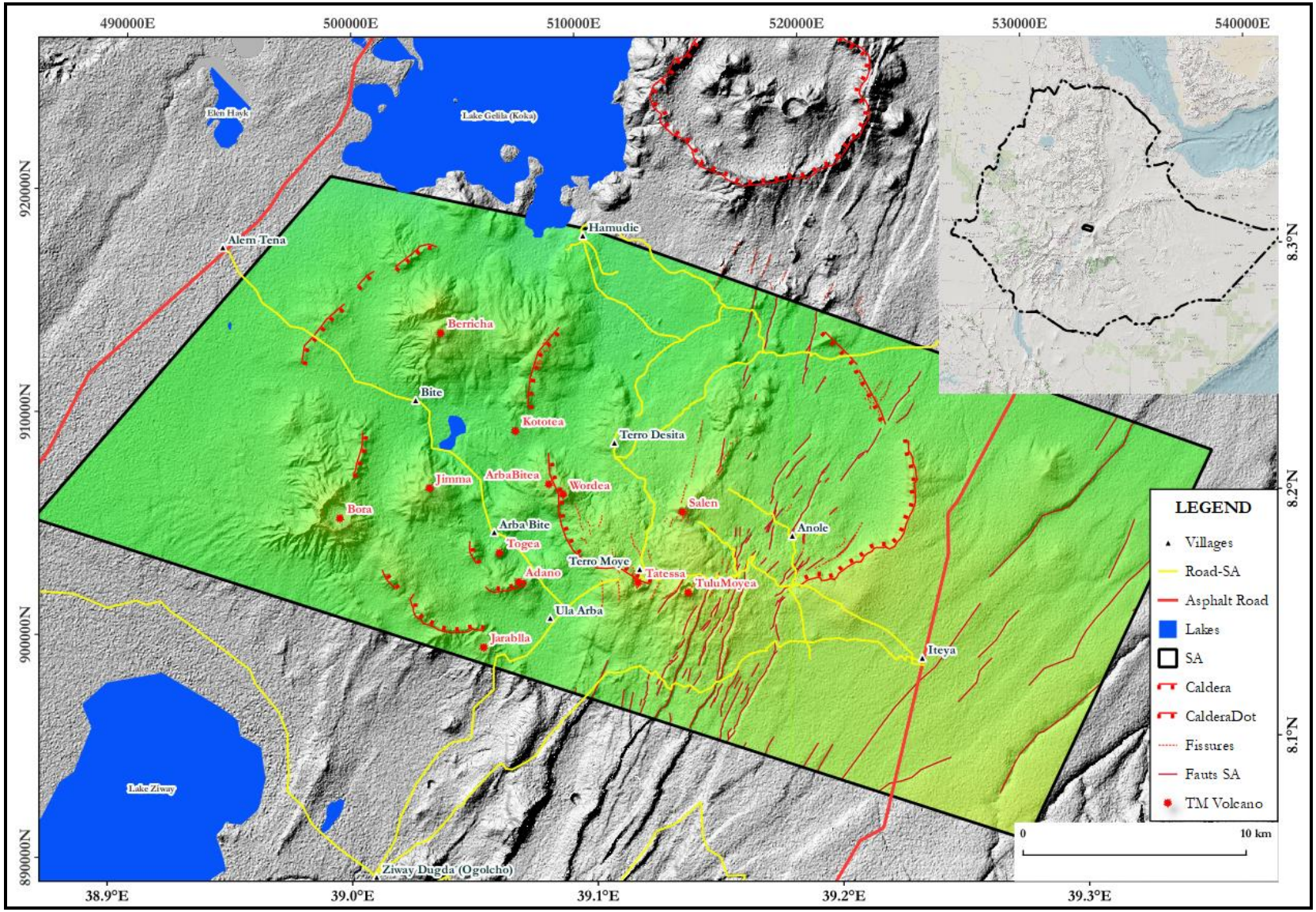

Figure I. Location map of the study area

1.2. Physiography of the study area

The study area is closer to the Easter Escarpment than the Western Escarpment. This implies it is more rugged in the eastern part of the project area than the western part in terms of relief. There are many volcanoes within the oldest and biggest Anolea Caldera among which Mount Werdi, Dimma and Adano (Figure 2) which range up to 1950m above sea level and three major volcanos have altitude 2285 m above sea level namely Tulu-Moye, Bora and Berriccha. Figure 2 shows the physiography of the study area (Mamo, T, et al., 2016**).**

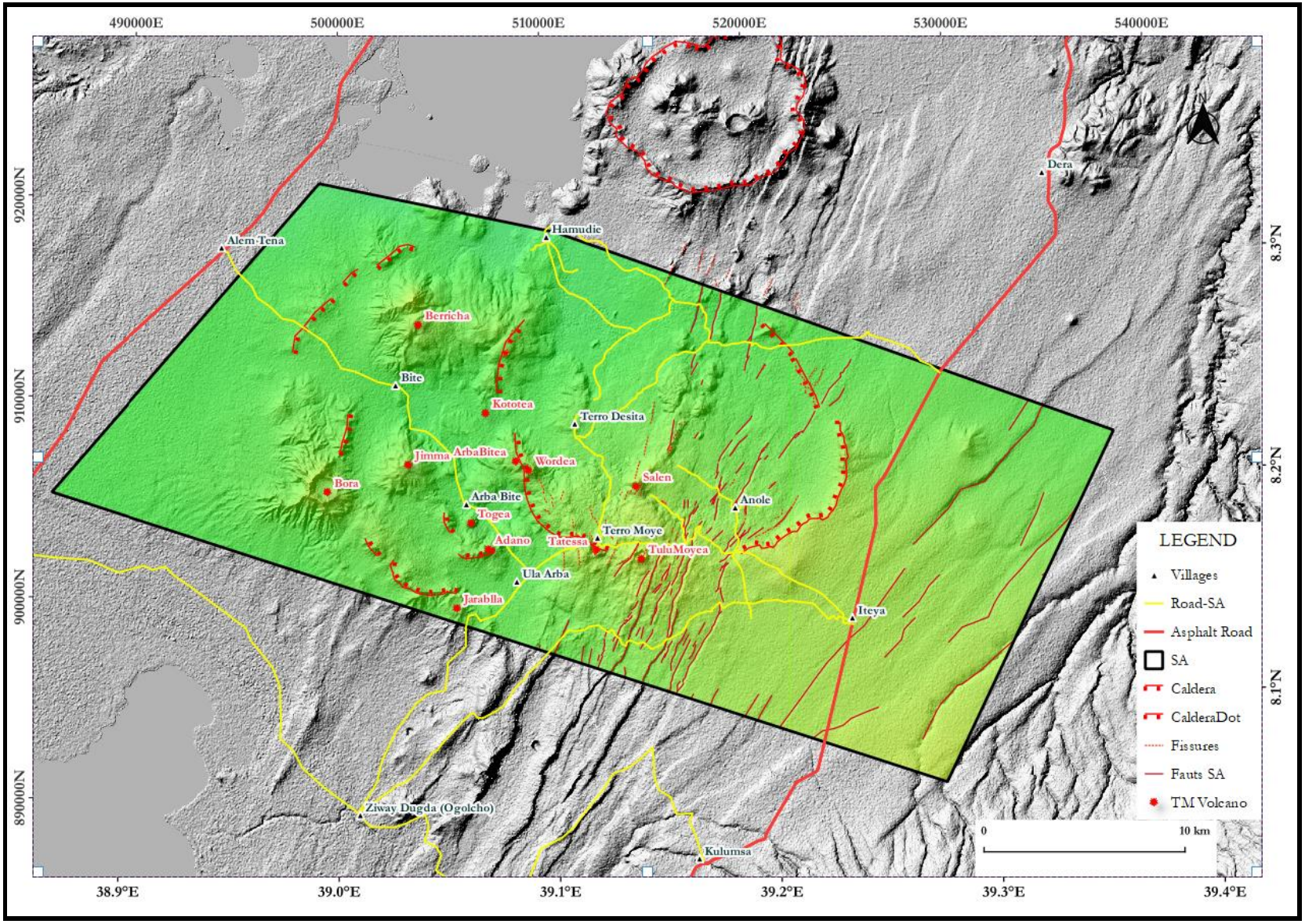

Figure 2. Physiographic map of the study area

1.3. Statement of the problem

The Central Main Ethiopian Rift has been investigated by various geoscientists to understand its nature in relation to formation of the earth and to identify its geothermal potential. Such studies have been rife all over the East African Rift System (EARS). Geophysics has been one of the vital techniques deployed together with other geoscientific tools to acquire data, analyses and interpret it bearing in mind the main purpose. In the course of the geophysical endeavor made to understand the areas' crustal structure, crust mantle relation, geothermal exploration gravity and magnetic exploration methods have played vital roles. Most of the studies carried out could retrieve valuable geoinformation about the area.

However, none of the studies tried to generate 3D models by jointly inverting gravity and magnetics data particularly for geothermal potential assessment. This thesis research takes this gap into consideration and uses gravity and magnetics data collected in the Tulu Moye Volcanics Complex to generate density and magnetics susceptibility 3D models based on joint inversion of the two signals.

The 3D models generated and included in this thesis are the first for the study area and is thought to initiate others to continue such endeavor in their attempt to understand the signatures of signals in three dimensions in general and inverting at least two signals together which certainly minimize non-uniqueness solution.

1.4. Research questions.

This research has basic question on how to identify geothermal energy reservoir using 3D join inversion of magnetic and gravity data among which:

1. How can a geothermal reservoir component be related to a rock matrix physical property particularly to density and susceptibility anomaly signatures?
2. What does the 3D join inversion of gravity and magnetics result indicate in relation to identifying the presence of a geothermal source components? And
3. What additional geoscientific information could supplement the gravity and magnetic data/results to fulfill the outlined research objectives?

I.5. Objectives of the study

I.5.1. General objective

The object of the study is basically bringing all available geoscience data, generate 3D jointly inverted density and magnetic susceptibility model and characterize the probable geothermal reservoir which is believed to exists beneath the Tulu Moye volcanic complex.

I.5.2. Specific objectives

The specific objectives are,

i. Generate 3D density and susceptibility models,

ii. Identify the presence of the following geothermal reservoir components,
   - heat source
   - Cap Rock/ Clay Cap
   - permeable zone
   - recharge area

iii. Estimate reservoir capacity of the geothermal resource that exists beneath the Tulu Moye volcanic complex.

I.6. Expected outcomes of the research work

The study attempts to understand the area in relation to geothermal source presence beneath the Tulu Moye Volcanic Complex mainly by deploying 3D joint inversion of gravity and magnetic signals/ data. This study generates 3D density and magnetic susceptibility models through joint inversion technique. The obtained models, supplemented by priori geoinformation, are related to geothermal source indicating components and ultimately be used to draw conclusion on the presence of a geothermal reservoir. Moreover, the study estimates the possible volume of a geothermal reservoir beneath the Tulu Moye Volcanics Complex.

I.7. Significance/contribution of the study

The 3D joint inversion of the two potential fields has never been applied and never been a model produced so far in the study area at least to the knowledge of the author. So, in addition to its new nature in its output, it will be an energy to other researchers to go further and see this area in 3D which is produced by joint inversion technique and take the experience to apply in other places in the field of geothermal or other exploration fields.

1.8. Literature Review

There are many geoscientific studies carried out within this study area. Surface geology, structural, geochemical, geophysical, hydrogeological studies were undergone based on ground and remotely sensed data. These studies were carried out to understand the geological, tectonics, surface and ground water conditions, geothermal potential, etc. of the area. So, literature review was done on studies (published, unpublished), theses, and technical reports considering relevance, type, and time of study (heed is given to the latest ones). The following briefly reviewed literatures are found pivotal during interpretation.

- **Birhan et al. (2023),** in their research to understand the constraints on the ground deformation process at the Tulu Moye Volcanic Complex, Main Ethiopian Rift used InSAR data. In the study the presence of deformation with consistent uplift at a velocity of 50mm/year in the year 2014-2017 and decreasing 12mm/year in the year 2022 was indicated. The study also delineated that the location of the deformation is about 10km west of the TM Geothermal Operations Plc drilling location. It is located between Bora, Berriccha and Tulu Moye volcanoes. The trend of deformation is NW-SE. The study also highlighted the size and depth of the body which caused the deformation. It is identified to be a sill which has 8.7x1.2km size and 7.7km depth below the surface. This body showed a velocity of volume change of $8.9x10^6 m^3$/year in the year 2014-2017.
- **Martina et al. (2023),** in their study to see and understand evidence on fluid induced earthquake swarms using high resolution earthquake and relocation in the Main Ethiopian Rift felt the knowledge gap that exists on the role of fluids in generating earthquakes in some of the main continental rifts. The study utilized a large seismic catalog dataset that covers both the Main Ethiopian Rift axis and margins and investigated the interaction between fluids and faults. The study carried out cross correlations on four major earthquake clusters to substantially improve precision of the earthquake comparative relocations and to measure families of earthquakes in which waveforms are alike.

  Analysis was also performed on variation in the seismicity rate and seismic moment release in time for the clusters. The exploration discovered that the depth of the earthquake relocations in all four clusters are 5-15 km and related to explicit N-NEN trending and steep (>60°) dip planes. This study summarized that fluids such as water and carbon dioxide that come from deep Earth can arise to the surface through fractures and faults. When this occurs, fluid can displace the faults, resulting in several feeble seismic signals in a short period of time and on the same plane. The study's major results are that earthquake swarms within the rift exhibit features consistent with earthquakes caused

by fluid movement along faults. In contrast, earthquakes along the rift's edges have a different character, implying that they are caused by plate tectonic motion rather than fluid migration.

- F. Albino et. Al, (2020), using sentinel-1 SAR data 18 ground deformation signals were identified across 14 volcanoes, with six in Afar, six in the Main Ethiopian Rift, and two in the Kenya-Tanzanian Rift. New instances of uplift were observed at Tullu Moje in 2016 and Suswa in mid-2018.while long-lasting subsidence signals were detected at Gada Ale and Kone. The subsidence signals can be attributed to various factors such as the post-eruptive changes in magma reservoirs (e.g., Alu-Dallafila), lava flow compaction (e.g., Nabro), and pore-pressure variations linked to geothermal or hydrothermal activities (e.g., Olkaria). The findings indicate that approximately 20% of the Holocene volcanoes in the East African Rift System exhibited deformation over the course of this 5-year period, highlighting the range of processes at play.
- Tim Greenfield et al. (2019) in their study to understand and determine what caused the low frequency earthquakes beneath TM volcano used detected low frequency seismicity data collected by Southampton university. Detector lasted in the area at their locations for ~ 1.5 years within the Tulu Moye volcano complex. The study analysis of the seismicity data collected brings to light that its sources are from two locations at a depth of 1–5 km below sea level. The study suggested that seismicity is caused by the release of volatiles (likely H2O/CO2 mixes) from a shallow magma body located under TM. The fluid source is likely a cooling magma from Tulu Moye's very recent eruption, which took place 100-200 years ago. The two clusters are locations where the pore fluid pressures are risen to high enough potential to initiate fracturing but with slow rupture velocities. This is the cause for the presence of the low-frequency earthquakes in the area. Based on the research the presence of a magmatic beneath Tulu Moye was suggested which believed to have a minimum depth of 4km below the surface. Th body believed to have high volatile content. This indicate that the bod is reach in silica-rich and has been fractionated significantly. It is then likely that the body releases volatiles.
- Hjálmar Eysteinsson et al. (2016) in their resistivity study using Magnetotelluric and Transient Electromagnetic data identified a resistivity structure which is common to high enthalpy geothermal systems. That is clay cap with low resistivity at shallow depths could be delineated. The depth to the clay cap generally ranges 500-1000m but its shallowest in the 200-500m range. The study also determined the resistivity of this clay cap which is less than 10 Ωm within the Anolea Caldera and higher outside. This study also identified the presence of a deep-seated conductive layer which is 10-

20 km deep. The layer is mainly confined in the Anole Caldera. It could be the heat source in the area.

- Temesgen et al (2016) in their study to draw environmental baseline for Tulu Moye Geothermal Project outlined as the area is hydro-geologically identified by local to extensive aquifers which have low to moderate productivity. The ground water has the characteristics of flows in the shallow and deep aquifers around Lake Ziway and Koka Reservoir where the flow in the Ziway -Koka corridor for deep aquifer system. In addition to this, the report pointed out that the main source of recharge in the area is the rain fall in the southeastern highlands. There is also base flow recharge from Ziway Lake, Koka Reservoir, Ketar and Meki Rivers. It also pointed out that most of the stream courses and wetlands in the region are highly controlled by intensive faulting that also favours recharge. Most of the recharge in the area and the region goes to the deep circulation that indicate the potential of geothermal aquifer in the area.
- G. Wadge et al, (2016), compiled volcanism history and stress state in the East African Rift System (EARS) and among which Tulu Moye is one of them. According to this research Tullu Moje has a widespread field of vents. Giano lava flows (Bizouard and Di Paula, 1979) erupted from a fissure on the rift floor southeast of Lake Koka. Gouin (1979, p. 105) reported that a "pitchstone" ashfall ruined crops in 1900. Another eruption was documented in 1775 ± 25 years. The Giano Flows are believed to be the result of the 1900 eruption.
- E. Admassu et. Al, (2015), The faults in the region's formation and growth can be attributed to three distinct phases of faulting. Two fault models have been put forward to elucidate the progression of faulting, fracturing, and lava flow occurrences. The volcanic events in the area are predominantly influenced by the active faults and extension fractures of the Wonji Fault Belt (WFB). A survey on fault morphology revealed the diverse nature of fault and fissure morphology, primarily influenced by variations in strike within the geological units. A comprehensive link between Quaternary faulting and magmatism was established in the Tulu-Moye geothermal prospect.
- Tesfaye et al. (2004), in their study to investigate the role of preexisting structures for the origination, propagation and architecture of faults in the Main Ethiopian Rift indicated the presence of faults with various orientations. The study used Landsat Thematic Mapper images and high-resolution digital elevation models (DEM) to identify the presence of faults which have trends of N-S to NEN-SWS, NE-SW, E-W and NW-SE. The study also used ground gravity data and relate anomalies with faults which have NW-SE directions.

I.9. Methodology

The methodology applied in this study is ground gravity and magnetic data joint 3D inversion to identify and characterize the probable geothermal resource under Tulu Moye (Volcanic Complex) Geothermal Field. This kind of inversion is vital not only to show the variations of the physical properties': density and magnetic susceptibilities in three dimensions but also helps to constrain the dimensions of the body which is probably related to geothermal resource indicators. As a standard practice, a geothermal reservoir is characterized by a heat source, clay/cap rock, fractured rock, and source of recharge. This study mainly considers, in addition to the potential fields which are mainly used, all available geological, hydrogeological resources and geophysical survey results. Resources from these studies were used in one way or another in constraining mainly the 3D gravity models which in turn be used as a regularizer/ constraining factor in the attempt of undergoing a 3D joint inversion with magnetic data. This approach was selected because the gravity data precision (according to the meta-data obtained) is high.

The 3D inversion method is preferred to 2D inversion because 2D inversion involves either lateral (X: EW-Y: NS) or vertical (EW or NS with Z) density and susceptibility variations whereas the 3D inversion can show variations in the three directions (X, Y, Z) which can give better picture of a body beneath the surface of the earth. Here heed is given to the importance of 2D maps along with 3D models to divulge geoscientific information in a better view.

The gravity and magnetic methods are common geophysical methods applied in the realm of geothermal resource studies. They help in identifying geothermal resource components including heat source, clay cap/ cap rock, fractured zones, and recharge areas. A recharge area is basically obtained from hydrogeological findings but existence of facilitating factors (like faults, fractures, etc.) in the study area can be inferred or identified from the join inversion of the potential field or the 2D models/maps in addition to the geological findings available.

This approach was chosen to see the variations of the density and magnetic susceptibility values which is vital in constraining the dimensions of a magmatic body which probably exist in the area and up dooms and be responsible for the presence of heat beneath the study area. Such bodies could have higher density and lower magnetic susceptibility if existed in the area. Heat sources are one of the prime entities in the realm of geothermal resource studies. Therefore, identifying the presence of this entity in an area is crucial to characterize a geothermal resource in an area (though not the only one). Thus, with a proper usage and analysis of this potential fields using constraining values like density and depth, it is possible to get a reliable density model. The obtained model can be used as a regularize / constraining factor in the process of 3D

joint inversion of gravity and magnetic data. The above arguments have led the researcher to select this method and forward his MSc research proposal.

The ground magnetic and ground gravity data are owned by TM Geothermal Operations Plc which is performing geoscience exploration including deep drilling of various well trajectories to develop electric power from geothermal resources.

I.10. Thesis Structure

The work plan of this project is carved in such a way that it maximizes the use of literature and secondary gravity and magnetic data to generate new 3D models of density and magnetic susceptibility (Figure 3).

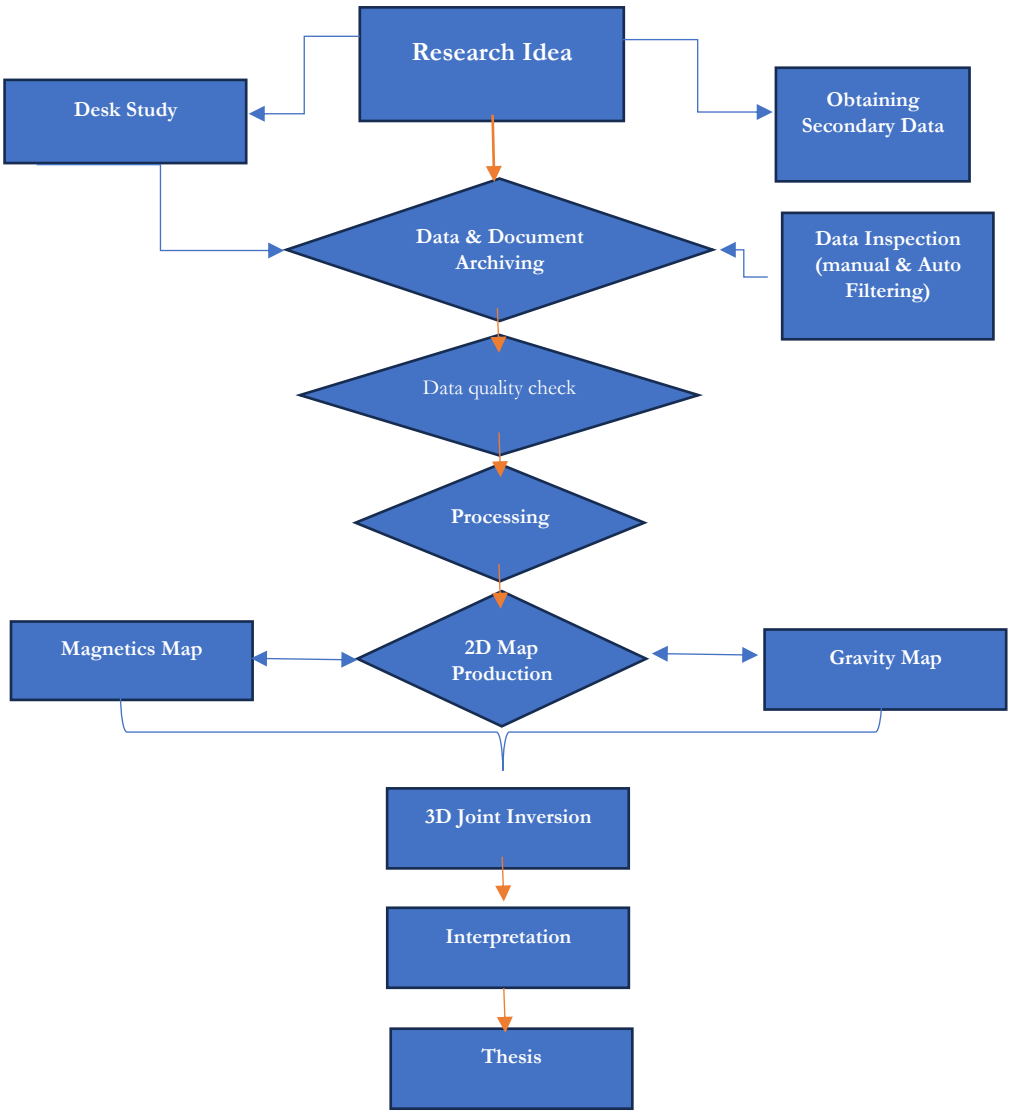

Figure 3. general work procedure and inversion flowchart.

CHAPTER 2

2. Geology and Structural setting

2.1. Geology and structure of the MER

The research area is in the middle sector of the Main Ethiopian Rift (MER) (Figure 5), which is a component of the Great East African Rift System (EARS) (Figure 4), running typically in the NEN-SW direction. The Ethiopian Rift (MER) is the northern portion of the East African Rift system that divides the South-eastern and Western Ethiopian plateaus. It runs from the triple junction of Lake Abbe in Afar, south-southwest, to Lake Turkana. The Main Ethiopian Rift (MER) is a huge graben that is around 800 km long and up to 60-80 km wide, with an average elevation of roughly 1600 m. The edges of the rift forms flat shoulders around 2200 meters, on which volcanic centres such as Chike, Chilalo, and Kaka (which reach altitudes of up to 4200 meters) have been built (Lecture note by Gezahegn Y. 2013)

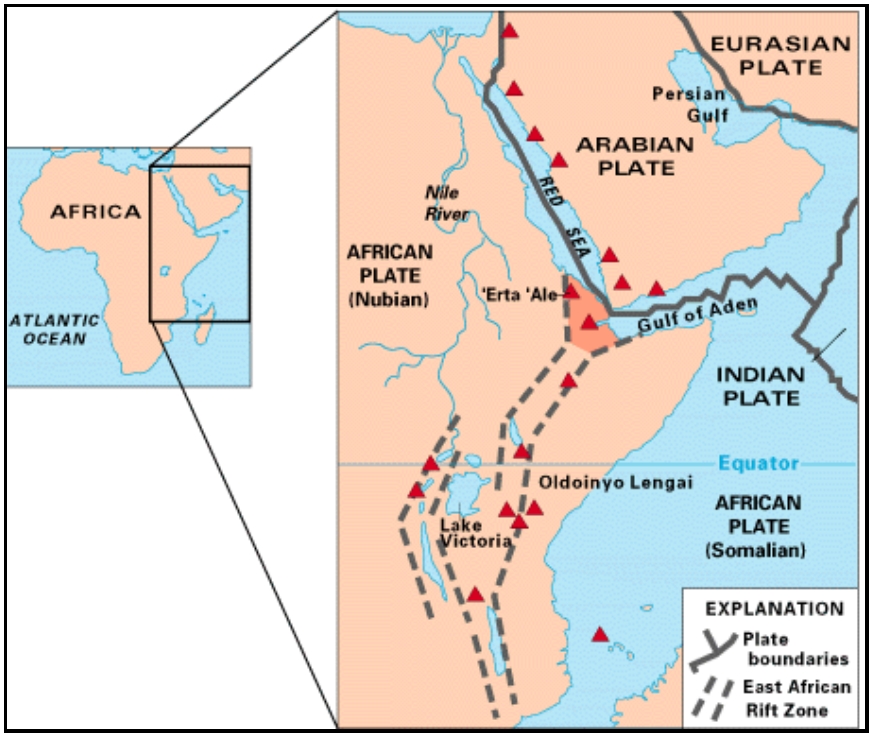

Figure 4. East African Rift System

(https://en.wikipedia.org/wiki/File:Tectonical_map_of_East_Africa.png)

The rift system's origin dates to the early Tertiary (Upper Eocene), when the Afro Arabian dome experienced initial uplift around the Afar triple junction (Mohr,1971). This was followed by fissural eruptions of widespread flood basalt volcanism with alkali to transitional compositions, known as the Trap Series, which included the Alagi basalt. According to Kazmin and Seife (1978) and other experts, the Ethiopian Rift originated in the Lower Miocene. This episode was followed by extensional tectonism, which caused the crust to thin, leading in the formation of the Ethiopian Rift valley.

Volcanism spread northward, forming the Afar Stratoid Series around 4.1 million years ago (ELC, 1987). They are mostly made up of basalts and tiny amounts of silicic products. There had been multiple instances of rift development and volcanism (Kazmin and Seife, 1978; Di Paula, 1970). The creation of a fractured eastern escarpment around the Nazret area led in silicic volcanism, often known as the Nazret Group. This was followed by an event of rift floor subsidence, faulting, and escarpment tilting, which resulted in the extensive extrusion of the Nazret group's ignimbrite and the creation of trachytic volcanism along the rift's shoulder. The present-day volcanic centers of Chilalo, Badda, and Kaka, which are exposed on the eastern escarp, are the product of volcano-tectonic activity. Following this event, Older Basalt and Bofa basalts erupt on the rift floor. Volcano-tectonic sinking resulted in the formation of a caldera while also widening and sinking the main Ethiopian Rift.

The final stage of volcano-tectonic activity occurred in the MER from the Pleistocene to the recent past and is associated with the axial extensional zone, the Wonji Fault Belt (WFB). The WFB is structured in an "en echelon" configuration, which is a common Rift phenomenon (Di Paola, 1970, ELC, 1987, and others). The activity culminated in the construction of a NEN-SWS trending series of faults that shattered the rift floor, generating a fissure in the rift structure (Mohr, 1971), resulting in step-like structures and volcanism (Wonji Group). These tectonic motions created extremely deep fractures through which basaltic magma lava flows emerged. During the latter phases of young tectonic activity damaged the previous formations and produced in the fissural outbursts alkali rhyolitic volcanoes of Bora, Bereccia, and others (Di). (Di Paola, 1970).

Based on the simplified geology map (Figure 5) of the main Ethiopian Rift the rift is basically dominated by quaternary central volcanics and pyroclastic layers including quaternary lacustrine sediments and interbedded pyroclastic.

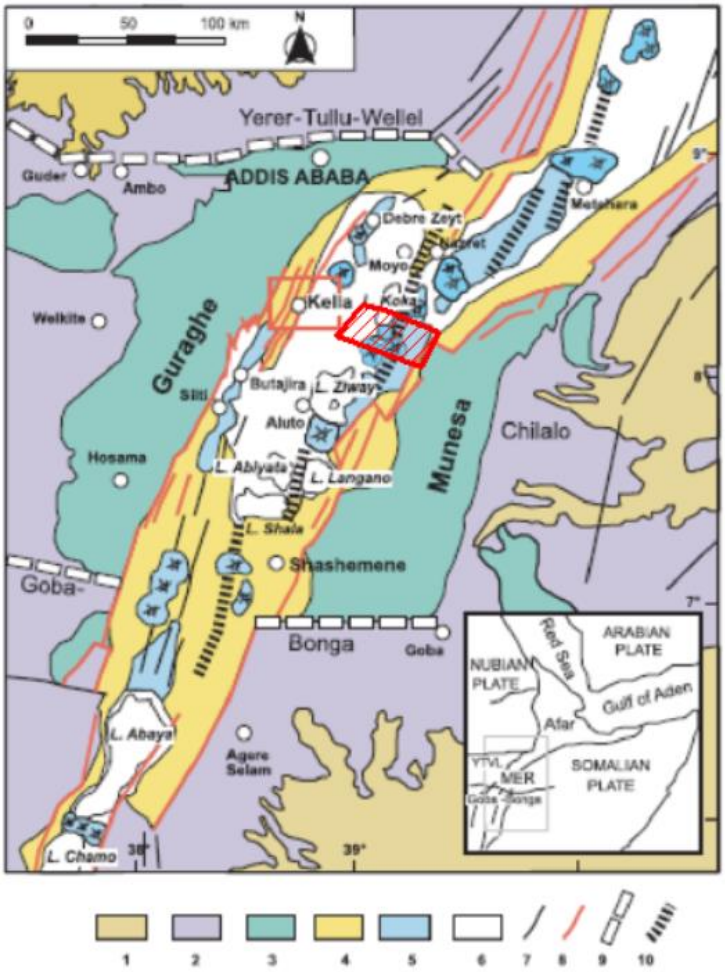

LEGEND

1. Pre-Tertiary sediment and crystalline basement
2. Oligocene (32-29 Ma) and lower Miocene (12-8 Ma) plateau volcanics
3. Miocene-Pliocene rift-shoulder trachytic-rhyolitic volcanics and pyroclastic layers
4. Plio-Pleistocene rift floor
5. Quaternary central volcanics and basaltic lava flows, associated scoria cones and phreato-magmatic deposits,
6. Quaternary lacustrine sediments and interbedded pyroclastics
7. Faults
8. major rift border faults
9. major transversal tectonic lineaments in the basement
10. Wonji fault belt segments

Survey area.

Figure 5. Simplified Geology Map of Main Ethiopian Rift (MER)

(modified after Jepsen and Athearn 1997)

2.2. Geology and structures of the CMER

The Main Ethiopian Rift (MER) has three sections based on surface geology and geomorphology namely, Southern Main Ethiopian Rift (SMER), Central Main Ethiopian Rift (CMER) and Northern Main Ethiopian Rift (NMER). The Tulu Moye area is in the CMER which extends from Lake Koka in the north to Lake Hawasa in the south with border faults trending N30°E-N35°E. The eastern margin faults show an average trend of N30°E and WNW dipping Assela –Langano Fault System (Figure 6), (Corti, 2009). The border fault systems are normally segmented and characterized by transverse structures. The estimate of the age of the faulting is 8.5 -9.3 Ma (Woldegabriel et al., 1990).

The rift floor under the MER is affected by significant deformation because to faulting along the Wonji Fault Belt. (Mohr, 1967, Dereje A and Bekele A. 2021.). The WFB are normally short, closely spaced and displayed in small throws (<100 m) Boccaletti et al., 1998 and Hoffman et al, 1997). They are characterized by steep sub vertical scarps and are commonly en-echelon and linear or curved associated with the faults are open fissures with or without vertical displacement and rhombus shaped structures (Asfaw, 1998; Williams et al., 2004).

These features reflect a change in the deformation style from the rift margin to the rift floor, where the extension is accommodated by few widely spread faults with substantial vertical displacement, and deformation occurs through dense fault swarms with minor vertical offset. (Boccaletti, et al., 1995 and Ebinger and Casey, 2001).

The eastern part of the research region, near the Tulu Moye Volcanic Complex, is distinguished by NEN-SWS trending, closely spaced fault swarms, and open tensional fissures. This zone is currently the active axis of the rift structure. The latest basalts and obsidians erupted via these structures (Di Poala, 1972). The alignment of thermal manifestations also indicates NW-SE trending transversal structures traversing the research area. (Tadesse M, et al. 2016).

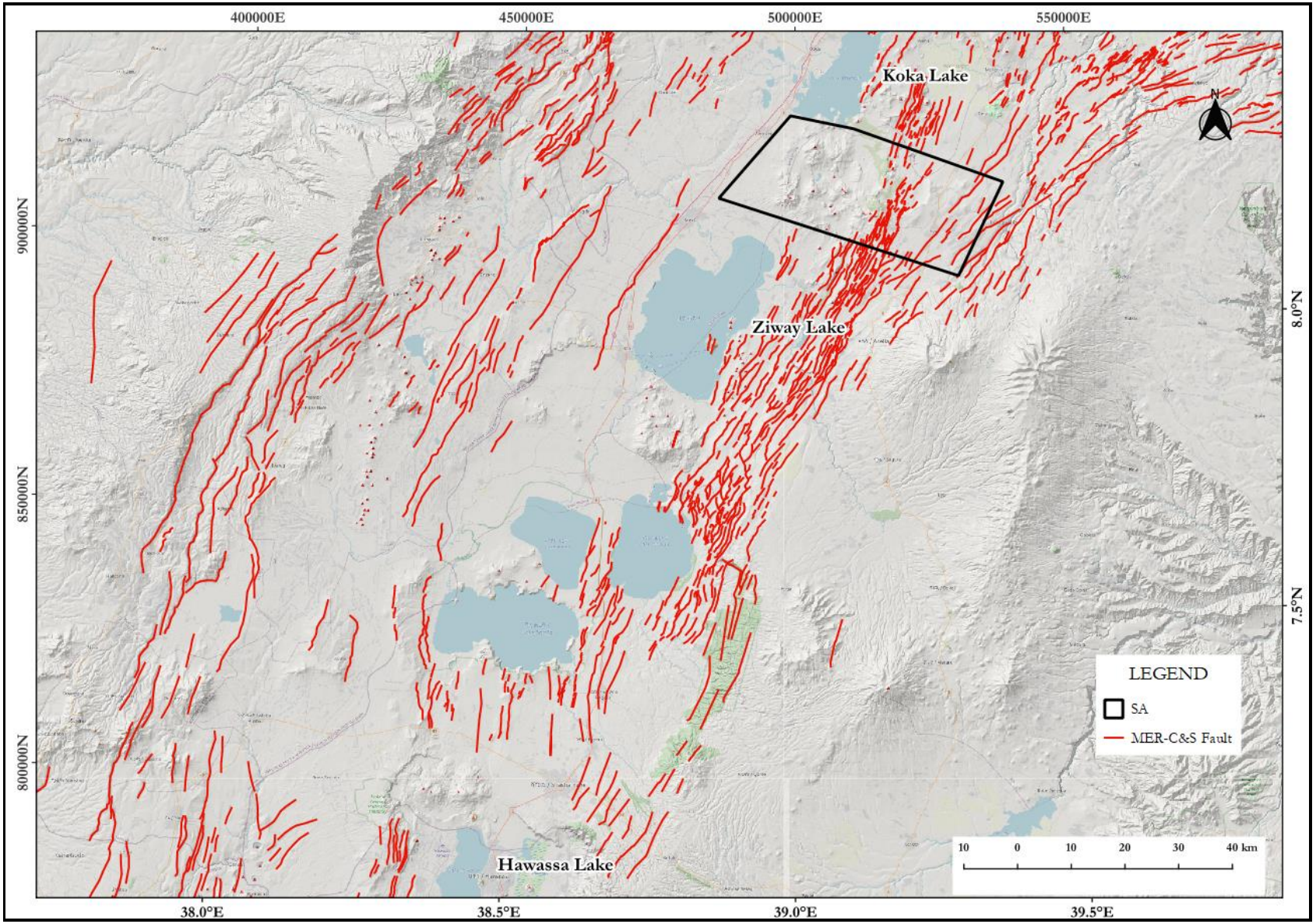

Figure 6. Tectonic sketch map of Central Main Ethiopian Rift

2.3. Geology of Tulu Moye area

Geology of the Tulu Moye area (Figure 7.) is described below from oldest to the youngest as follows according to Di, Paola, 1970, ELC 1987, Abebe, 1987, Mamo, 2000, 2001 and later RG in 2014 and 2015.

Older basalts (QWpb): Basaltic lava and associated with scoria cones. They mostly outcrop in the eastern and the southeastern part of the area (Figure 7). They are coarsely porphyritic (plagioclase feldspar sometimes as big as 2cm). The phenocrysts are mainly plagioclase feldspars (labradorite-bytowanite), olivine (partially idingsitized) and pyroxene. The groundmass is mainly glass and plagioclase lath.

Rhyolites (QTr): Form acidic lava domes and pyroclastics mostly pumice flows and falls. There are numerous rhyolite centres having perfect domes with subordinate craters are abundant and irregularly shaped and are scattered, in most cases they are fractured. Predominantly they are concentrated in the centre, northeast and southwest of the study area associated with pumice breccia (Figure 7). The rhyolites are less porphyritic and, in most cases, crystalline and vitric. The major constituents of the phenocrysts are alkali feldspars (sanidine and anorthoclase) and micro phenocysts of pyroxene (augite) quartz and amphibole (hornblende). Groundmass is mainly volcanic glass and with associated opaque minerals, leucoxene and iron-oxides. The rhyolites are of peralkaline nature (Di Poala, 1978).

Pumice pyroclastics and poorly welded tuffs (QTpu): The pumiceous pyroclastics and poorly welded tuff is mainly characterized by pumice breccia and sometimes by lithic breccia (obsidians and rhyolites). The pumice breccia fill valleys and flow over pre-existing topographic features (mostly they are concentrated in the centre of the study area). The rhyolitic pumice pyroclastics are of peralkaline nature (Di Poala, 1978).
This unit covers most of the studied area especially western half of the area. It is associated, at depth, with poorly welded pumiceous ignimbrite.

Basalts (QWb): Mostly fresh, fine grained with vesicles and sometimes scoriacious. There are different varieties of lavas. The basalt lavas cover most of the north-eastern part of the area and some on the southern end of the area. They have aphanitic texture, scarce micro phenocrysts of plagioclase, olivine and pyroxene, and the groundmass is dominated by plagioclase lath, olivine, pyroxene, and iron oxide.

Trachytes (QTt): Form moderate domes and are concentrated on the eastern part of the area. They outcrop on the eastern and southeastern part of the area and near Bite Lake. The rock has a trachytic texture with phenocrysts of alkali feldspars (anorthoclase) and plagioclase (andesine), olivine (idingsitized) and minor pyroxene (partially altered) and quartz. The groundmass is dominantly plagioclase lath, pyroxene and opaque minerals (Fe-oxides). The trachytes are oversaturated to pantelleritic lavas (ELC, 1987)

Obsidians (QTo): Common in the study area and form thick viscous lava flows mainly porphyritic but there are also the non-porphyritic flows highly fractured and having high permeability. They are outcropping mainly on the eastern side of the study area, around Mt. Gnaro and Mt. Jano following the NNE-SSW structures.

They have partially porphyritic and vitro porphyritic texture with phenocrysts of sanidine and anorthoclase and with minor pyroxene, quartz, and iron oxides. The groundmass is totally glassy. The obsidians are mainly viscous glassy commendites (Bizouard and Di Poala, 1978).

Lacustrine Sediments (Ql): There are also sedimentary rocks, which cover mostly the lower depression of the rift. Exposed section of the unit contains fine ash, sand, and clay. It shows alternate graded bedding (10 to 20 cm apart). It has been described by many researchers (Lloyd, 1977; UNDP, 1973; ELC, 1987 and others) that the sediments are widespread in the central part of the Main Ethiopian Rift. They are 0.1 My old as this is the age suggested by Laury and Albritton (1975). Recent alluvial products (Ql) mainly constituted by clay, silt and sand cover the low-lying flat plains.

The significance of the geology (section 2.3) and structure (section 2.4) of the study area for geothermal resource occurrence is described in section 2.5.

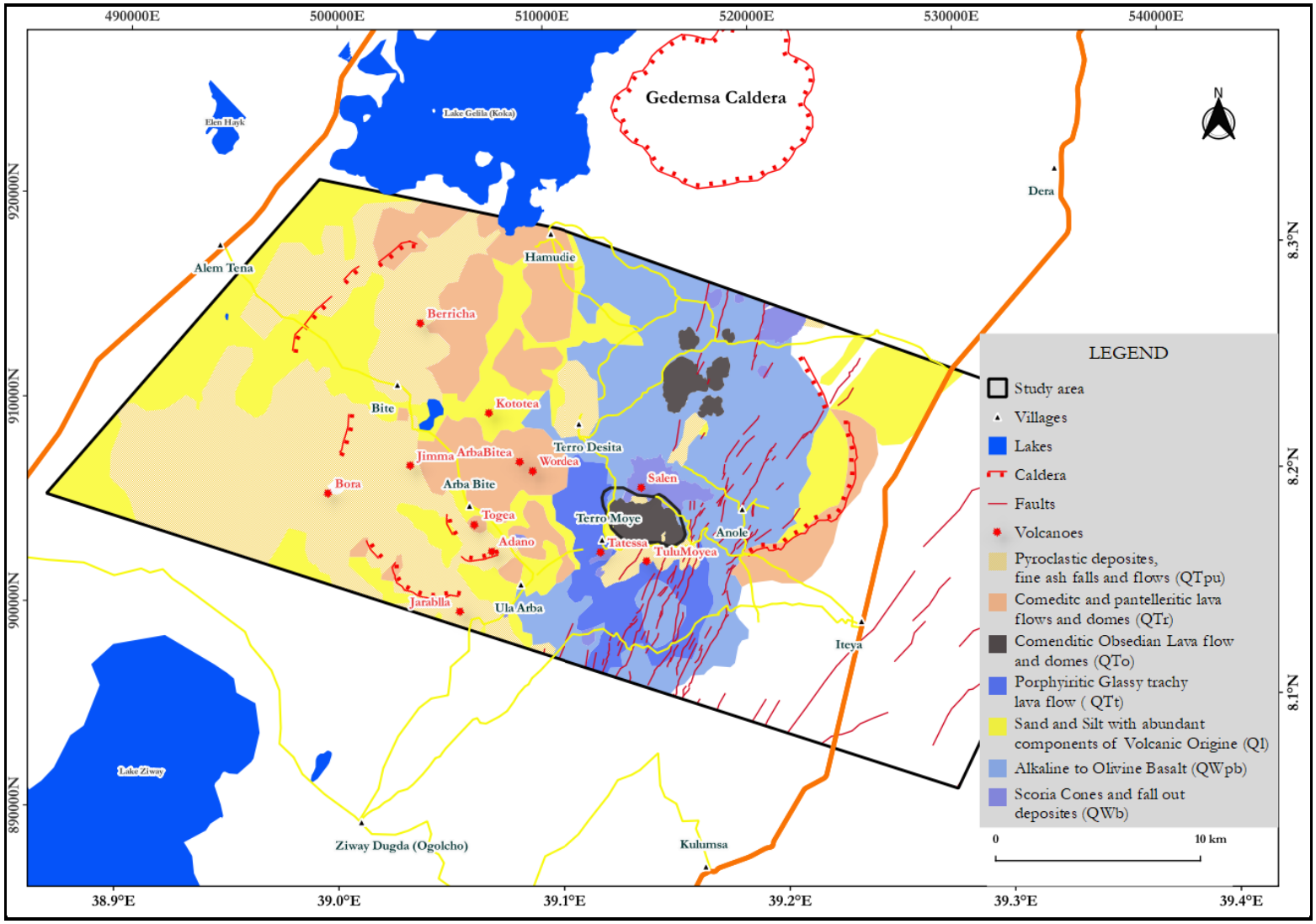

Figure 7. Lithology Map

(Adapted from Tulu Moye Geothermal Prospect Surface Exploration Geology report, Tadess M. et al., 2016)

2.4. Structures of Study area

The Main Ethiopian Rift (MER) has three sections based on surface geology and geomorphology. The Tulu Moye area (Figure 8) is in the Central Main Ethiopian Rift (CMER) which extends from Lake Koka in the north Lake Hawasa in the south with border faults trending N30°E-N35°E. The eastern margin faults show an average trend of N30°E and WNW dipping Assela –Langano Fault Sysem, (Corti, 2009). The estimate of the age of the faulting is 8.s -9.3 Ma (Woldegabriel et al., 1990). The border fault systems are normally segmented and characterized by transverse structures.

The rift floor under MER is affected by widespread deformation related to faulting along the Wonji Fault Belt (Mohr, 1967).

The Wonji Fault Belt

The alignment of caldera structures, cinder cones, and volcanic fissures indicates that volcano-tectonic activity from the Quaternary to Recent MER is linked to the Wonji Fault Belt. In general, generates a compact network of faults distinguished by fresh, steep fault scarps. The eastern margin is characterized by closely spaced sets of horsts, graben and half graben fault plane that have high angle geometry with dip generally >65° (Corti, 2009).

The WFB is segmented at the surface and at depth tomographic images reveal along axis segmentation in crust and upper mantle velocity patterns that follow the same right stepping pattern as the magmatic segment of the WFB (Casey et al., 2006). Meyer et al. (1975) recognizes the WFB as a tectonic and magmatic rift stages transitional between continental and oceanic rifting a narrowing zone of magma intrusion.

The WFB is the most recent fault system in the MER and has been divided into three areas:

- Shone-Awassa: Southernmost area with dominant N-S fault lines.
- Chilalo-Arbagugu: East of Gedemsa caldera, from the 8°00 N and 8°30 N with three major fault direction E-W, NE-SW, and NEN-SWS.
- Assela-Wonji: West of the Chilalo-Arbagugu margin and is the most active segment of the WFB. The dominating fault direction is NEN-SWS. The study area is with in this section.

The study area is in the central part of the Main Ethiopian Rift (MER) where it is affected by the Wonji Fault Belt (WFB) (Mohr, 1967). It consists open fractures trending NEN-SWS. The major structures are trending following WFB they are intersected by NW-SE trending transverse faults, where most of the

hydrothermal activities are concentrated (Tadesse M, et al 2016). The volcanic centres are aligned in the NEN-SWS directions.

The eastern part of the area around Tulu Moye is characterized by NEN-SWS trending, closely spaced fault swarms and open tensional fissures (fractures). This zone is presently active axis of the rift structure. The Recent basalts and obsidians have erupted through these structures (Di Poala, 1972). There are also inferred NW-SE trending transvers structures crossing in the study area observed from the alignment of the thermal manifestations (Tadesse M, et al. 2016).

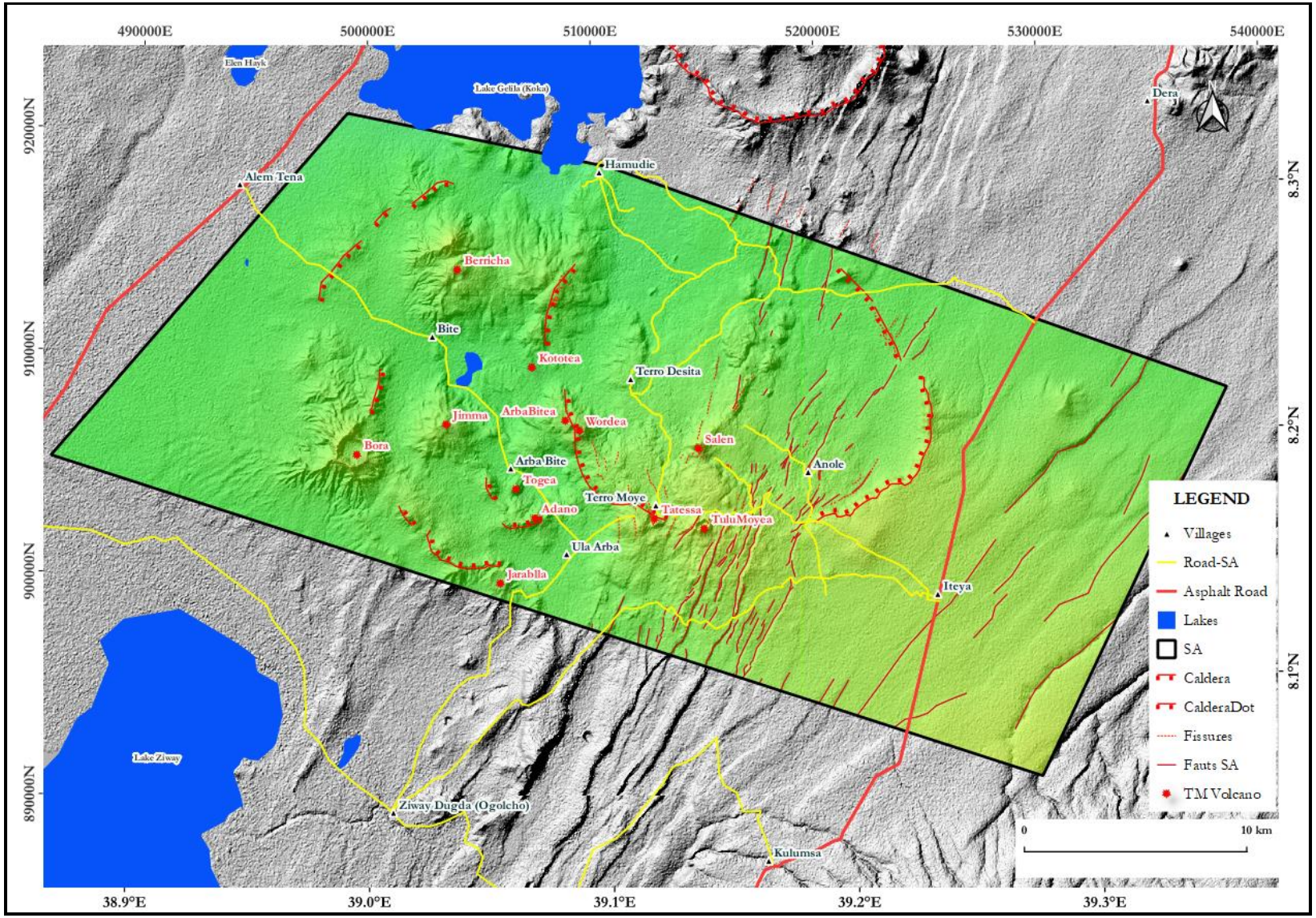

Figure 8. Structural Map of the Tulu Moye Volcanic Complex and its Surroundings.

2.5. Geological and Structural conditions for Geothermal

As it is pointed out in the previous sections (2.1 to 2.4) and its subsections, volcanic activity and volcanic eruptions are recent events in the area less than 200 years old (Tim Greenfield et al., 2019) which probably indicate presence of active volcanoes in the area which intern indicate the possibilities of the presence of heat sources at relatively shallow depths in the area. In addition to the volcanic activities and their favourable conditions in contributing one of the major components of a geothermal system, the WFB presence and its orientation, the transversal faults in the area which have NW-SE trend have effect on facilitating or hindering ground water flow into the probable geothermal reservoir which is believed to exist beneath the surface of the study area. Though the hydrogeological conditions (especially ground water flow directions) and the structures effect on ground water condition is presented in Section 1.8, it is possible to point out that the WFB facilitates ground water flow in the NE-SW and downward direction but impede flows against it. Thus, the WFB could have positive contribution in recharging the geothermal system in the area or could have impact on cooling it.

CHAPTER 3

3. Theoretical background

3.1. Introduction

Geophysical methods are based on the study of the propagation of different physical fields inside the Earth. The most important geophysical fields are gravity, magnetic, electromagnetic, and seismic wave fields. The observations of these fields first depend on the physical properties of the rock. Traditional geophysical data analysis methods include the establishment of different geological models and observational data. Numerical modeling of geophysical data for a given model parameter is often referred to as a forward problem. The solution to the forward problem enables us to predict geophysical data from specific geological structures. The ultimate goal of geophysical observations is to determine geological structures from geophysical data. Due to the complex internal structure of the earth, this is a very difficult problem. Usually, we use a more or less simple model to approximate the real geology and try to determine the model parameters from the data. We call this problem an inverse problem (see Figure 8). The success of geophysical interpretation depends on whether or not we can approximate the true geological structure through a reasonable model and effectively solve the corresponding inverse problems.

3.2. Gravity

3.2.1. Basic Theory

The gravity survey method relies on Newton's Law of Gravitation, which states that the force of attraction (F) between two masses (m_1 and m_2) with small dimensions is proportional to their distance (r).

$$F = \frac{Gm_1m_2}{r^2} \quad \text{.....3.1}$$

where G is the Gravitational Constant (6.67 X $10^{-11} m^3 kg^{-1} s^{-2}$).

Consider the gravitational attraction of a spherical, non-rotating, homogeneous Earth of mass M and radius R on a small mass m on its surface. It is relatively simple to show that the mass of a sphere acts as though it were concentrated at the center of the sphere and by substitution.

in equation (3.1)

$$F = \frac{GM}{R^2} m = mg \quad \text{.....3.2}$$

Gravitational acceleration ($g = GM/R^2$) refers to the relationship between force and mass. The weight of a mass is represented by m.

On such an Earth, gravity would be constant. The Earth's ellipsoidal form, rotation, variable surface relief, and interior mass distribution result in varying gravity over its surface.

The gravitational field is most usefully defined in terms of the gravitational potential U:

$$U = \frac{GM}{r} \quad \text{.....3.3}$$

The gravitational acceleration g is a vector quantity with magnitude and direction (vertically downward), whereas the gravitational potential U is a scalar with magnitude only. The first derivative of U in any direction determines the component of gravity in that direction. Therefore, a potential field approach offers computational flexibility. Equipotential surfaces can be defined as those with constant U. The sea-level surface, also known as the geoid, is the most recognizable equipotential surface. It is horizontal and perpendicular to gravity.

3.2.2. Units of gravity

The average gravity at Earth's surface is 9.8m s^{-2}. Differences in gravity induced by density differences in the subsoil are on the order of 100 mms^{-2}. The gravity unit (gu) is a measurement of micrometers per second. Gravity surveys on land can achieve an accuracy of ±0.1 gu, which is approximately one hundred millionth of the usual gravitational field. At sea, accuracy is approximately ±10 gu. The c.g.s. unit of gravity is the milligal (1 mgal = 10^{-3} gal = 10^{-3} cm s^{-2}), which equals 10 gu.

3.2.3. Measurement of gravity

Gravity, being an acceleration, may be measured using length and time. Gravity surveying requires precision and accuracy, making seemingly simple observations challenging to achieve.

Measuring the absolute value of gravity is hard and time-consuming. Large pendulums or falling body approaches, such as those described by Nettleton (1976) and Whitcomb (1987), can achieve a precision of 0.01 gu. Historically, instruments for measuring absolute gravity in the field were big, expensive, and slow

to read (Sakuma 1986). A new generation of absolute reading instruments (Brown et al. 1999) is being developed to overcome these disadvantages and may become more widely used in the future.

Gravity surveying often measures relative gravity values (differences between places), which is a simpler method. To obtain absolute gravity values at survey stations, refer to the International Gravity Standardization Network (IGSN) of 1971 (Morelli et al. 1971). The IGSN is a network of stations where absolute gravity values have been determined based on measurement sites (see Section 6.7). To establish the absolute value of gravity at a specific site, use a relative reading instrument to measure the difference in gravity between an IGSN station and the field location.

Previous relative reading tools relied on small pendulums or torsion fiber oscillations, which were portable yet time-consuming to read. Gravimeters are modern instruments that can rapidly measure gravity.

Gravimeters are essentially spring balances with a constant mass. The length of a spring varies with the weight of the mass, indicating the change in gravity. In Figure 9, a spring with an initial length s is stretched by an amount δs due to a rise in gravity (δg) and the weight of the hanging mass (m). Hooke's Law states that the extension of a spring is proportionate to its extending force.

$$m\delta g = k\delta s \quad \text{and} \quad \delta s = \frac{m}{k}\delta g \qquad \ldots\ldots.3.4$$

where k is the elastic spring constant.

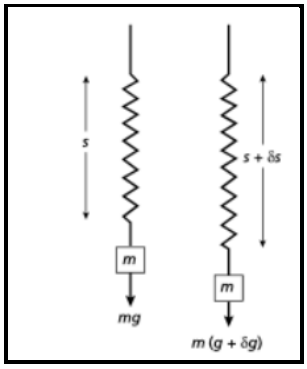

Figure 9. Principle of stable gravimeter operation.

δs should be measured with precision of I: 108 using surveying equipment suitable for gravity measurement on land. Using a big mass and weak spring can boost the instrument's sensitivity (m/k ratio) but can also lead to system collapse. In actuality, the expansion requires amplification through optical, mechanical, or electrical means.

Early gravimeters, also known as steady or static gravimeters, had limited sensitivity due to the spring's dual function of supporting the mass and acting as a measuring device. Modern meters (unstable or astatic) use

an extra force that functions similarly to the spring's extension or contraction, amplifying movement directly. The LaCoste and Romberg gravimeter is an unstable instrument. The meter consists of a hinged beam with a mass supported by a spring mounted above the hinge (Figure 10). The spring's moment on the beam is proportional to its extension and the sine of the angle (Θ). As gravity increases, the beam depresses, and spring expands.

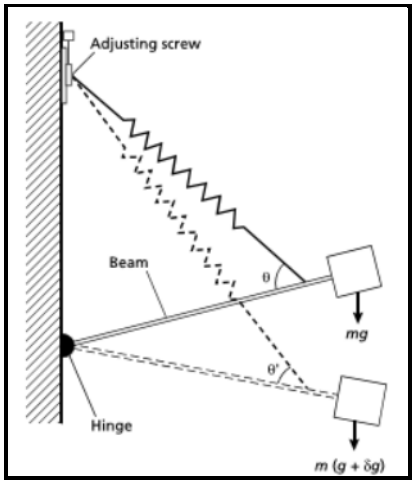

Figure 10. Principle of the LaCoste and Romberg gravimeter.

As the restoring force of the spring increases, the angle Θ decreases to Θ'. Designing the spring and beam geometry can minimize the increase in restoring moment as gravity increases. Using regular springs would limit the instrument's functioning range significantly. Using a 'zero-length' spring, which is pretensioned during manufacturing and has a restoring force proportionate to its physical length rather than extension, instruments can have a highly sensitive response across a wide range. To get reading from the instrument, adjust the vertical position of the spring attachment using a micrometer screw to bring the beam back to the horizontal. A battery-powered thermostat removes thermal impacts. The instrument's range is 50,000 gu.

Gravimeters for general surveying can measure gravity changes with an accuracy of 0.1 gu. A new generation of efficient zero-length springs has been developed. Microprocessor-controlled instruments can be self-level within certain limitations and enable for quick observations. Gravimeters are also available for more specialized surveys capable of detecting gravity changes as tiny as 1 microgal ($10\text{-}8ms^{-2}$).

Gravimeters have a limitation called drift. This refers to a steady shift in readings over time, visible when the instrument is left at a fixed location. Drift is caused by the springs' poor suppleness, which leads to creep over time. Temperature fluctuations might cause expansion or contraction of the measuring equipment,

leading to discrepancies in results that are not related to gravity changes. Drift is tracked using daily meter readings at a fixed point.

3.2.4. Gravity Surveying

Gravity survey station spacing can range from a few meters in detailed mineral or geotechnical surveys to many kilometers in regional reconnaissance surveys. Accurate measurement of gravity gradients is crucial for interpretation; hence station density should be highest in areas with rapid gravity field changes. To compare results with other gravity surveys, a base station with known absolute gravity measurements is necessary. If the nearest IGSN station is too far away, a gravimeter can be used to create a local base by measuring the difference in gravity between the two locations. To avoid instrumental drift, looping is used instead of direct recording. To create drift curves (Figure 11), alternate readings at recorded times are taken at both sites. To calculate the drift-corrected gravity difference, average the ordinate measurement discrepancies ($\Delta g_{1\text{-}4}$) between the two stations.

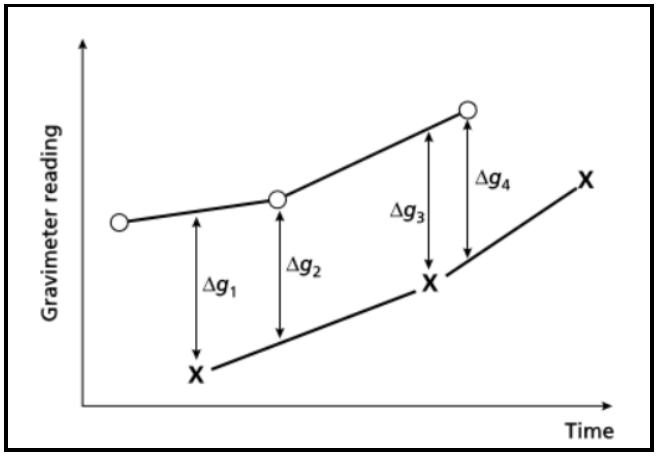

Figure 11. The principle of looping.

Crosses and circles represent alternate gravimeter readings taken at two base stations. The vertical separations between the drift curves for the two stations ($\Delta g_{1\text{–}4}$) provide an estimate of the gravity difference between them.

A gravity survey involves reading the gravimeter at a base station at a frequency determined by the instrument's drift characteristics. Each survey station records location, time, elevation, water depth, and gravimeter readings.

To obtain a reduced gravity value of ±1 gu, the gravimeter must be read to a precision of ±0.1 gu, and the station's latitude and elevation must be known to ±10m and ±10mm, respectively.

3.2.5. Gravity Reduction

To properly interpret gravity survey results, it's important to account for fluctuations in the Earth's gravitational field that are not caused by density variances in the underlying rocks. Gravity reduction (LaFehr 1991) or reduction to the geoid refers to using sea-level as the most appropriate datum level. Lists of gravity reduction are drift, Latitude, elevation, Simple and complete bouguer correction, and isostatic correction. Formulas and methods on how to carry out these corrections can easily be found from standard geophysical books (like An Introduction to Geophysical Exploration. Third Edition by Philip Kearey et al. 2002).

3.3. Magnetics

3.3.1. Introduction

A magnetic survey aims to examine subsurface geology by identifying abnormalities in the Earth's magnetic field caused by underlying rocks. Although the majority of rock-forming minerals are not magnetic, some rock types do contain enough magnetic minerals to generate large magnetic anomalies. Magnetic surveys are used for a variety of purposes, including detecting buried metallic items in engineering or archeological surveys, as well as investigating regional geological structure on a larger scale. Magnetic surveys can be conducted on land, sea, or in the air. Airborne surveys are extensively used due to their speed of operation, making them an attractive option.

3.3.2. Basic concepts

A bar magnet produces magnetic flux that flows from one end to the other (Figure 12). A Small compass needle floating within this flux can be used to trace its directions. The poles of a magnet are the spots where flux converges. A freely hanging bar magnet aligns with the Earth's magnetic field. The north-seeking or positive pole of a magnet points towards the Earth's north pole, whereas the south-seeking or negative pole at the opposite end has the same strength.

The force F between two magnetic poles of strengths m_1 and m_2 separated by a distance r can be expressed as

$$F = \frac{\mu_0 m_1 m_2}{4\pi\mu_R r^2} \quad \text{.....3.5}$$

The variables μ_0 and μ_R represent the magnetic permeability of vacuum and the medium separating the poles, respectively. When the poles have opposite signs, the force is attracting, while when they have the same signs, it is repulsive.

The magnetic field B caused by a strong pole at a distance r is defined as the force exerted on a unit positive pole at that point.

$$B = \frac{\mu_0 m}{4\pi\mu_R r^2} \quad \text{.....3.6}$$

Magnetic fields can be defined in terms of magnetic potential. They behave similarly to gravitational fields. For a single pole with strength m, the magnetic potential V at a distance r from the pole can be calculated as

$$V = \frac{\mu_0 m}{4\pi\mu_R r} \quad \text{.....3.7}$$

To calculate the magnetic field component in a specific direction, take the partial derivative of the corresponding potential.

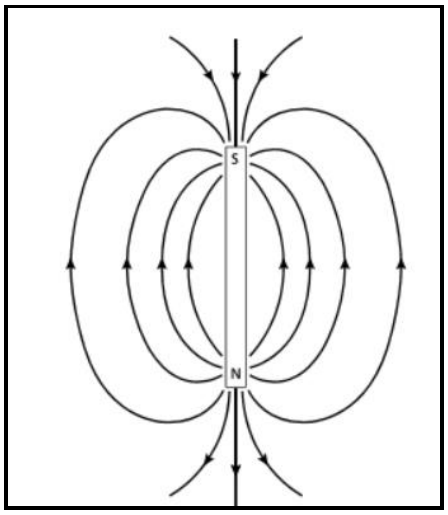

Figure 12. The magnetic flux surrounding a bar magnet.

Magnetic characteristics in the SI system are defined based on electrical current flow (Reilly 1972,). When a current flows through a coil with multiple turns of wire, a magnetic flux flows through and around the annulus due to a magnetizing force (H). H is proportional to coil turns and current strength, but inversely

proportional to wire length. It is given in Am^{-1}. The magnetic field B of a coil refers to the density of magnetic flux measured perpendicular to the flow direction. B is proportional to H, and the constant of proportionality, m, is known as magnetic permeability. Lenz's law of induction states that the rate of change of magnetic flux in a circuit is proportional to the voltage created inside it. This is written as B in Vsm^{-2} (Weber $(Wb)^{m-2}$). The unit of the Wbm^{-2} is the tesla (T). Permeability is represented as $WbA^{-1}m^{-1}$ or Henry $(H)m^{-1}$. The gauss (G) unit represents magnetic field strength and is comparable to 10^{-4} T.

To measure minor magnetic anomalies induced by rocks, a subunit called nanotesla (nT) is used instead of the tesla ($1nT = 10^{-9}$ T). The c.g.s. system uses numerically comparable gamma (g) equal to 10^{-5} G.
Common magnets are called dipoles because they have two poles. The magnetic moment (M) of a dipole with poles of strength m and distance l apart is given by

$$M = ml \quad \ldots\ldots.3.8$$

A current-carrying coil's magnetic moment is proportional to its number of turns, cross-sectional area, and current magnitude, represented in Am^2. When a substance is placed in a magnetic field, it may develop magnetization in that direction, which is then lost when withdrawn.
Induced magnetization, also known as magnetic polarization, occurs when elementary dipoles within a material align in the direction of the field. Magnetic poles are dispersed across the material's surface, corresponding to the ends of dipoles (Figure 13). The intensity of induced magnetization (Ji) is defined as the dipole moment per unit volume of the substance.

$$J_i = \frac{M}{LA} \quad \ldots\ldots.3.9$$

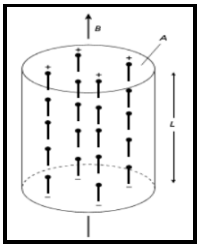

Figure 13. Schematic representation of an element of material in which elementary dipoles align in the direction of an external field B produces an overall induced magnetization.

M represents the magnetic moment of a sample of length L and cross-sectional area A. J_i is then expressed in Am^{-1}. In the c.g.s. system, magnetization intensity is measured in $emucm^{-3}$ (emu = electromagnetic unit),

where 1 emucm^{-3} equals 1000Am^{-1}. The intensity of magnetization is proportional to the magnetizing force H of the inducing field.

$$J_i = kH \quad \text{.....3.10}$$

where k is material's magnetic susceptibility. Susceptibility in the SI system is dimensionless since J_i and H are both measured in Am^{-1} units. In the c.g.s. system, susceptibility is dimensionless. However, rationalizing the SI system results in SI susceptibility values that are 4π higher than equivalent c.g.s values.

In a vacuum, the magnetic field strength (B) and magnetizing force (H) are related by $B = \mu_0 H$, where μ_0 represents the vacuum permeability (4π X 10^{-7} Hm^{-1}). Air and water have similar permeabilities to μ_0, which can be used to represent the Earth's magnetic field when not affected by magnetic elements. When a magnetic material is placed in this field, it creates an extra magnetic field with a strength equal to $\mu_0 J_i$. The total magnetic field or magnetic induction in the body, B, is given by,

$$B = \mu_0 H + \mu_0 J_i \quad \text{.....3.11}$$

Substituting equation (3.10)

$$B = \mu_0 H + \mu_0 kH = (1+k)\mu_0 H = \mu_R \mu_0 H \quad \text{.....3.12}$$

The dimensionless constant μ_R represents the relative magnetic permeability. The magnetic permeability μ is equal to the product of relative permeability and vacuum permeability, with the same dimensions as μ_0. For air and water, μ_R is near to unity.

At the atomic level, all substances have magnetic properties. Atoms operate as dipoles due to their electrons' spin and orbital route around the nucleus. According to quantum theory, two electrons can reside in the same state (or electron shell) as long as their spins are opposing. Paired electrons have cancellable spin magnetic moments. Diamagnetic materials include entire electron shells and no unpaired electrons. When electrons are placed in a magnetic field, their orbital trajectories rotate, resulting in a magnetic field opposite the applied field. As a result, diamagnetic substances exhibit weak and negative susceptibility. This is still a pretty weak effect.

Small grains of paramagnetic substances with unpaired electrons exhibit magnetic coupling between nearby atoms via their spin dipoles. Such a grain is thus considered to be a single magnetic domain. The connection between electron orbits can be parallel or antiparallel, based on their degree of overlap. Ferromagnetic materials have parallel dipoles (Figure 14), resulting in substantial spontaneous magnetization

even without an external magnetic field and high susceptibility. Ferromagnetic substances, such as iron, cobalt, and nickel, are scarce in the Earth's crust.

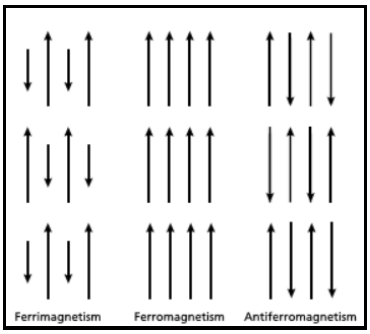

Figure 14. Schematic representation of the strength and orientation of elementary dipoles within ferrimagnetic, ferromagnetic and antiferromagnetic domains.

In antiferromagnetic minerals like hematite, dipole coupling is antiparallel, with an equal number of dipoles in both directions. The dipoles' magnetic fields are self-cancelling, therefore there is no external magnetic influence. Defects in an antiferromagnetic material's crystal lattice structure can result in parasitic antiferromagnetism, which is a small net magnetization. In ferrimagnetic minerals like magnetite, the dipole coupling is antiparallel, although the strength of dipoles in each direction varies. Ferrimagnetic materials have strong spontaneous magnetization and high susceptibility.

Magnetization strength of ferromagnetic and ferrimagnetic material diminishes with temperature and disappears at Curie temperature. Above a certain temperature, interatomic distances become too large to allow electron coupling, resulting in the material's normal paramagnetic behavior.

To reduce total magnetic energy, bigger grains can be subdivided into discrete volume elements (magnetic domains) with widths of the order of a micrometer and parallel coupling of dipoles. Without an external magnetic field, domains align to lessen magnetic forces between them. The Bloch wall is a limited zone that prevents dipoles from crossing from one domain to another.

When a multidomain grain is exposed to a weak external magnetic field, the Bloch wall unrolls, leading to the expansion of domains magnetized in the field at the expense of domains magnetized in other directions. Removing the applied field causes the domain walls to rotate back to their original configuration, resulting in loss of induced magnetization. Applying stronger fields causes domain walls to unroll irreversibly across minor flaws in the grain, resulting in irreversible enlargement of domains magnetized in the field direction. After removing the applied field, the inherited magnetization is known as remanent or permanent magnetization J_r. When greater magnetic fields are applied, the material becomes magnetically saturated, allowing for all potential domain wall movements. Primary remanent magnetization can occur when an

igneous rock solidifies and cools due to the Curie temperature of its magnetic minerals (thermoremanent magnetization, TRM) or when sedimentary magnetic particles align in the Earth's field during sedimentation (detrital remanent magnetization). Secondary remanent magnetizations can occur when minerals recrystallize or develop during diagenesis or metamorphism, resulting in chemical remanent magnetization (CRM). Viscous remanent magnetization (VRM) occurs when the major magnetizations of a rock relax in the direction of an ambient magnetic field over time.

Magnetic minerals in rocks can have both induced and remanent magnetizations (J_i and J_r). The Königsberger ratio (Jr : Ji) is often used to express the relative intensities of induced and remanent magnetizations. These can be in multiple directions and vary significantly in magnitude. The magnetic effects of such a boulder are caused by the resultant J of the two magnetization vectors (Figure 15). The magnitude of J determines the amplitude of the magnetic anomaly, while its orientation affects its shape.

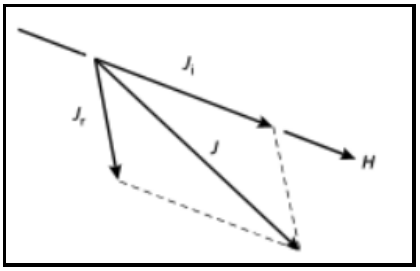

Figure 15. Vector diagram illustrating the relationship between (Ji), remanent (J_r) and total (J) magnetization components.

3.3.3. Rock Magnetism

Rocks have a low magnetic susceptibility due to the presence of few magnetic materials. These minerals can be found in only two geochemical groupings. The iron-titanium-oxygen group includes magnetic minerals such as magnetite (Fe_3O_4) and ulvöspinel (Fe_2TiO_4). Haematite (Fe_2O_3), another common iron oxide, is antiferromagnetic and does not cause magnetic anomalies. However, parasitic antiferromagnetism can occur. Pyrhotite (FeS_{1+x}, $0<x<0.15$) is a magnetic mineral with varying susceptibility based on its composition. The most prevalent magnetic mineral is magnetite, with a Curie temperature of 578°C. Rocks can be classified based on their overall magnetite content, although the size, shape, and dispersion of magnetite grains can impact their magnetic properties. Figure 16 shows a histogram of the susceptibilities of common rock types.

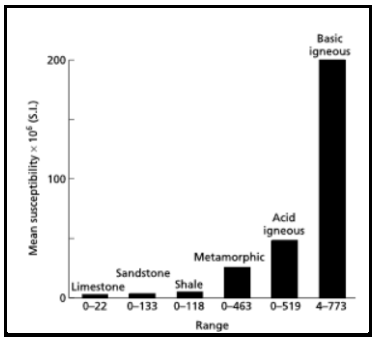

Figure 16. Histogram showing mean values and ranges in susceptibility of common rock types.

(After Dobrin & Savit 1988).

Basic igneous rocks have considerable magnetite concentration, making them strongly magnetic. As acidity increases, the amount of magnetite in igneous rocks decreases. As a result, acid igneous rocks are typically less magnetic than basic rocks. Metamorphic rocks have varied magnetic properties. Low oxygen partial pressure causes magnetite to be resorbed and iron and oxygen to be integrated into other mineral phases during metamorphism. High oxygen partial pressure can lead to the development of magnetite as an accessory mineral in metamorphic events.

Magnetite concentration and susceptibility of rocks vary greatly, with significant overlap amongst lithologies. Magnetic information alone cannot reliably determine the lithology of an anomaly. Sedimentary rocks are non-magnetic unless they include significant amounts of magnetite in their heavy mineral fractions. Magnetic anomalies over sediment-covered areas are typically induced by an underlying igneous or metamorphic basement or intrusions into the sediment.

Magnetic anomalies are commonly caused by dykes, faulted sills, lava flows, huge basic intrusions, metamorphic basement rocks, and magnetite ore deposits. Magnetic anomalies can range in amplitude from a few tens of nT in deep metamorphic basements to hundreds of nT in basic intrusions, and even thousands of nT in magnetite ores.

3.3.4. The geomagnetic field

Rocks can generate localized magnetic anomalies in the Earth's normal magnetic field, known as the geomagnetic field. Understanding the geomagnetic field is crucial for reducing magnetic data and interpreting anomalies. The geomagnetic field is more complex than the gravitational field on Earth, with irregular variations in orientation and magnitude with latitude, longitude, and time.

A magnetic needle suspended on the Earth's surface will align with the geomagnetic field in the surrounding area. This will typically be at an angle to both vertical and geographical north. The magnetic field vector is described using geomagnetic elements (Figure 17). The total field vector B consists of a vertical component Z and a horizontal component H in the magnetic north direction. The dip of B corresponds to the inclination I of the field, while the horizontal angle between geo-graphic and magnetic north is declination D. B's strength ranges from 25,000nT in equatorial regions to 70,000nT at the poles.

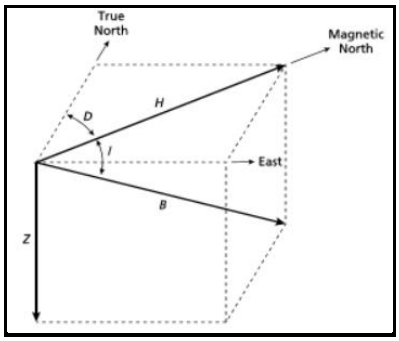

Figure 17. The geomagnetic elements.

In the northern hemisphere, the magnetic field typically dips to the north and becomes vertical at the north magnetic pole (Figure 18). In the southern hemisphere, the dip is mainly upwards towards the north. The magnetic equator is the line of zero inclination that roughly aligns with the geographic equator.

A theorized magnetic dipole in the Earth's center, inclined at 11.5° to the axis of rotation, accounts for approximately 90% of the Earth's field. The magnetic moment of the fictitious geocentric dipole can be derived using the observed field. Subtracting the dipole field from the observed magnetic field can approximate the residual field with a smaller dipole. To recreate the observed geomagnetic field to a desired level of accuracy, keep adding dipoles with diminishing moments. Spherical harmonic analysis, similar to Fourier analysis in spherical polar coordinates, uses successive approximations of the measured field to account for the effects of each fictitious dipole. The method was used to calculate the IGRF formula, which describes the theoretical undisturbed magnetic field at every place on the Earth's surface. In magnetic surveying, the IGRF removes magnetic changes caused by this theoretical field from the data.

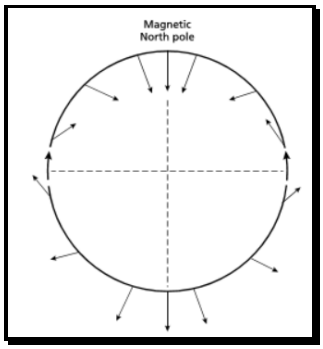

Figure 18. The variation of the inclination of the total magnetic field with latitude based on a simple dipole approximation of the geomagnetic field.

(After Sharma 1976.)

The geomagnetic field cannot be caused by permanent magnetism in the Earth's deep interior. The required dipolar magnetic moments exceed practical expectations, and the temperatures exceed the Curie temperature of any known magnetic material. The geomagnetic field is caused by the dynamo action of charged particles in coupled convective cells within the Earth's outer core. Paleomagnetic investigations suggest that the periodic changes in polarity of the geomagnetic field are caused by the exchange of dominance between these cells. The circulation patterns in the core are not fixed and alter gradually over time. Secular variation refers to the gradual changing of all geomagnetic elements throughout time. Predictable variations exist, such as the progressive rotation of the north magnetic pole around the geographic pole.

External magnetic factors generate daily fluctuations in the geomagnetic field, resulting in diurnal changes. Normal conditions (Q or calm days) result in a smooth and regular diurnal variation with an amplitude of 20-80nT, with polar regions seeing the highest levels. The flow of charged particles inside the ionosphere towards the magnetic poles causes fluctuation in circulation patterns and diurnal variations, which are affected by the tidal forces of the Sun and Moon. This is known as the graphic pole.

D or disturbed days are characterized by irregular diurnal changes and short-term geomagnetic disturbances of up to 1000nT, known as magnetic storms. These days are typically connected with high solar activity and the arrival of charged particles in the ionosphere. During storms, magnetic surveying should be avoided as it is impossible to adjust for quick and high amplitude changes in the magnetic field.

3.3.5. Magnetic anomalies

Magnetic anomalies created by rocks are overlaid on the geomagnetic field, much as gravity anomalies are superimposed on the Earth's gravitational field. The geomagnetic field varies in both magnitude and direction, unlike the gravity field, which is always vertical. The normal geomagnetic field is represented by a vector diagram (Figure 19(a)), which shows how the geomagnetic elements are connected.

$$B^2 = H^2 + Z^2 \quad \text{.....3.13}$$

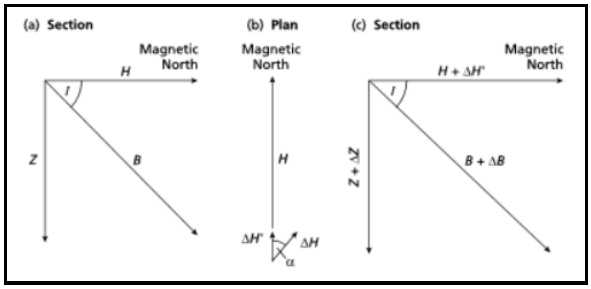

Figure 19. Vector representation of the geomagnetic field with and without a superimposed magnetic anomaly.

A magnetic anomaly affects the Earth's field, altering the strength of vector B. Assume the anomaly causes a vertical component ΔZ and a horizontal component ΔH at an angle δ to H (Figure 19(b)). Only ΔH in the direction of H, namely ΔH', contributes to the anomaly.

$$\Delta H' = \Delta H \cos\alpha \quad \text{.....3.14}$$

It is possible to include the magnetic anomaly using a similar vector diagram.

$$(B + \Delta B)^2 = (H + \Delta H')^2 + (Z + \Delta Z)^2 \quad \text{.....3.15}$$

Expanding this equation, substituting equation 3.13, and ignoring negligible terms in Δ^2 results in:

$$\Delta B = \Delta Z \frac{Z}{B} + \Delta H' \frac{H}{B} \quad \text{.....3.16}$$

Substituting equation 3.16 with angular representations of magnetic element ratios yields

$$\Delta B = \Delta Z \sin I + \Delta H \cos I \cos\alpha \quad \text{.....3.17}$$

where I is the inclination of the geomagnetic field.

This method calculates the magnetic anomaly generated by a small isolated magnetic pole with strength m, defined as its influence on a unit positive pole at the observing site. The pole is located at depth z, horizontal distance x, and radial distance r from the observation point (Figure 20). Substituting $\mu_R=1$ into equation (3.1.3.1) yields the force of repulsion (ΔB_r) on the unit positive pole in direction r.

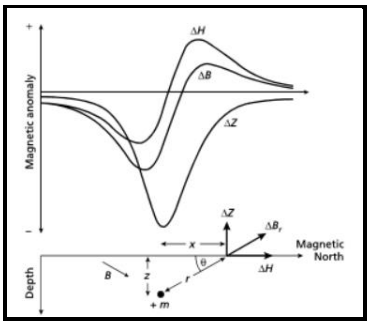

Figure 20. The horizontal (ΔH), vertical (ΔZ) and total field (ΔB) anomalies due to an isolated positive pole.

$$\Delta B_r = \frac{Cm}{r^2} \quad \text{.....3.18}$$

where $C = \frac{\mu_0}{4\pi}$

Assuming the profile aligns with magnetic north, the horizontal(ΔH) and the vertical (ΔZ) component of the anomaly can be estimated by resolving in the appropriate directions.

$$\Delta H = \frac{Cm}{r^2}\cos\theta = \frac{Cmx}{r^3} \quad \text{.....3.19}$$

$$\Delta Z = \frac{-Cm}{r^2}\sin\theta = \frac{-Cmz}{r^3} \quad \text{.....3.20}$$

The vertical field anomaly is negative, as the z-axis is typically positive downwards. Figure 20 displays plots illustrating the form of these anomalies. The horizontal field anomaly is a positive/negative couplet, while the vertical field anomaly is centered above the pole. Substituting the formulas of equations (3.1.3.13) and (3.1.3.14) into equation (3.1.3.12) yields the total field anomaly ΔB with $\delta = 0$. If the profile is not aligned with magnetic north, angle δ represents the angle between magnetic north and the profile direction.

3.3.6. Magnetic survey instrumentation

Geomagnetic field signals have been developed since early 1900. The measuring unites are named magnetometer. A lot has been done to improve the precision of measurement, accuracy, and mode of measurements. These days it is possible to deploy modern magnetometers for measurements on land (ground magnetic survey), in air (Aeromagnetic survey) and on sea (Marine survey).

3.3.7. Ground magnetic survey.

Ground magnetic surveys typically cover small areas on a pre-defined objective. Station spacing typically ranges from 10-100m, however smaller distances may be used in areas with large magnetic gradients. Avoid taking readings near metallic things that may disrupt the local magnetic field, such as railway lines, cars, roads, fencing, or houses. Similarly, operators of magnetometers should avoid carrying metallic objects. Fluxgate and proton magnetometers do not drift, hence base station values are not necessary for monitoring instrumental drift. However, they are useful for monitoring diurnal fluctuations (see Section 7.9). Magnetic surveys on land are faster than gravity surveys due to the absence of the need for precise levelling.

3.3.8. Aeromagnetic and Marine survey

Magnetic surveys are typically conducted in the air, with the sensor towed in a 'bird' housing to avoid aircraft magnetic effects or fixed in a 'stinger' in the aircraft's tail, where inboard coil installations compensate for the aircraft magnetic field. Aeromagnetic surveying is quick and cost-effective, often costing 40% less per line kilometer than ground surveys. Remote surveying allows for quick and cost-effective coverage of large areas, including difficult locations, without requiring field personnel. Positioning has historically been the most challenging aspect of airborne surveys. Nowadays, however, the availability of GPS eliminates the locating issue.

Marine magnetic surveying techniques are comparable to those used in aircraft surveys. To reduce magnetic influences, the sensor is pulled in a 'fish' at least two ship lengths behind the vessel. Marine surveying, while slower than aeromagnetic surveying, is often used in conjunction with other geophysical procedures like gravity surveying and continuous seismic profiling, which cannot be done in the air.

3.3.9. Reduction of magnetic observation

Magnetic data must be reduced to eliminate non-subsurface causes of fluctuation. The following are the reductions that need to be applied to magnetic data.

i. Geomagnetic correction

Geomagnetic correction removes the influence of a geomagnetic reference field from survey data, similar to gravity surveying latitude correction. The IGRF (International Geomagnetic Reference Field) is the most rigorous method for geomagnetic correction. It represents the undisturbed geomagnetic field in terms of several harmonics and incorporates temporal terms to account for secular variation. The IGRF is sophisticated and requires computer calculations for corrections. The IGRF is imperfect as it relies on observations from a small number of distributed magnetic observatories. The IGRF predicts future spherical harmonics based on observatory data. As a result, the IGRF in places far from observatories may have significant errors.

ii. Elevation and Terrain correction

The geomagnetic field has a vertical gradient of only 0.03nTm-1 at the poles and -0.015nTm-1 at the equator, so elevation correction is typically not necessary. Topography can have a significant impact on ground magnetic surveys, but its effects are unpredictable due to the magnetic characteristics of the topographic features. Therefore, in magnetic surveying, terrain corrections are rarely used. After applying diurnal and geomagnetic adjustments, any remaining magnetic field changes are likely due to spatial differences in the sub surface's magnetic characteristics, known as magnetic anomalies.

3.3.10. Formulation of Forward and Inverse Problems

When studying geophysical approaches, we must remember that certain sources can produce geophysical fields. Therefore, the generic forward and inverse problems can be described as follows:

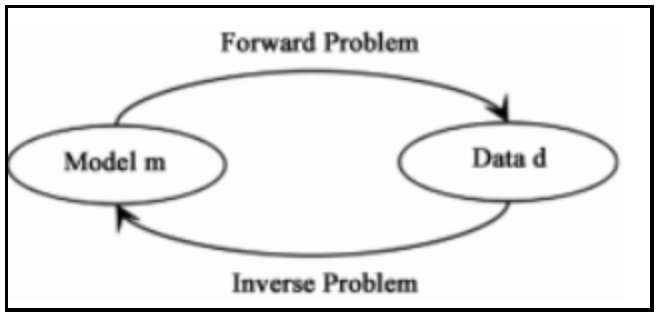

Figure 21. Traditional definition of forward and inverse problems.

Forward Problem

$$\text{Model } \{\text{model parameter m, sources s}\} \rightarrow \quad \text{data d:}$$

$$d = A_s\,(m)\ldots\ldots\ldots\ldots....3.1$$

Where, A_s is forward problem operator de3pending on s.

Inverse Problem

$$\{\text{Data d, source s}\} \rightarrow \text{model } \{\text{model parameter m}\}$$

$$m = A_s^{-1}(d)\ \ldots\ldots\ldots\ldots....3.2$$

Where, A_s^{-1} is inverse problem operator.

In some geophysical applications, the inverse problem is solely expressed in terms of the sources of the observed field.

$$\{\text{data d}\} \rightarrow \{\text{source s}\}\ \ldots\ldots\ldots\ldots....3.3$$

The problem (3.3) is called the inverse source problem. In this situation, the model parameters (the medium's physical properties) are presumed to be known. Typical examples of this problem are the gravity inverse problem and seismological inverse problem. In the first scenario, the gravity field comes from the rock's density distribution. In the second case, the goal is to estimate the location and type of seismic source from the observed seismic field.

In the solution of any inverse problem, three crucial questions emerge:

i. Does the solution exist?
ii. Is it unique?
iii. Is it stable?

The presence of the solution is related to the mathematical formula for the inverse problem. Because we investigate the actual geological structure within the Earth, there should be a physical solution. However, from a mathematical standpoint, there may be no appropriate numerical model to fit our observed data to a given set of models.

The formula below illustrates the solution's uniqueness. Suppose we have two different models, m_1 and m_2, and two different sources s_1 and s_2, that produce the same data d_0:

$$A\,(m_1, s_1) = d_0,\ A\,(m_2, s_2) = d_0$$

In this scenario, it is impossible to discriminate between two models, m1 and m2, using the data. That is why uniqueness difficulties are critical for inversion.

The final issue is solution stability, which is also an important issue in Inversion Theory. Geophysical data is always tainted by noise (δd). The issue is if the variation in responses between different modes is higher than the noise level. For example, if two separate models, m1 and m2, and two different sources, s1 and s2, generate two different data sets, d1 and d2, as follows:

$$A(m_1, s_1) = d_1, A(m_2, s_2) = d_2$$

Assume that the two models and the source are different obviously, while the data difference is within the noise level ε:

$$\|\delta m\| = \|m_1 - m_2\| > C, \|\delta s\| = \|s_1 - s_2\| > C,$$

$$\|\delta d\| = \|d_1 - d_2\| < \varepsilon, C >> \varepsilon$$

Where, the symbol ‖. ‖ denotes some norm, or measure of difference between two models, sources, and data sets.

In this situation, the two models are indistinguishable from the observed data.

Given the relevance of these three concerns in the solution of the inversion problem, Hadamard, a well-known French mathematician, stated that if all three issues are answered positively, a mathematical problem can be expressed accurately. In other words, a mathematical issue is deemed well-posed if its solution exists, is unique, and stable. According to Hadamard (1902), an ill-posed issue is one in which the solution does not exist, is not unique, or is not a continuous function of the data. Hadamard believed that ill-posed mathematical problems were not physically or mathematically meaningful. However, it turns out that most mathematical physics and geophysical problems (in fact, most natural science problems) are ill-posed. Fortunately, it was eventually shown that Hadamard's viewpoint was incorrect: the ill-posed problems are both physically and mathematically significant and can be solved.

In the middle of the twentieth century, Andrei N. Tikhonov laid the groundwork for the idea of ill-posed problem solutions. He developed a regularization method to approximate an ill-posed problem with a set of well-posed problems.

CHAPTER 4

4. Instrumentation, Data acquisition, Processing and Presentation

Instrumentation, acquisition, processing for the two methods is conducted given heed to data quality and distribution.

4.1. Instrumentation

4.1.1. Gravity

Ground gravity data was collected using LaCoste & Romberg G781 gravimeter which has an accuracy of 0.001mGal. In addition to the instrument's sensitivity and accuracy collected elevations qualities are high. Since latitude and elevation accuracies play a key role in gravity data reduction, based on direct involvement of the researcher in the survey and according to the meta-data of gravity, serious heed was given to this measurement. GNNS (Global Navigation Satellite System) privileges were used from 13 station and RTK (Real Time Kinematics) observation tool was deployed which enabled obtaining the lowest accuracies of 0.0026 and 0.0069 with mean square error of 0.0016 and 0.0038 in the horizontal and vertical. The data owner is TM Geothermal Operations Plc where the researcher is an employee and entitled to use it free.

4.1.2. Magnetics

The GSM-19T v7.0 proton precession magnetometer which has 0.01nT resolution and 0.2nT absolute accuracy (GSM-19 v7.0 Instruction Manual 2008) was deployed to acquire data. Data was collected along roads, tracks, trails giving special attention to crossing the main geological strikes of the area during the survey time. The data owner is TM Geothermal Operations Plc where the researcher is an employee and entitled to use it free.

4.2. Data acquisition

4.2.1. Gravity

The information below was obtained both from meta-data and by being part of the survey endeavor. This data was not collected during the study time. It was collected for a private company (TM Geothermal Operations Plc) which is engaged in the geothermal resource utilization for electric power production. The purpose of the survey was to draw a baseline before any abstraction of the geothermal resource and be used

as a reference while production. The researcher had direct involvement in the planning and the gravity data acquisition processes apart from other issues. So, the researcher has full information on how the data acquisition was carried out. The owner of this data is TM Geothermal Operations Plc. No publications have been produced using this data so far.

Gravity data acquisition was carried out along six profiles which have WNW-SES orientation (Figure 22) using LaCoste & Romberg G781 gravimeter for relative gravity measurements and the combination of GNSS and RTK systems were applied for coordinate/ position and elevation surveys. The survey profiles are 3-4 km apart with 2-4 km station intervals. However, data density is high and spacing is small in the central part of the study area. Special heed was given in the central part of the survey area considering the presence of major volcanic centers, rift axis segments, Wonji Falt Belt (WFB), etc. in the area. Figure 9 shows survey coverage. 204 corrected and reduced gravity data points values are used for this study.

4.2.2. Magnetics

The researcher has direct involvement in planning, designing, and participating in this data acquisition. So, the researcher has full information on the data collected. It was primarily collected for the company which is mentioned in the previous sub-section but not meant to draw baseline rather get information on the subsurface condition which could be reflected by the anomaly signature and be related to magnetic susceptibilities.

GSM-19 v7.0 Proton Precession Magnetometer was deployed to acquire magnetic data. The magnetometer is equipped with an internal clock to record reading time and an external GPS is connected to its port on the main consol to read and register data station location and elevation. The data is collected in the continuous mode/walking mode set to read and record the survey data (Total Magnetic Field, Easting, Northing, Elevation and Time). It is collected following road, tracks, trails, and free spaces which run across the main geological features (like Wonji Faults, Rift axis, etc.) to acquire meaningful data. However, base station data was collected at a point which is free from any cultural noises for about six hours to understand the trend of the diurnal variation of the field in the study area to select survey times and apply correction. 214262 corrected ground total magnetic intensity data points are used to compile this thesis. Figure 22 shows survey data coverage of both methods.

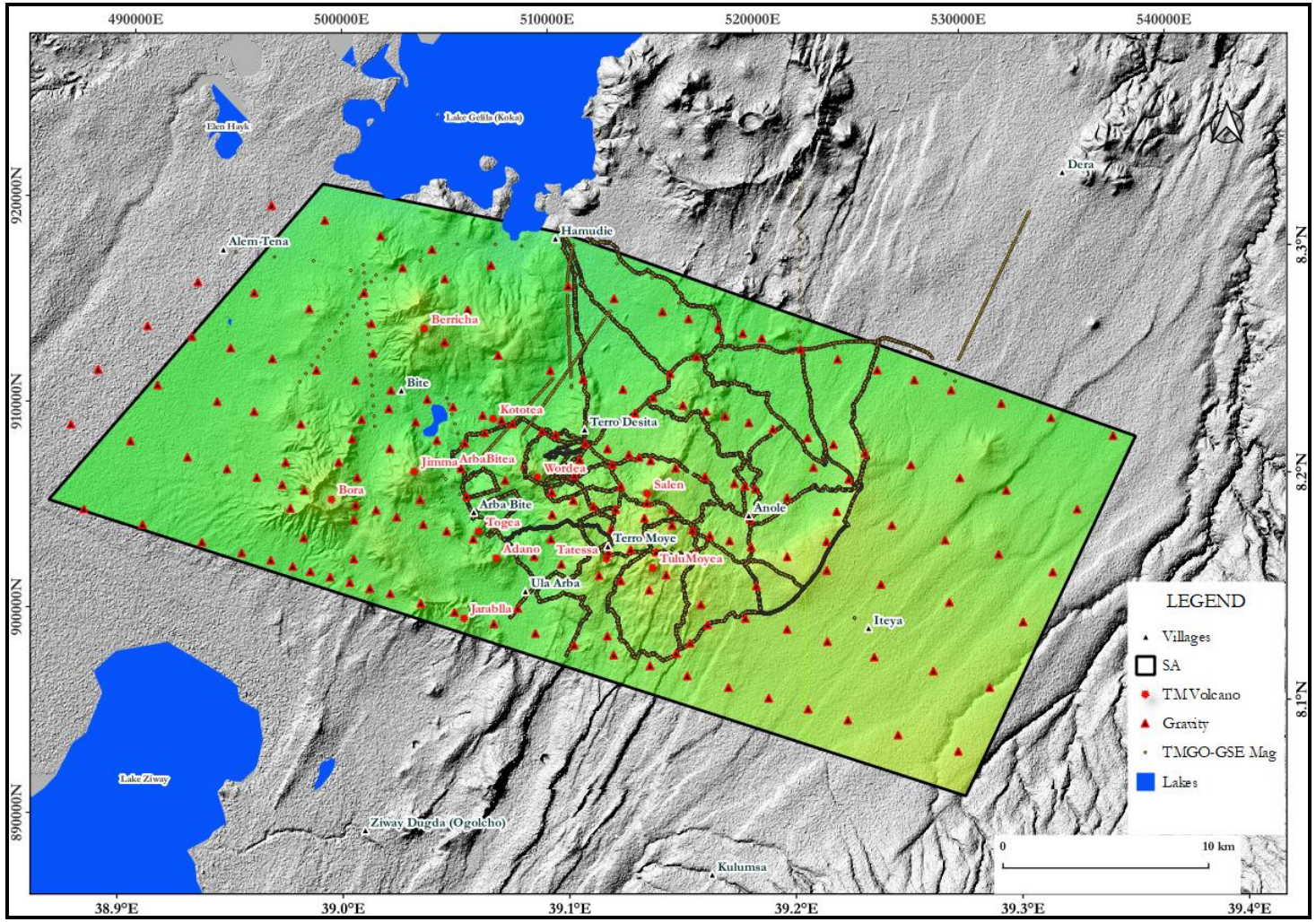

Figure 22. Gravity and magnetic data coverage map.

4.3. Data reduction

4.3.1. Gravity

Gravity data, once relative readings are changed to absolute gravity values, reduction encompasses Latitude, Free air, Bouguer Slab, and Terrain corrections to remove/ avoid all fictitious anomaly sources. The researcher underwent all data reduction using the absolute gravity value. In the reduction process Oasis montaj (Version 6.42.) was used to reduce the absolute gravity values to complete Bouguer Anomaly.

4.3.2. Magnetics

It is a standard practice that magnetic data doesn't show fictitious anomaly due to topographies undulations or masses excess/ deficit under them. So, correction related to such irregularities need not be applied to the raw data. However, diurnal correction needs to be applied and was applied to the raw data to eliminate variations caused on the total magnetic field only because of reading time difference (Figure 23). A base station whose location is within the survey area was selected which is quiet and free from any cultural noises to carry out survey on the diurnal variation of magnetic field in the survey area. Reading started at 9:30AM which lasted until 3:55Pm for a total time of 6hours and 25 minutes. Figure 23 shows a linearly decreasing trend in the total magnetic field variation in the survey with increasing time. This implies it is possible to undergo total magnetic field survey in the mentioned duration time and undergo diurnal correction using straight line equation.

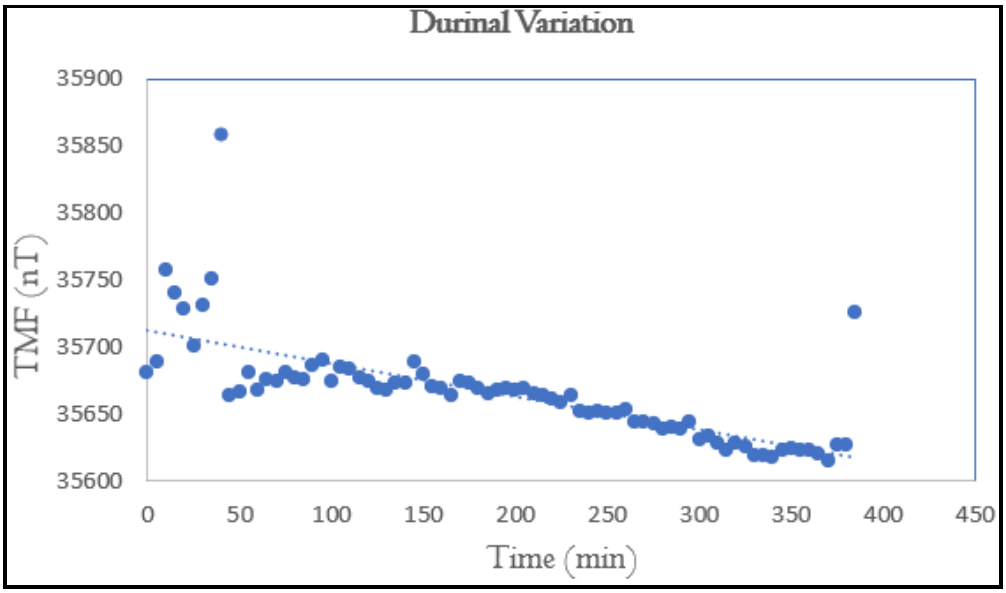

Figure 23. Diurnal variation of total magnetic field in the survey area.

4.4. 2D Data Processing / Analysis

Since the study used two potential field data: magnetics and gravity the processing encompasses both independently in the 2D processing step and together in the 3D joint inversion processes.

4.3.1. 2D Data processing

Data processing in 2D proceeded by checking data quality followed by changing discreet data to continuous surfaces. The data quality of both data sets was checked using geospatial auto-correlation method bearing in mind that data spatially close to each other have to show similarity (Figure 24 a and b). The figure shows variogram and sample pairs as a function of distance. The total magnetic data variogram (Figure 24a) indicates,

i. Nugget = 0 which indicates low, or no noise is included in the data as a result of measurement or operator problem,
ii. Sill = 129091 where the variogram starts flattening which is the beginning of low auto-spatial correlation, and
iii. Range = 8397m which shows the distance to which data/ sample pairs are auto-spatially correlated

Whereas the gravity variogram (Figure 24b) indicates,

i. Nugget = 0 which indicates low, or no noise is included in the data as a result of measurement or operator problem,
ii. Sill = 4348 where the variogram starts flattening which is the beginning of low auto-spatial correlation, and
iii. Range = 39316m which shows the distance to which data/ sample pairs are auto-spatially correlated

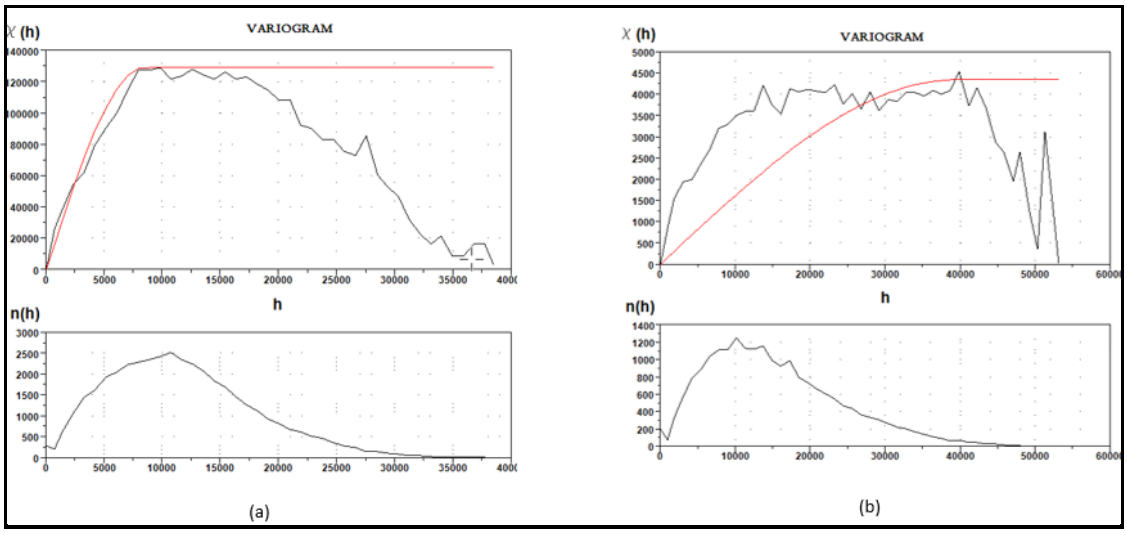

Figure 24. Variogram of (a) magnetic and (b) gravity data.

4.3.1.1. Magnetics

The discreet data is grided to a 2D grid map using a statistical interpolation method called kriging to change it to continuous surface so that various kinds of filtering and enhancement, in addition to derivatives anomaly maps production, can easily be applied to it. Therefore, the IGRF corrected magnetics discreet data is interpolated, and a total magnetic field anomaly map is obtained. A filtering known as curve fitting, which is the process of generating a curve, or mathematical function, that has the best match to a set of data points, is performed to separate the regional and residual anomalies and to isolate the effect of deep and shallow magnetic anomaly sources. As a 2D map the residual component is used here for subjective interpretation of anomalies due to sources that exist underlying the magnetic anomaly signatures.

Along with magnetic anomaly, typical models (Figure 25) are presented how a magnetic anomaly due to a magnetized body with identical magnetic property looks like at different locations/ magnetic inclinations on earth. The models help in the interpretation of magnetic data in this study. As can be seen from the model, the magnetic anomalies from a magnetized body placed at the pole and equator are exactly opposite to each other. That is when a magnetized body is placed at the pole, its effect is reflected by high anomaly and when the same body is placed at the equator, its effect is shown by low anomaly. The geo-magnetic inclination at pole and equator are 90^0 and 0^0 respectively. At north magnetic latitude, where geo-magnetic inclination is 45^0, the magnetic anomaly due to the same magnetized anomaly is a bit complicated and the anomaly appears as if it were from two bodies with negative and positive anomalies. So, to avoid such complications when surveys are done in the magnetic latitude, it is advisable to apply various reductions like reduction to the pole, analytic signal, reduction to the equator, etc. to avoid ambiguity.

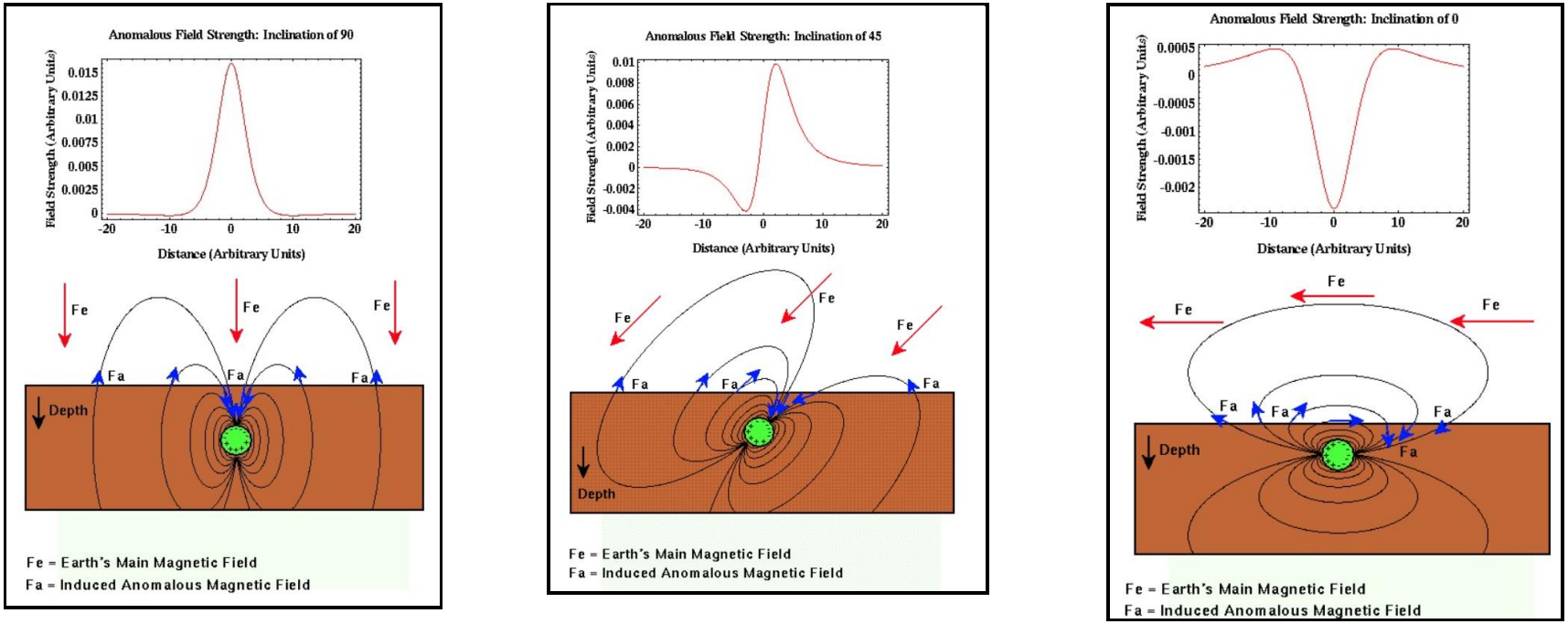

Figure 25. Magnetic anomaly patterns at three latitudes.

Obtained from
https://pburnley.faculty.unlv.edu/GEOL452_652/.

4.3.1.2. Gravity

The gravity data which is reduced to complete Bouguer Anomaly is used to produce 2D bouguer gravity anomaly. A statistical interpolation method called kriging was applied to change the discrete data into continuous surface so that various enhancement and filtering applied to get derivatives of the complete Bouguer Anomaly. The first step taken in this study to the Bouguer Anomaly is separating it into its regional and residual components. This filtering is useful to distinguish effects of deep and shallow gravity anomaly sources.

4.5. Data presentation and analysis

4.5.1. Magnetics

The residual magnetic anomaly which is considered for this study to reveal the effect of subsurface or shallow sources is presented in 2D is shown in figure 27. The anomaly map is produced by separating the regional and residual components from the total magnetic anomaly (figure 26) using curve fitting method which is the process of constructing a curve, or mathematical function, that has the optimum fit to a series of data points. Both total magnetic anomaly and residual magnetic anomaly appear to have similar anomaly trends. However, anomaly signature, both high and low, strengths are higher in the residual than the total magnetic anomaly. This may be interpreted as shallow anomaly sources dominate the survey area with respect to magnetic anomaly signature. Other anomaly maps like analytic signal map (Figure 28), horizontal derivatives in the X and Y directions (Figure 29 and Figure 30 respectively), horizontal derivative (165^0) anomaly (figure 31) and tilt derivative anomaly maps (figure 32) are also presented.

The analytic signal map is meant to put anomaly signatures over their sources since it avoids the dipolar nature of the magnetic field. The X and Y derivatives are useful in enhancing anomaly sources which are aligned in NS, EW and close to these directions respectively. It is possible to observe that the WFB is aligned with high negative gradients. However, the horizontal derivative (165^0) map shows the general trends of magnetic gradients in the survey area. According to horizontal derivative (165^0) map the high gradients generally have NE-SW trends basically aligned with the WFB, high positive gradient in the direction NW-SE observed north of Salen and most of the altered grounds and microseisms are delineated by high positive gradients.

The tilt derivative indicates positive values over magnetic sources, negative away from sources and zero over contacts. Miller and Singh (1994) computed a tilt-angle derivative in which the angle equals the ratio of the

first vertical to total horizontal magnetic gradient. Most of the microseisms and altered ground coincide with high tilt anomalies, Gnaro, the obsidian dome, in the area is dominantly delineated by negative anomalies. The general trends of the positive anomalies are NW-SE, EW, and NE-SW which are typical directions of structures in the area.

The residual anomaly map (Figure 27) delineates high, medium, and low magnetic anomaly signatures. The study area is situated in low magnetic latitudes and surface anomaly features basically show opposite subsurface condition in relation to susceptibility values. That is high magnetic anomalies basically indicate rock strata with low magnetic susceptibilities underlying it and vice versa. So, the possibility of the presence of rocks which are demagnetized underlying high anomalies is inevitable. It is a universal truth that rocks do lose their magnetic nature when heated up to curie temperature. The highest anomaly signature is found close to the central part of the study area which has WNW-ESE orientation. And this anomaly signature is bounded with caldera rims. It mainly indicates the presence of heat source underlying this anomaly signature.

The well-known geological feature, dominantly covered by obsidian flow in the study area, which is indicated by a blackline polygon in the map is delineated by medium to low magnetic anomalies which probably indicate that the area is underlain by rock strata with relatively high to medium magnetic susceptibility. The obsidian dome has been the core area for exploration and exploitation of the geothermal BH drilling site in the Tulu Moye Geothermal Project.

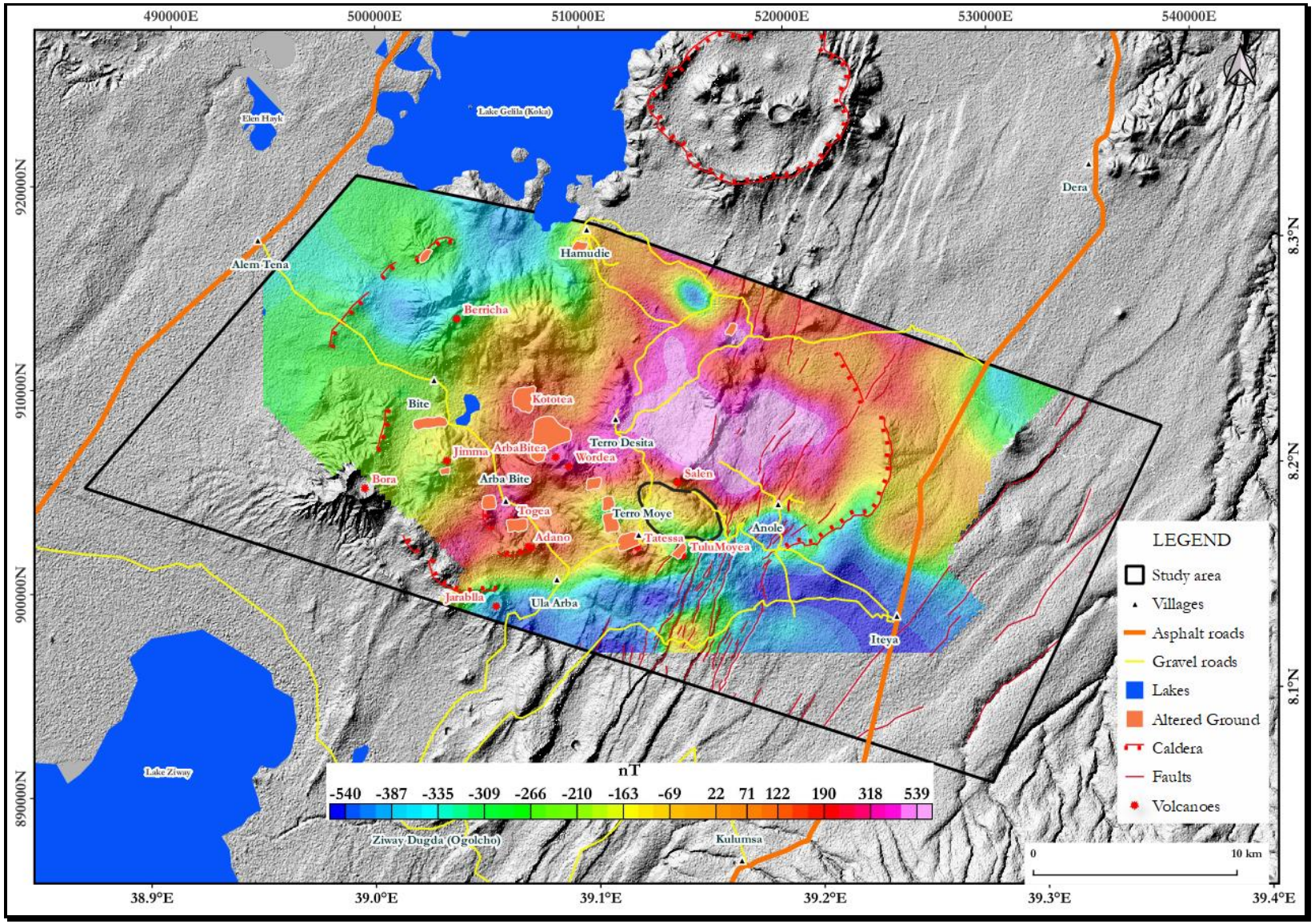

Figure 26. Total magnetic anomaly map

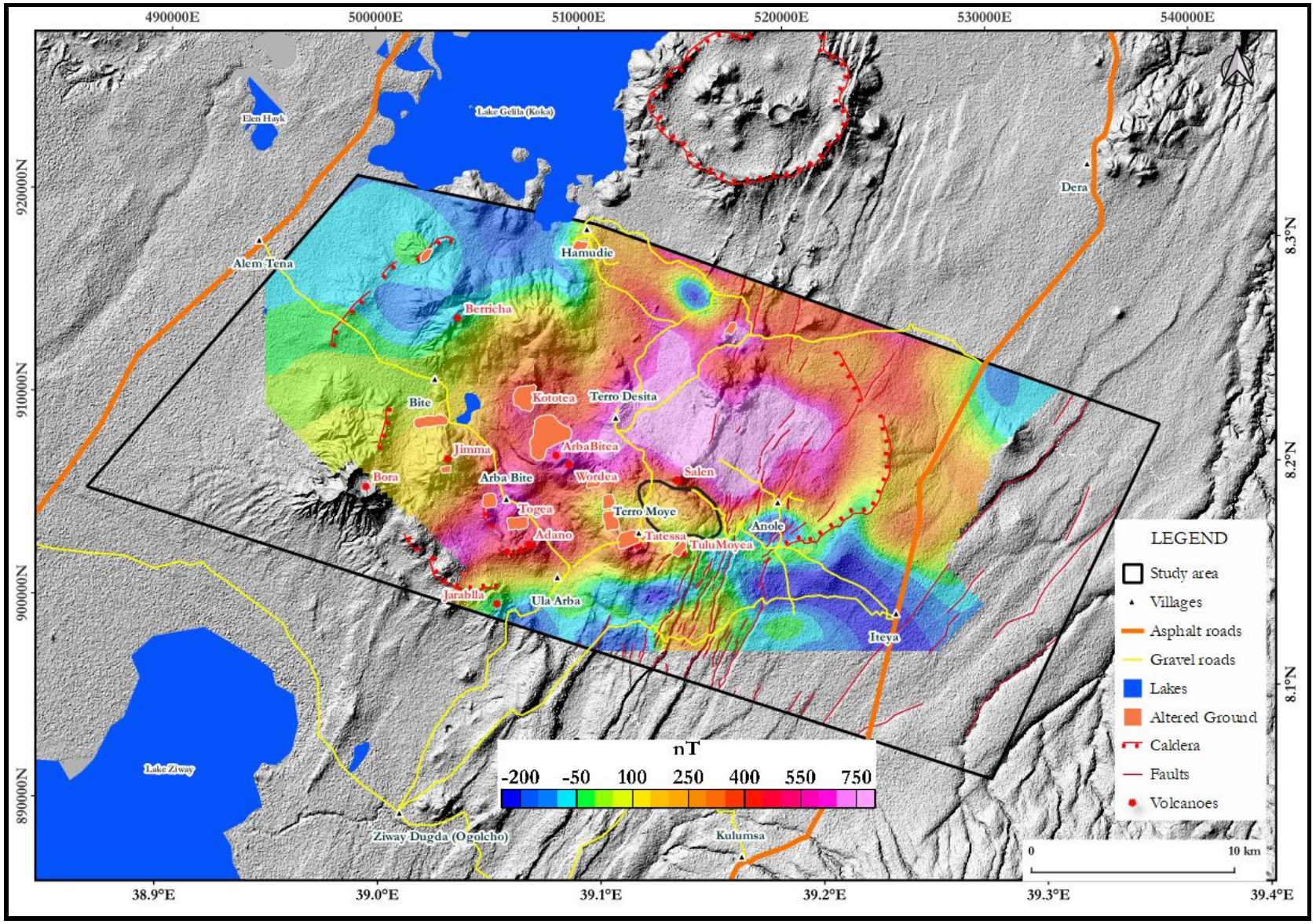

Figure 27. Residual magnetic anomaly map

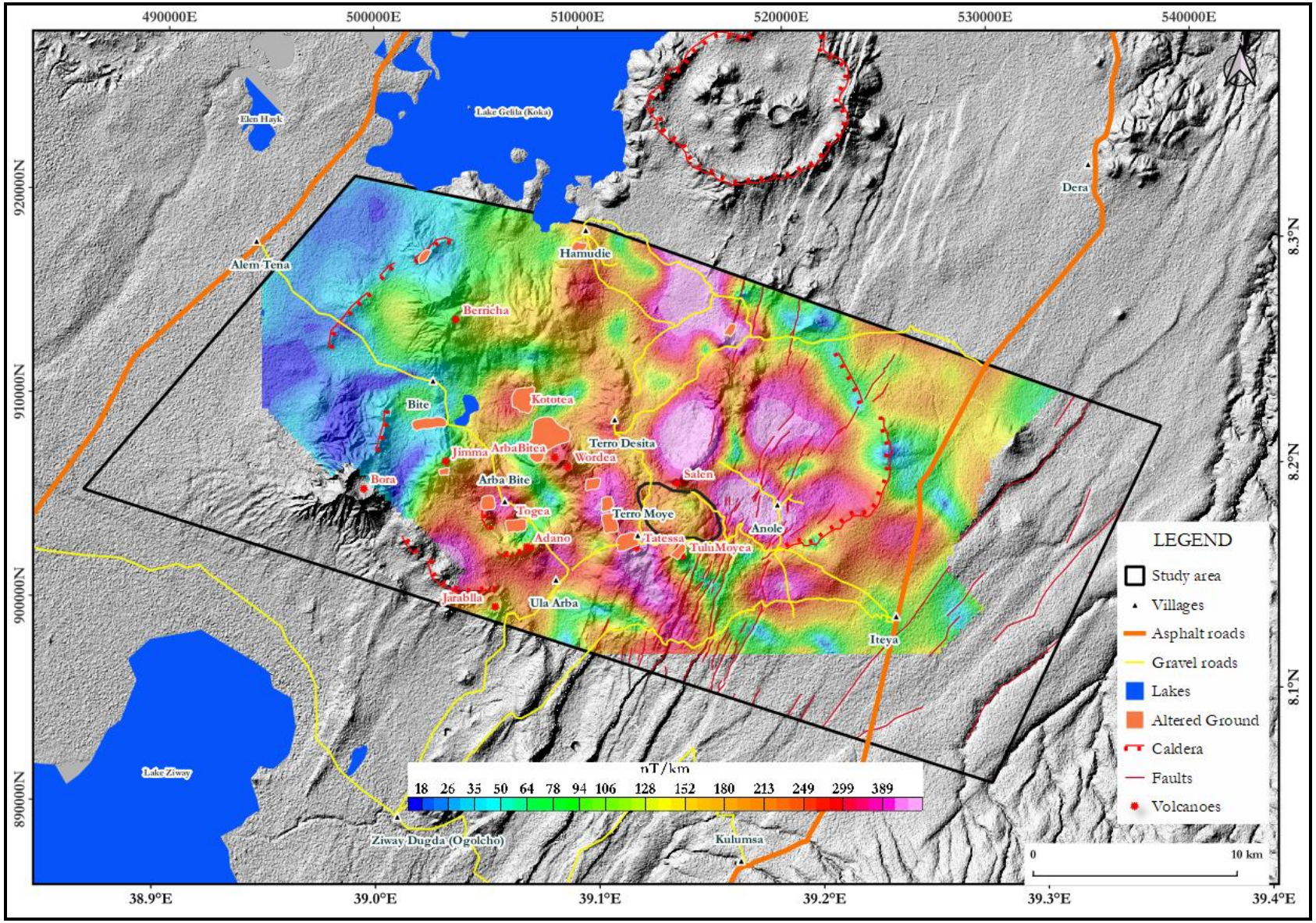

Figure 28. Analytic signal magnetic map

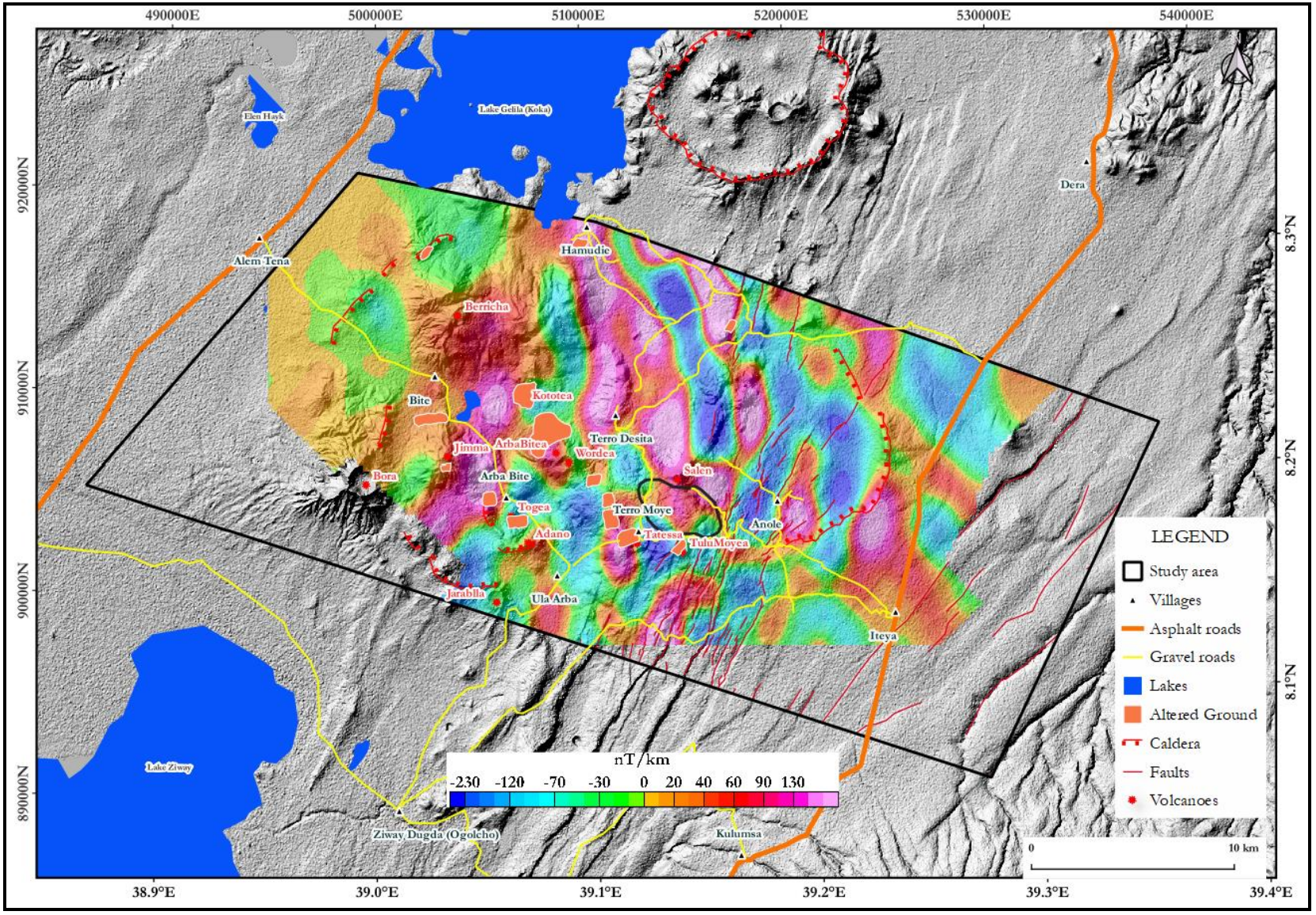

Figure 29. Horizontal derivative (dx) magnetic map.

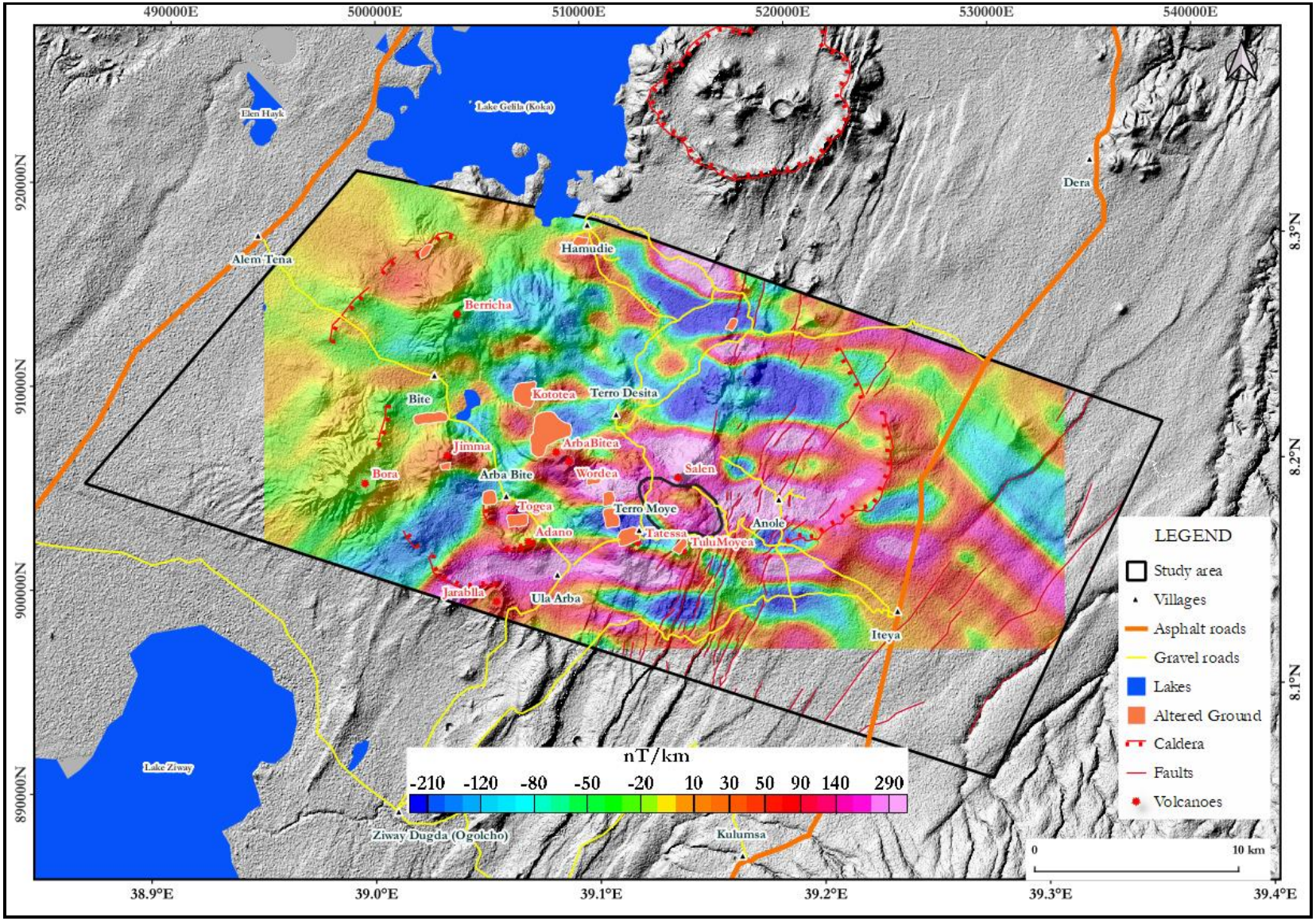

Figure 30. Horizontal derivative (dy) magnetic map

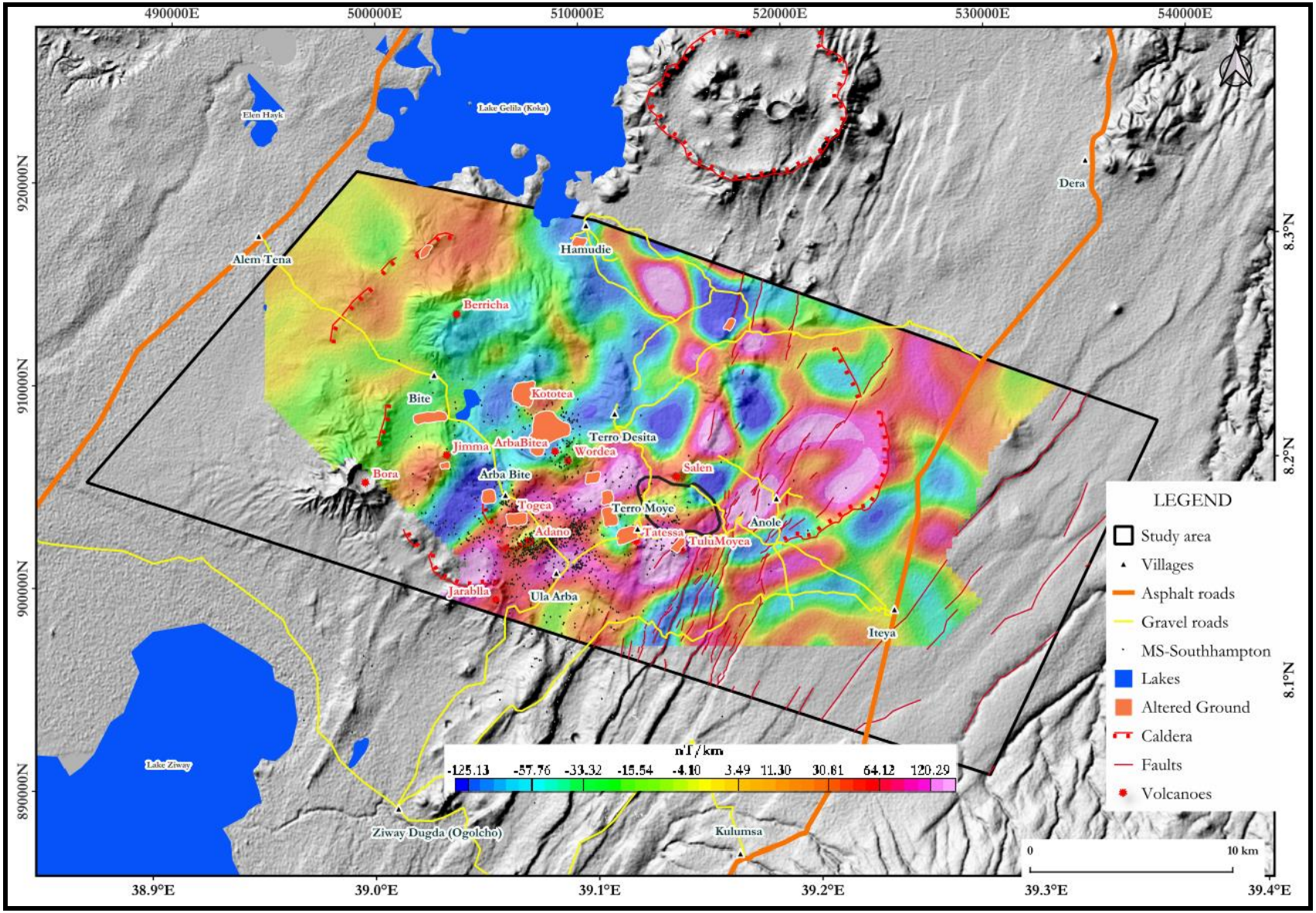

Figure 31. Horizontal derivative (165^0) magnetic map

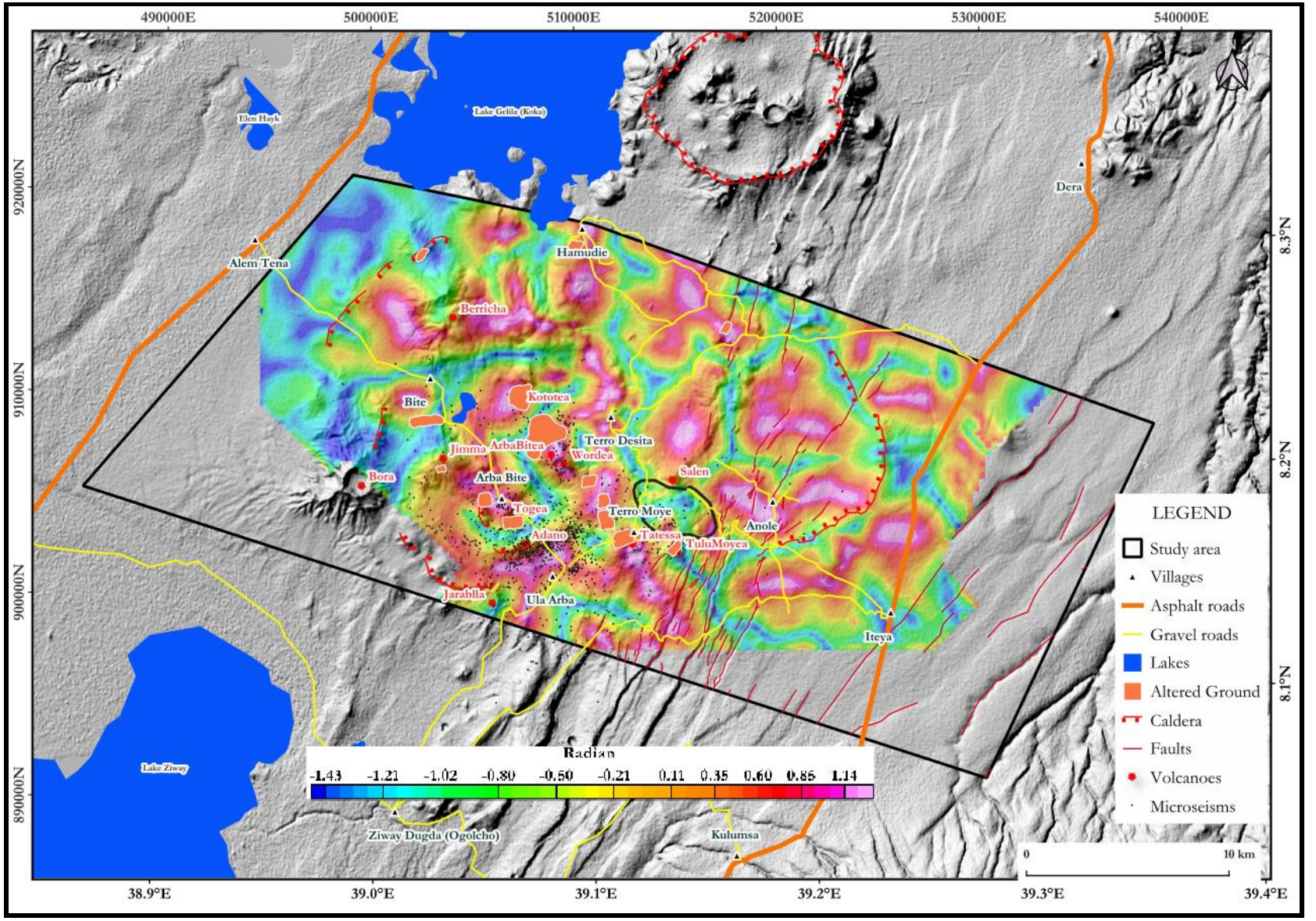

Figure 32. Tilt derivative magnetic map

4.5.2. Gravity

The residual gravity anomaly map compiled for the study area is shown in Figure 34. The map represents the residual Bouguer Anomaly which is produced by separating the residual from the regional using curve fitting method from the complete Bouguer anomaly map (figure 33). Along with the residual Bouguer Anomaly map horizontal derivatives in the x and y directions (Figure 35 and Figure 36 respectively), horizontal derivative (45^0) anomaly map and tilt derivative maps (figure 37) are presented here. Ther horizontal derivative (dX and dY) anomaly maps are useful in enhancing gravity anomaly signatures which have NS and EW general orientations. However, horizontal derivative (45^0) anomaly map shows general trends of gradients which could be related to density variation where crustal discontinuity or faults occur or exist. Based on this anomaly map high positive and negative anomalies assume WNW-ESE general orientation but in the SW extreme end of the survey area where the high gradient aligned in the NNW-SSE direction.

The tilt angle derivative map shows the presence of high-density sources which generally assume WNW-ESE orientations. Most of the microseisms and all of the altered grounds coincide with high tilt anomaly. However, north of Ulaarba village the microseisms are dense and located where the tilt anomaly is close to zero which is contact between the positive and negative tilt values. Miller and Singh (1994) used tilt angle to identify the limits of the source body. The positive contours of the tilt angle define the source, while negative contours represent the outside and zero contours reflect the source's vertical boundary.

It is possible to observe from the residual map (Figure 34) there are high residual anomalies extending from east to west. The anomalies orientation is nearly WNW-ESE. All the volcanoes mapped in the study are overlain by high residual anomalies but pronounced over areas where Bora, Berriccha and Salen are located. This probably indicates the presence of magmatic updomings beneath these volcanoes and the coming up of possible heat sources towards shallow depths. There is also an extended high residual gravity anomaly starting from Gnaro (the well-known obsidian Dome-black line polygon in Figure 34 towards the west. This could also be related to the presence of high-density units at shallow depths. It is notable though that the magnetic anomaly over this obsidian dome is not so high as it should be if the high density indicates possible heat source. The probable cause for low magnetic anomaly could be the effect of ground water in cooling the rocks beneath since Wonji Fault Belt is a likely a lateral and vertical conduit for ground water. The black dots represent hypocenters for microseisms. The microseisms are probably triggered by the upwelling and placement of magmatic units (higher density units) to shallower depths and putting the brittle crust in stress

and force it to rapture. On the other hand, as can be seen from the residual bouguer and magnetic anomaly maps there are altered ground (white polygons in Figure 34) which are aligned in NW to SE directions overlain by high anomalies. The altered zones are indications of geothermal fluids' effects in totally changing the nature of the geologic units used to cover the areas. This in turn indicates the fluid got passage to pass through which is an indication for the presence of permeable layers beneath. In addition to that microseisms can be initiated by hot fluid movement in regions at different hotness states. Consequently, the microseisms hypocenters are indicators of better permeabilities in that zone as well.

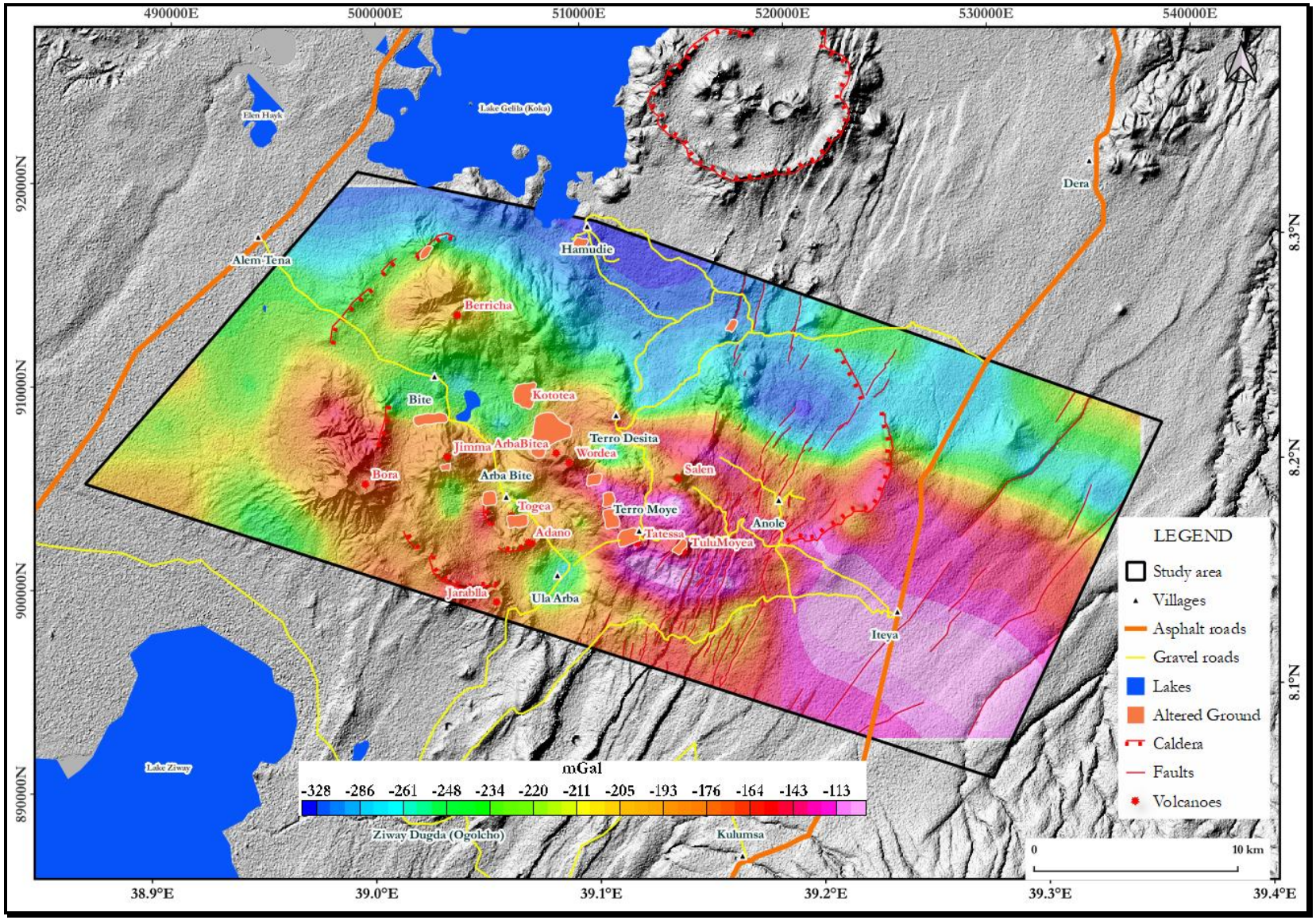

Figure 33. Complete Bouguer anomaly map

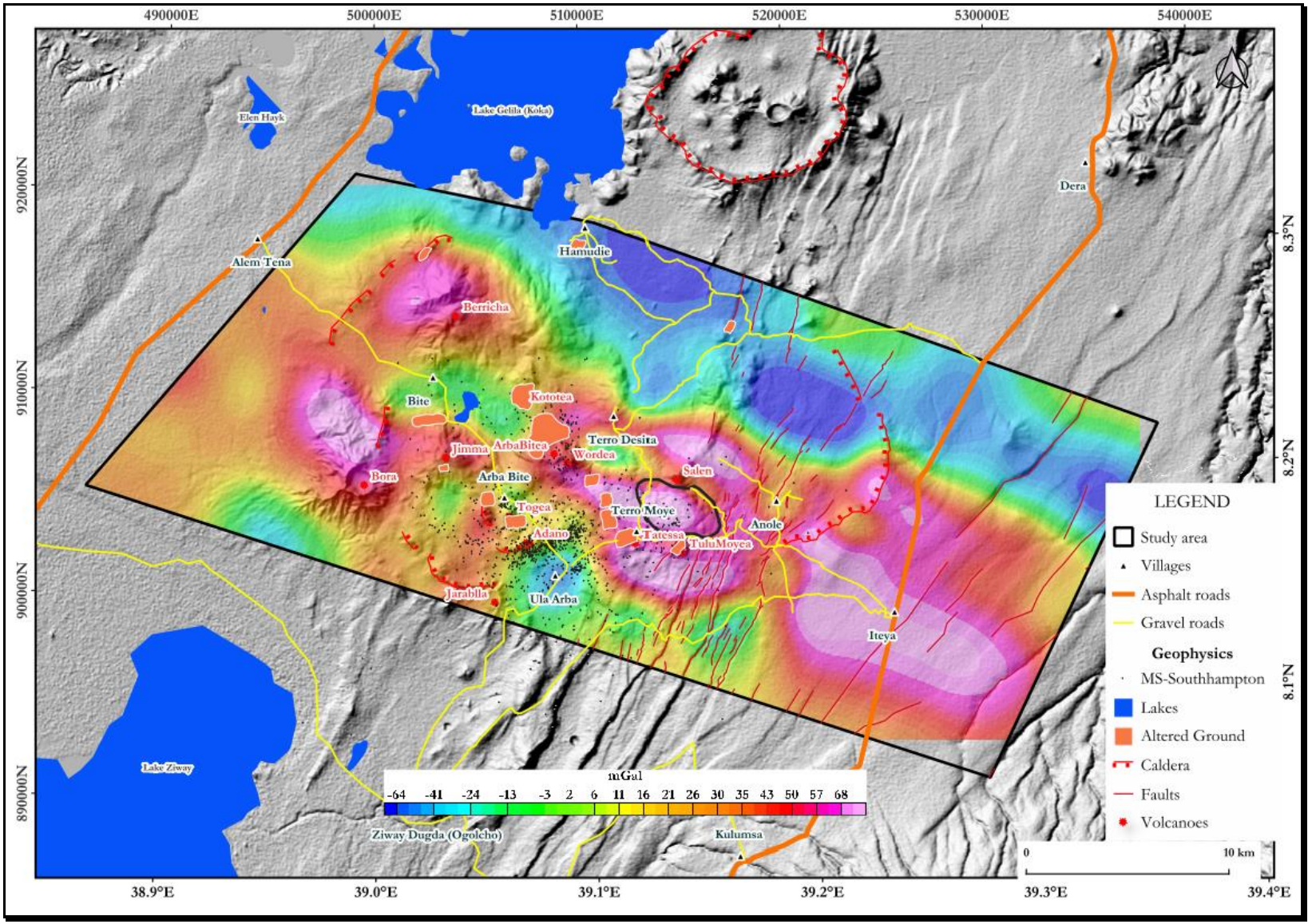

Figure 34. Residual Bouguer Anomaly map

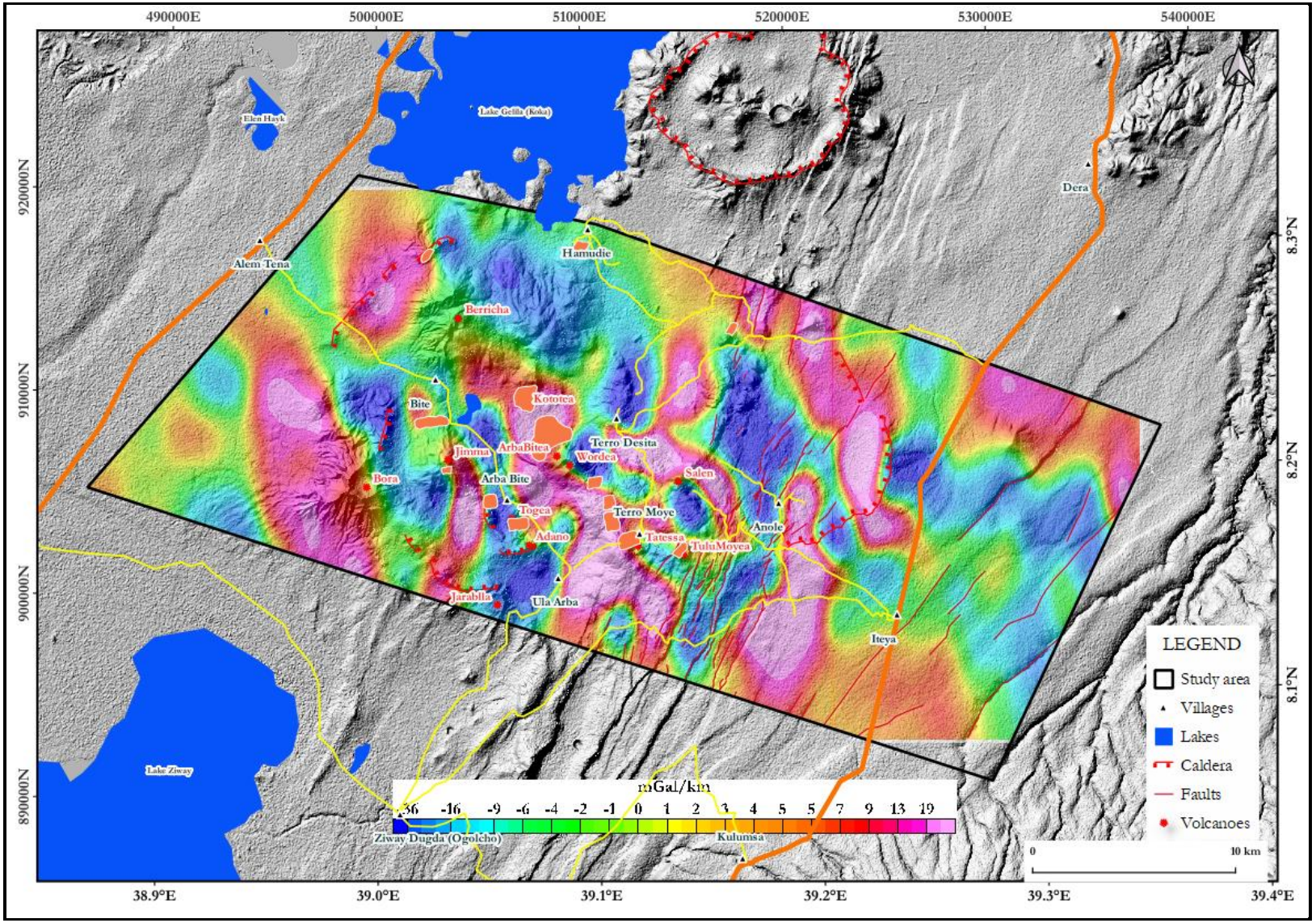

Figure 35. Horizontal derivative (dx) gravity map.

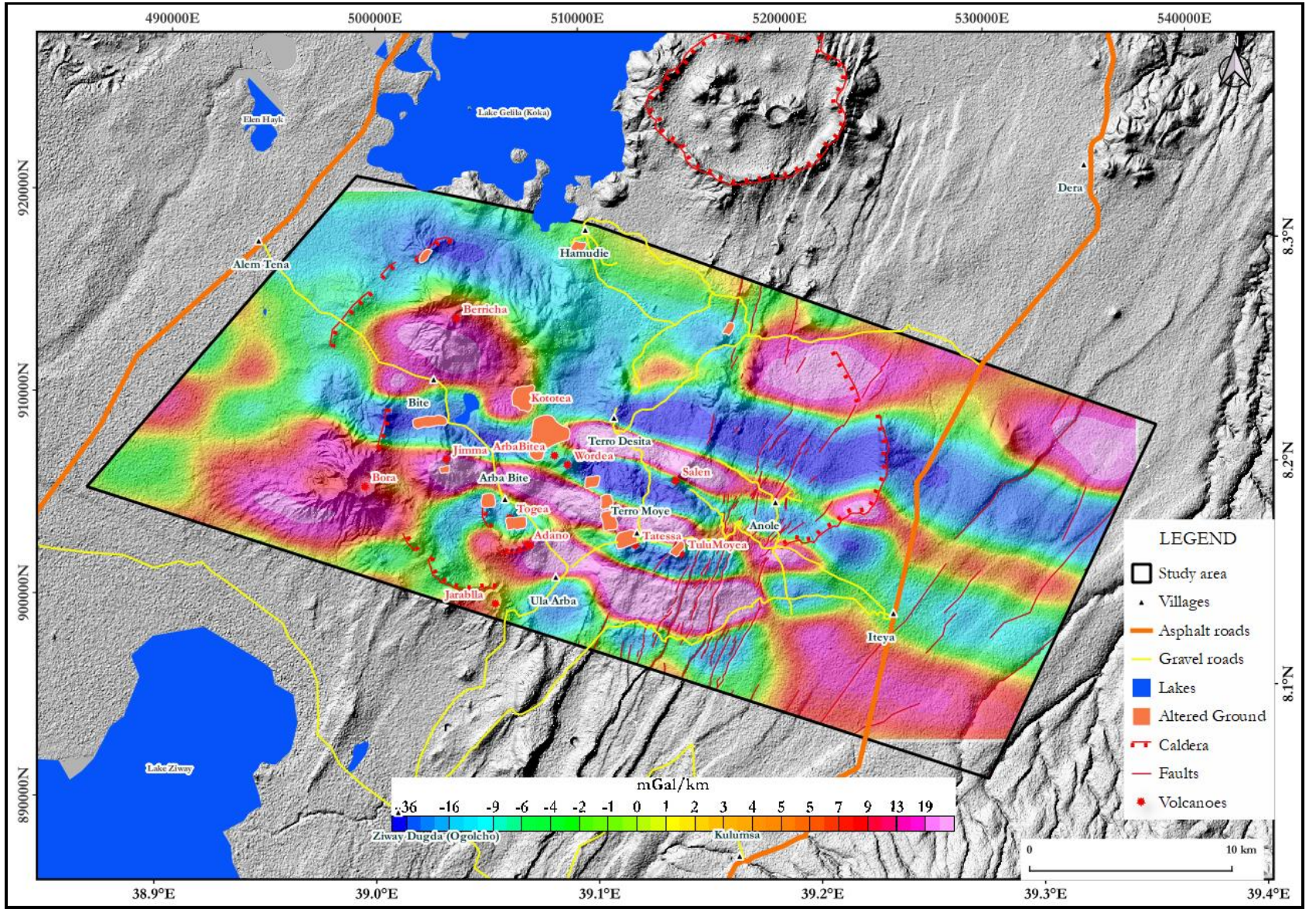

Figure 36. Horizontal derivative (dy) gravity map

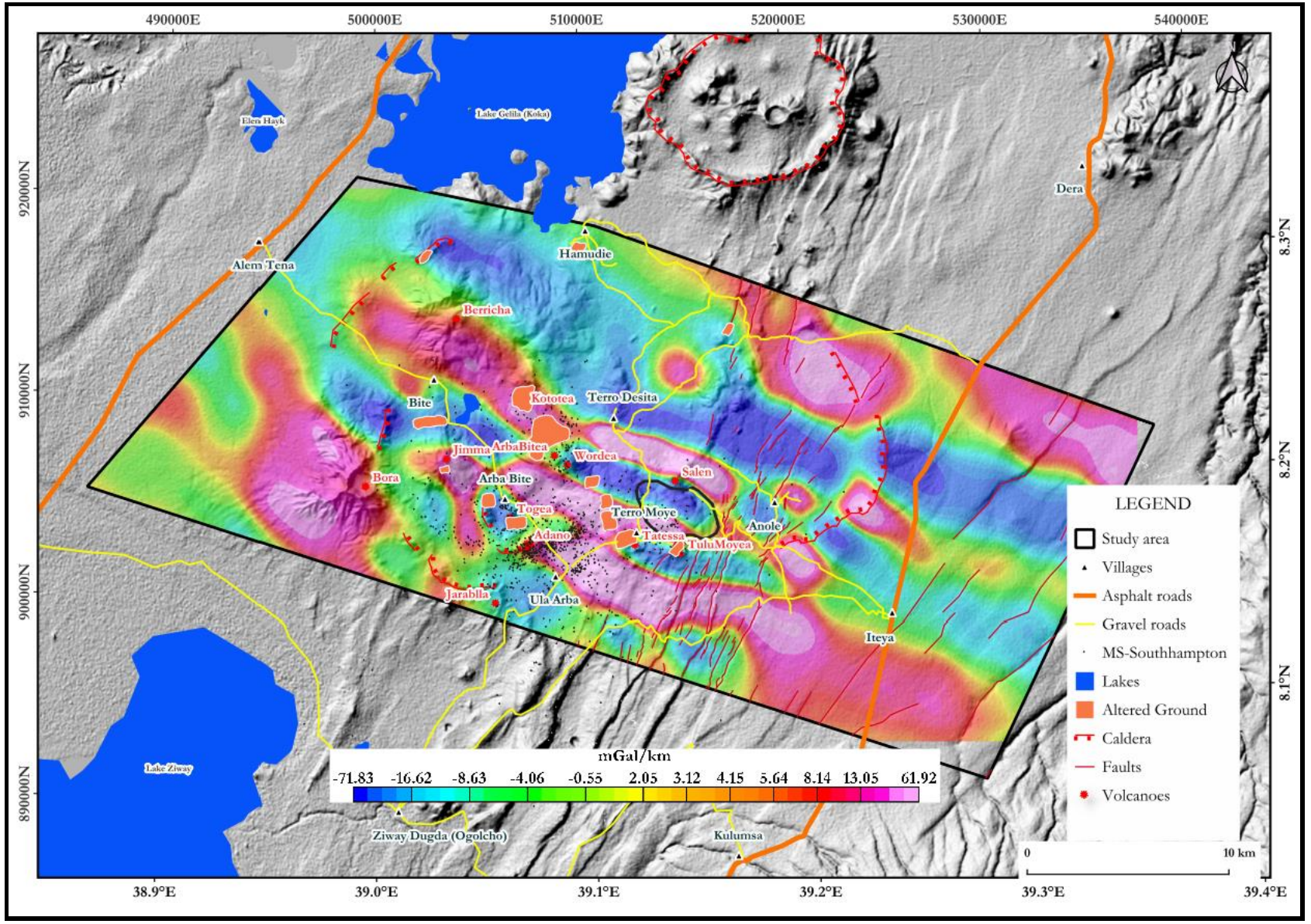

Figure 37. Horizontal derivative (45^0) gravity map

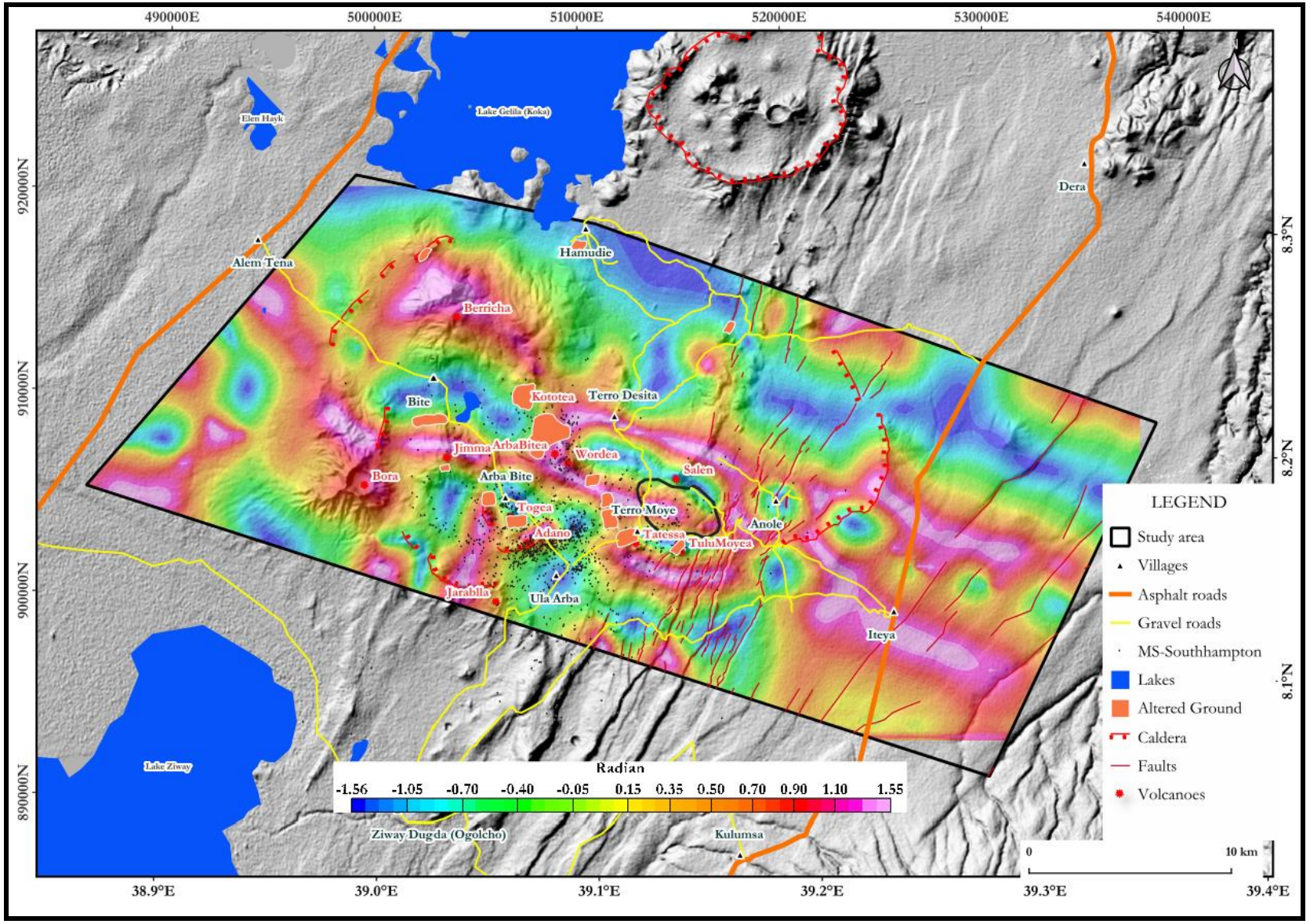

Figure 38. Tilt derivative gravity map

4.6. 3D Data processing

Geophysical inverse problems are commonly regularized to account for noise in the data and the mixed determined nature of most inverse problems. Moreover, non-uniqueness is a challenge in inversion due to limited data, leading to undetermined formulations. To address this issue, external constraints like a priori geologic information, smoothing, stochastic regularization, or inversion for a specific model type are typically introduced. While tomograms from a single geophysical data type can enhance various models, ambiguity may still persist.

A different method to decrease model ambiguity involves conducting joint inversion of multiple types of collocated geophysical data. This process generates a unified model that combines the information from each individual data set. Currently, the joint inversion of various geophysical and hydrological data types is becoming a prominent and effective approach for integrating quantitative data. The underlying principle of joint inversion strategies is the assumption that the reconstructed parameters are affected by a shared subsurface physical and/or hydrological property field (Infante et. al., 2010).

Vozoff and Jupp (1975) were the pioneers in introducing the concept of utilizing multiple geophysical datasets for geophysical inversion. The integration of data from various geophysical methods can be achieved through three primary approaches: i) conducting a joint interpretation by separately inverting different datasets, ii) performing a joint inversion of separate datasets to obtain a unified inversion parameter model, and iii) implementing coupled inversion, where distinct datasets mutually constrain each other based on a specific correlation equation or model (Doetsch et. al., 2012).

Joint inversions have gained significant popularity in the field of geophysics as a valuable tool for exploring subsurface models that align with data collected through various geophysical methods (Moorkamp et. al., 2016). By integrating datasets with distinct sensitivity and resolution characteristics within a unified framework, joint inversions effectively address challenges associated with inversion, such as limited resolution and non-uniqueness. The models derived from joint inversion inherently exhibit consistency across multiple data types, thereby enhancing interpretation, classification, and the establishment of petrophysical relationships (Jordi et. al., 2020).

The data processing in 3D is carried out using a software, which is being developed, called GRAVMAGINV3D (GMI3D) (www.gravmaginv.ru/en. Version 2024.03.01). Th processing is basically

joint inversion of ground gravity and magnetic data. Both the gravity and magnetic 2D grids were re-grided to give them the same lateral dimensions so the 3D joint inversion algorithm performs the task smoothly.

Initially ideal and nearly rectangular models were produced for both the ground gravity and magnetics data. These models were divided into infinitesimal density and susceptibility units of rectangular prisms which amount to non-masked cells of 368,098. However, calculations are set to be conducted taking into consideration the topography of the study area. During the process, 18,914 cells are found above the topography and only 349,184 are found to be valid cells for the joint inversion.

Following the creation of the 3D ideal rectangular models, forward calculations proceeded for both models. However, the initial gravity model is given a background density value 2.67 g/cm since this value is used in the gravity bouguer reduction and terrain effect calculations. Next to the forward calculations joint inversion applied to both gravity and magnetic anomalies. The process is applied simultaneously checking the susceptibility with the density calculated and vice versa. Figure 33 shows a 3D susceptibility anomaly model together with a 2D observed and calculated magnetic anomalies. This 3D model is obtained after jointly inverted with gravity data where a 3D density model (Figure 35) is generated concurrently. The observed and calculated 2D gravity anomaly maps are shown with the 3D model.

4.7. 3D model presentation

3D models of density and susceptibility fields were produced using joint inversion method. So, independent models of both density and susceptibility models are presented in this study. The presentation / analysis is commenced after observing and convinced by the similarity / fitting error between the observed and calculated anomalies.

4.7.1. 3D susceptibility model

The 3D susceptibility model (Figure 33) is obtained after joint inversion with gravity anomaly. The model shows sectors of high, medium, and low anomalies on the top surface (EW and NS direction) and with depth along the 3 visible faces of the model. On the top surface of the model, it is possible to see the presence of alternating relatively high and low values with an NEN-SWS general trend. The four numbers (1,2,3, and 4) labeled on the model represent Berriccha, Bora, Jarablla, and Tulu Moye Volcanoes. All the volcanoes correspond with low susceptibility values. These results show indications for the occurrence of magmatic

updomings beneath all the volcanos (Berriccha, Bora, Jarablla, and Tulu Moye). Therefore, it could be possible to deduce that the rocks beneath these volcanoes are heated by the magmatic bodies, which come to shallower depth, and lose their magnetic nature due to heat treatment indicating the presence of heat source which is one of the components of a geothermal reservoir. This basically occurs when rocks are heated to Curie's Temperature which is close to 280^{0}C.

However, it is necessary to cut out 2D slices from the compiled 3D model in order to see the detail of its interior high and/or low susceptibility values and relate their signatures with geothermal resource components (heat source, cap rock, etc.). Figure 34 shows three 2D slices cut out along profiles indicated on the observed and calculated 2D magnetic anomalies maps. The slices are presented together with the mapped hypocenters of microseisms. These slices indicate low susceptibility values aligned along the NEN-SWS directions with their breadth attenuating towards the SWS direction. However, microseisms occur being associated with the low susceptibility values and rife in the southwestern part of the study area.

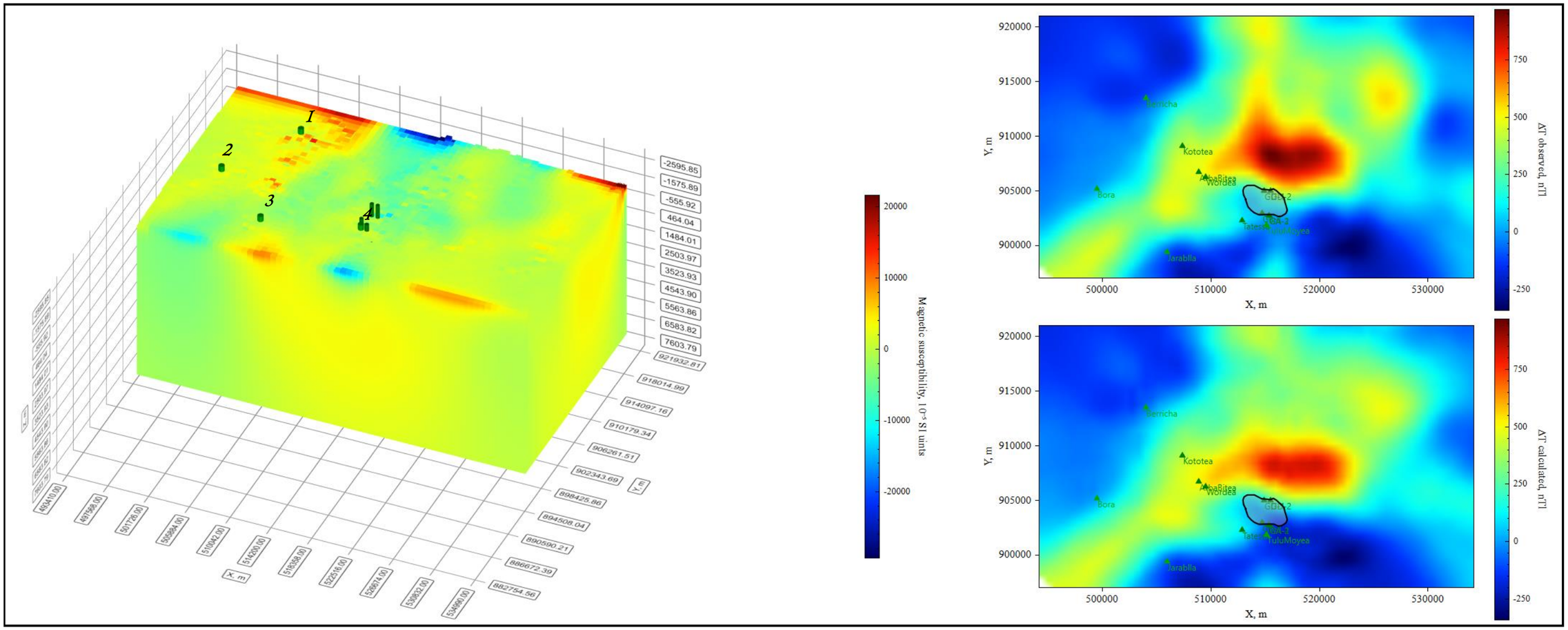

Figure 39. 3D Magnetic susceptibility anomaly model

(The four Red Picks 1-Bericcha, 2-Bora, 3-Jarablla, 4. Tulu Moye Volcanoes)

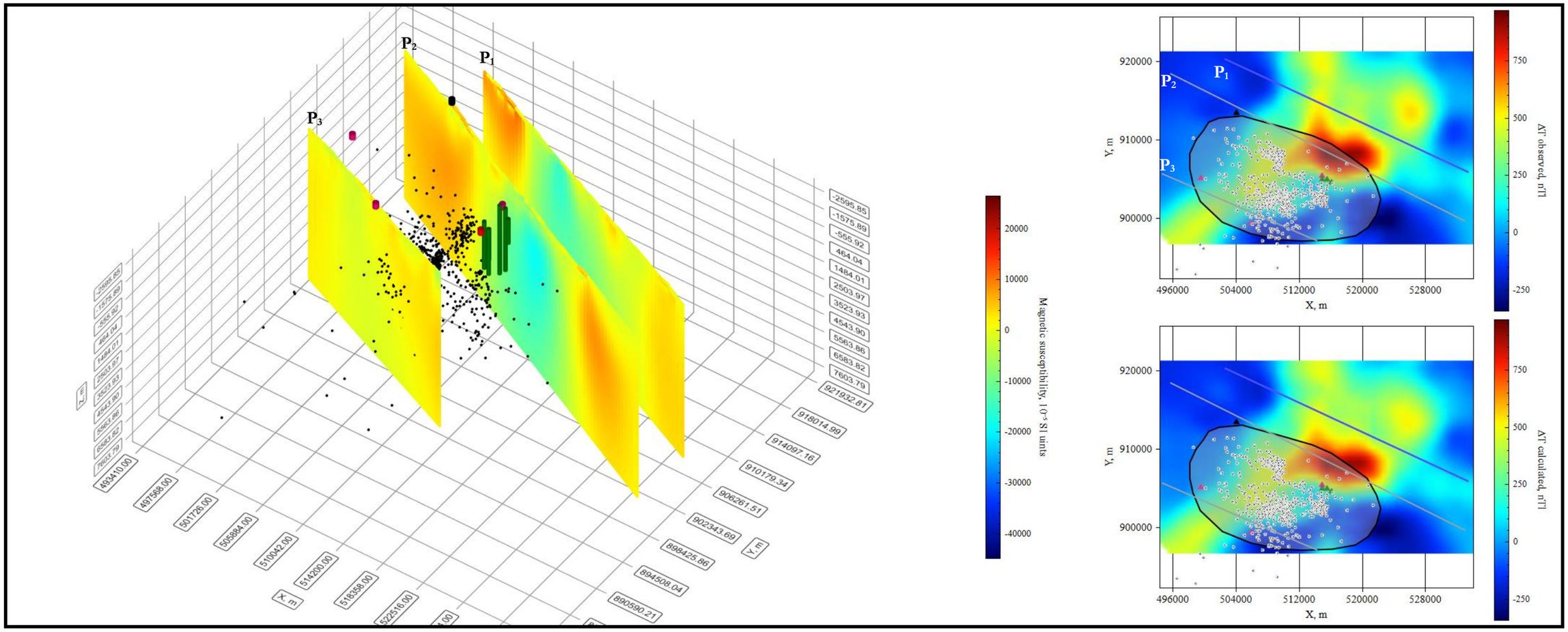

Figure 40. 2D Magnetic susceptibility slices cut out of the 3D magnetization model.

4.7.2. 3D density model

The 3D density model (Figure 35) is obtained after the joint inversion of the gravity anomaly with the magnetic anomaly. In this model, density values which range from low to high are observed. On the top surface of the model alternating strips of high and density values are observed dominantly oriented in the WNW-ESE direction. Relatively high- and low-density values are observed occurring beneath the four volcanoes indicated on the model by numbers (1, 2, 3, 4). The volcanoes occur over higher density values which indicate the presence of denser unit beneath each of them. As indicated in the aforementioned section it can be related to magmatic bodies placed at shallower depths. There is a prominent high-density body which extends from Tulu Moye to Bora Volcanoes which probably indicates the placement of high-density unit along this corridor and seismic clusters are also rife along and close by it.

2D density slices are also cutout of this model and presented along hypocenters of microseisms in Figure 36. The slices together with the microseisms show occurrence of a low-density zone where the seismic events are abundant. This is thought to indicates the presence of a fractured zone within the `study area. In addition to that the coincidence of the seismic events with low gravity indicate the stress imparted by the elongated magmatic body between Tulu Moye and Bora and in turn initiated microseismical events. This could be responsible for micro fracturing taking place within that area. So, it is possible to conclude that there is porosity/permeability within this section of the model. This could be taken as proof for the presence of another component of a geothermal system in the study area.

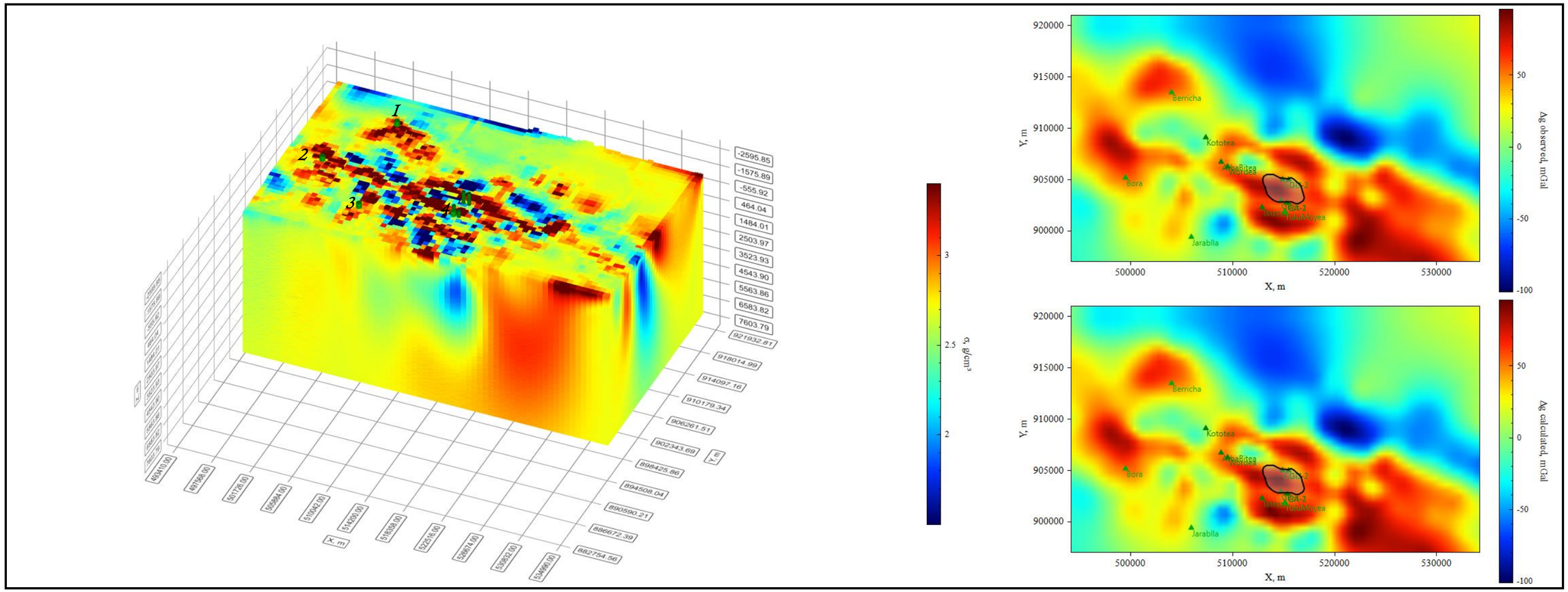

Figure 41. 3D Density anomaly model

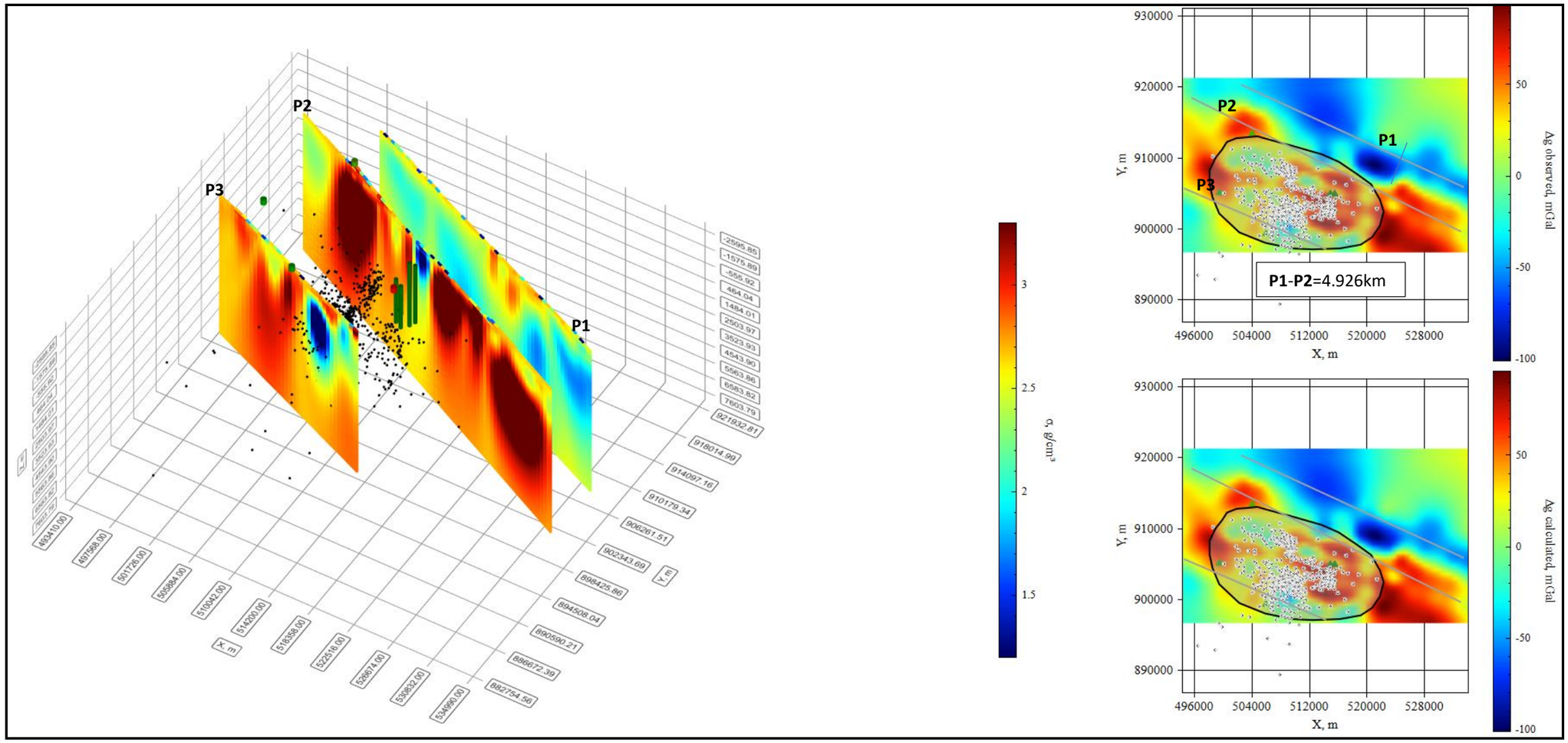

Figure 42. 2D Density anomaly slices cut out of the 3D density model.

CHAPTER 5

5.I. Interpretation and Analysis

5.I.I. Qualitative

The 2D gravity (Figure 30, 31, 32), magnetic field anomalies (Figure 26, 27, 28, 29) and the 3D density and susceptibility anomaly maps and models (Figure 33, 34, 35, 36) do show the probable presence of heat source and permeability. However, for the study to be complete and satisfy its objectives the presence of clay cap and possible sources of recharge must be defined. Both potential field signals analysis divulges important and main components of a geothermal system in combination with the micro seismic events and the hypocenters.

Clay cap layer has been calculated by Hjálmar Eysteinsson et al. (2016) using resistivity method from magnetotelluric, and TEM surveys done in the study area. This result is displayed along with a jointly inverted 2D profile to make correlation between them. Figures 37 and 38 show 2D magnetic susceptibility sections along with the top and bottom of clay cap calculated from resistivity survey in the study area. The two black lines are clay cap top and bottom depths. These maps show low magnetic susceptibility where the magnetic field strength is high, and the clay cap is well developed over this low susceptibility anomaly. This can be identified by the thickness of the clay cap. Within the clay cap the susceptibilities are relatively higher which indicates the anomalies coincide with the clay cap layer. This layer attenuates when traversing out of the low susceptibility anomaly zone. However, it gets thicker when traversing further to the SE (which is particularly visible in Figure 38) part of the section. This could be related to thick soil; volcanic ash falls deposit etc.

Hydrogeological studies in the area and its surroundings indicate that the main recharge comes from southeastern highlands which gets comparatively higher annual precipitation than the surrounding area (Temesgen et al 2016). This area can be considered as a source of recharge to the deeper parts of the possible geothermal system believed to exist in the study area. In relation to ground water flow directions, which is generally believed that groundwater flows south to north and east to west (Temesgen et al 2016). There are geological features which facilitate the flow. The CMER escarpments and the WFB (Wonji Fault Belt) are the main geological features responsible for facilitating ground water flow.

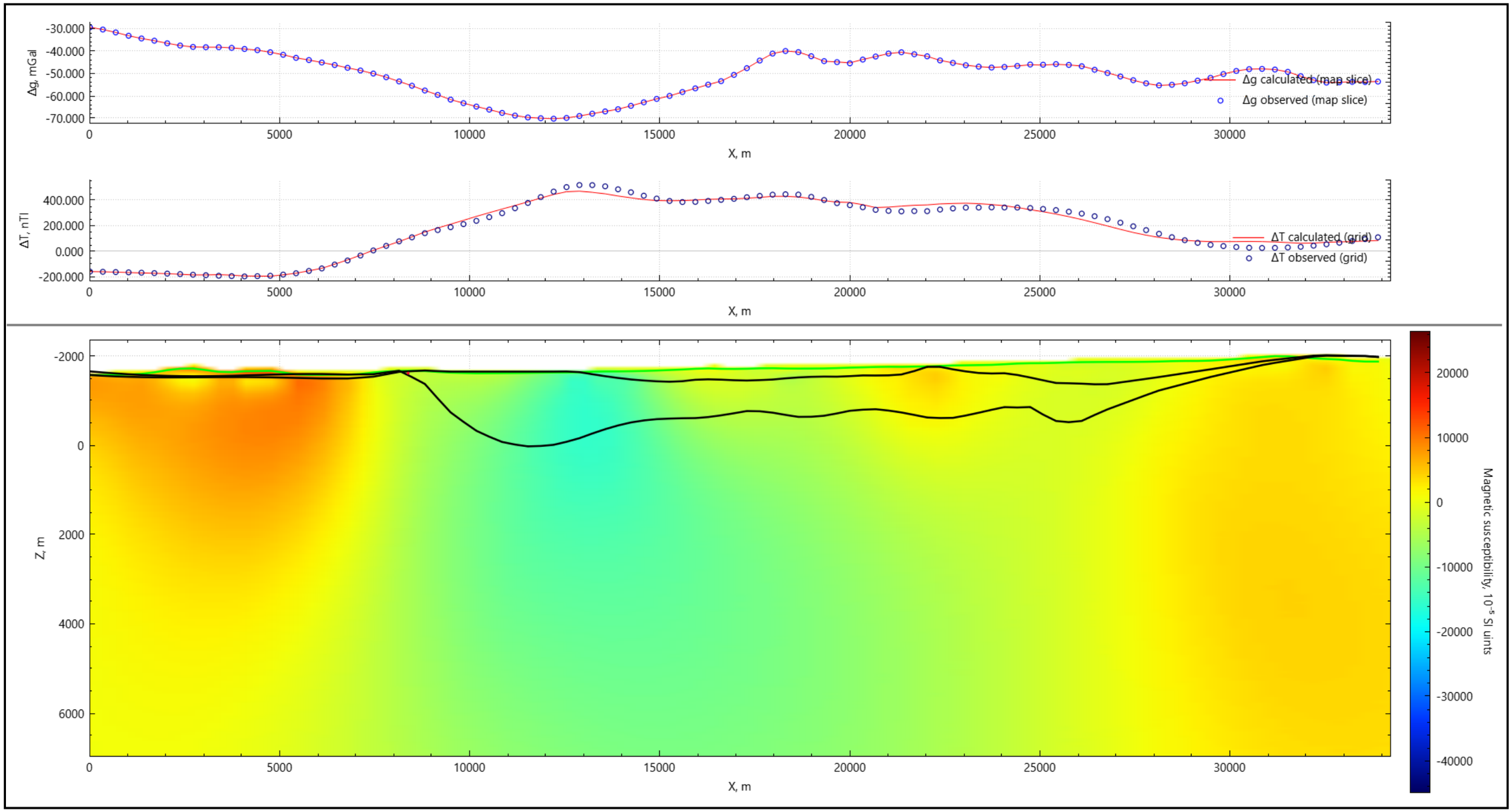

Figure 43. 2D Magnetic susceptibility section along profile I

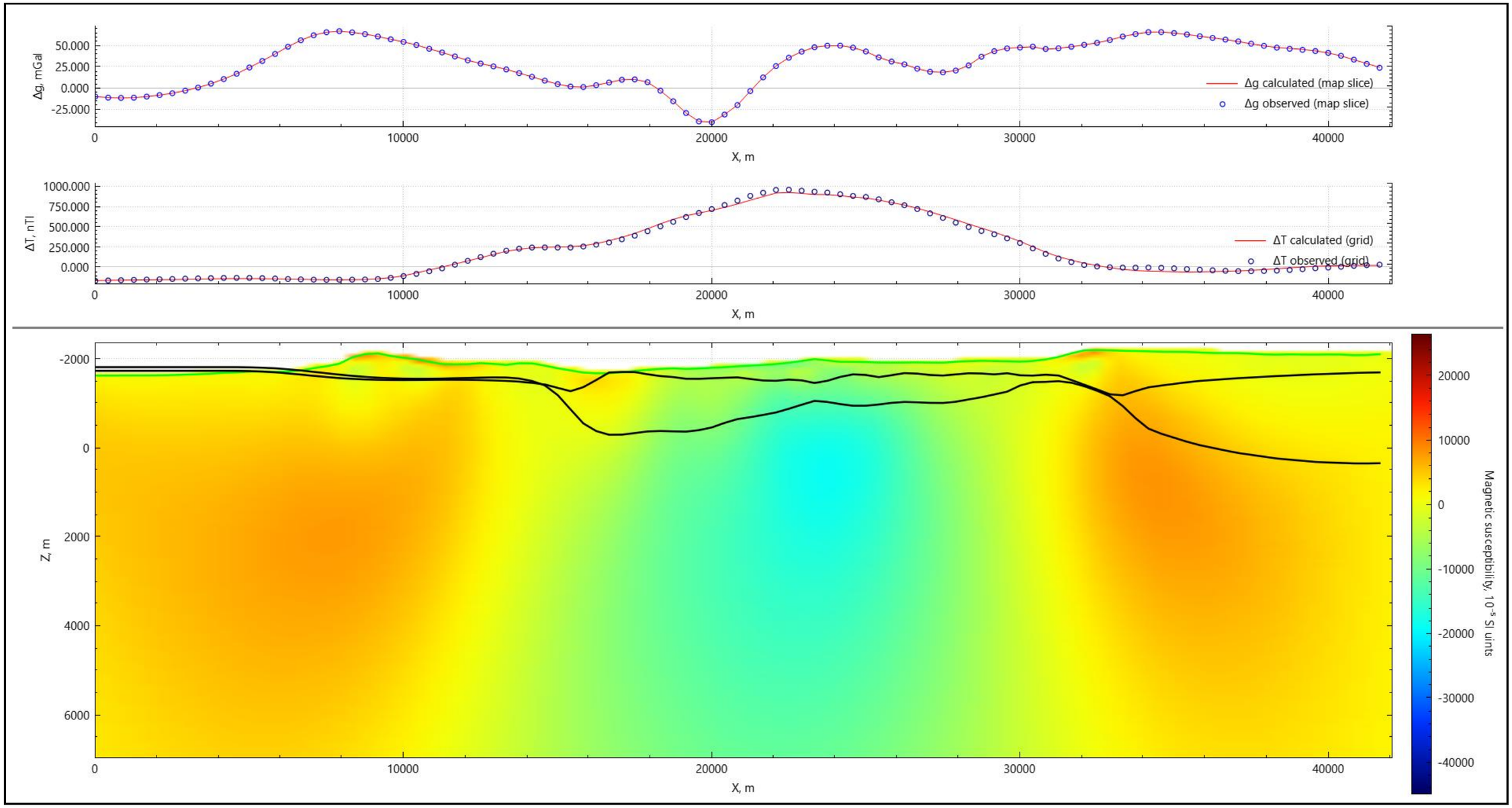

Figure 44. 2D Magnetic susceptibility Section along profile 2

5.1.2. Quantitative-Geothermal reservoir volume

This research thesis indicates the presence of the main geothermal reservoir components in the previous sections (4.5.1, 4.5.2, 4.7.1, 4.7.2 and 5.1.1). One of the objectives of this study is to define the geometry and volume of the possible geothermal reservoir in the study area. As indicated in the previous sections (4.5.1, 4.5.2, 4.7.1, 4.7.2 and 5.1.1), the existence of a heat source, permeable zone and clay cap have been determined using the main data (ground gravity and magnetic field) in combination with previous studies. All these components generally coincide with locations of the micro seismic events. This zone can be approximated by elliptical cylinder which completely encompasses the area covered by the epicenters of microseisms. The cylinder has major and minor axes *a* and *b* indicated on Figure39. The minor axis is ~ 13.8 km long whereas the major axis is ~24.8 km long and the height of the cylinder is approximately 9.1 km which is measured from the bottom of the clay cap to the bottom of the model.

Using the formula for an elliptical cylinder volume, the geothermal reservoir volume is calculated in the study area using the relation:

$$V = \pi abh = 9464 \text{ km}^3 \quad \ldots\ldots \quad (1)$$

Where V is Reservoir Volume, π =3.14, a is minor radius, b is major radius and h, is height of the cylinder

This volume is an approximate value which is calculated based on the current available data and processing capability. The produced 3D models and the reservoir volume approximation is the first for the study area and can be improved upon introduction of new additional data and data processing methods.

A drilling strategy can be carved based on the geometry of the investigated geothermal reservoir. This can be done using accessibility, ease to construct roads, laydown, camp site, water pipelines to rig site. Once rig site is selected and preparation is completed, it is possible to decide drilling methods and boreholes trajectory.

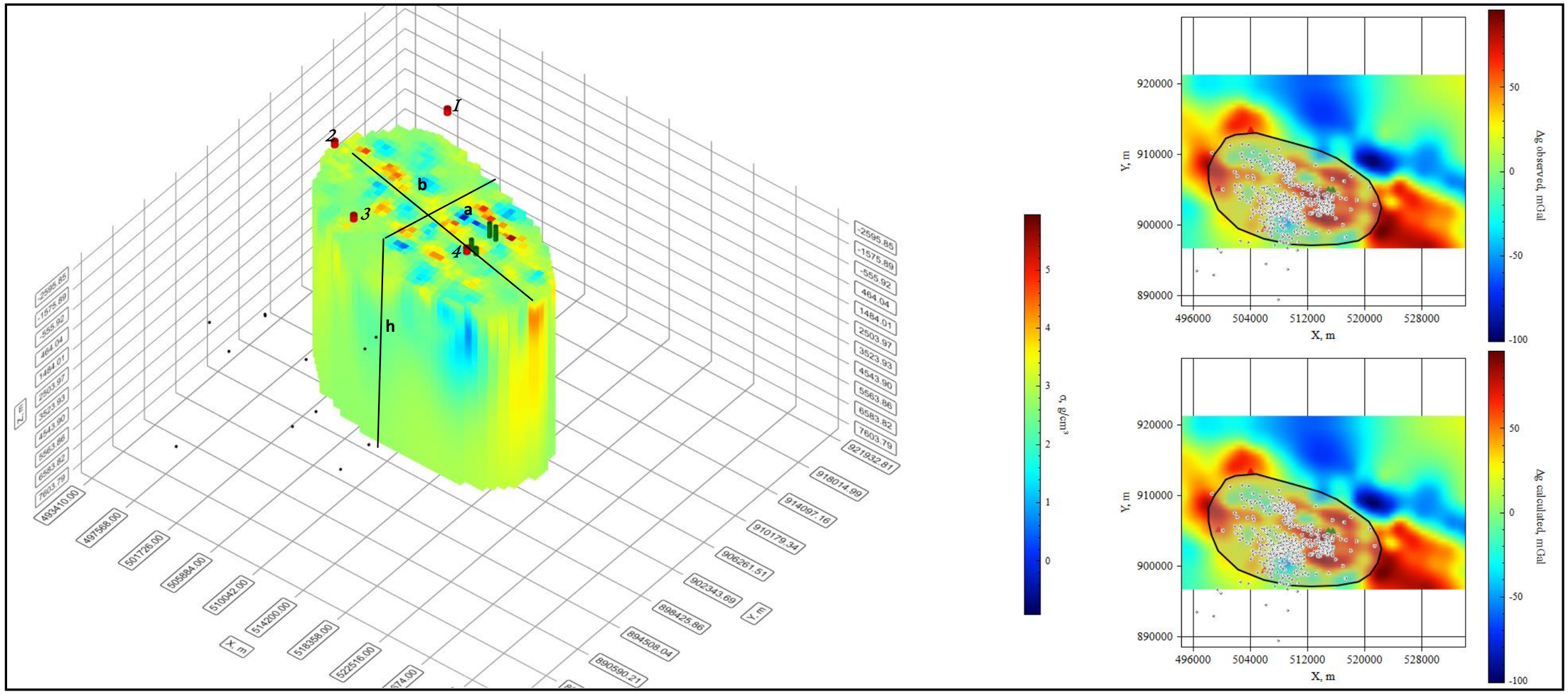

Figure 45. 3D Geothermal reservoir model.

(The four Red Picks 1-Bericcha, 2-Bora, 3-Jarablla, 4. Tulu Moye)

CHAPTER 6

6.I. Discussion

This thesis bases its foundation primarily on ground gravity, magnetic field data and the 3D joint inversion. The primary objective is to characterize the geothermal field and reservoir geometry beneath the Tulu Moye Volcanic Complex, Central Main Ethiopian Rift (CMER).

In the 3D model production residual anomalies of both data sets were used. However, the gravity data set has more areal coverage than the magnetics data set and the 3D processing software needs both data to have equal lateral and vertical dimensions. So, both were re-grided to the size of the magnetics data lateral dimensions before any processing actions were applied. In addition to data coverage magnetic data distribution is scares in the western part of the study area. Consequently, the 2D magnetic map is produced using large grid cell size while interpolating so as to cover the western part of the study area. So, the current interpretation in this study can be more refined and elaborated when more data is acquired in this part of the study area.

The gravity and magnetics data, mainly the 2D anomalies, were used in the joint inversion and divulged vital information in relation to the possible presence of geothermal resource components, in defining reservoir geometry, and reservoir extent. The availability of data and results from previous studies contributed to the present study to come up with results that were not obtained before in this study area. The clay cap layer's depths from resistivity survey by Hjálmar Eysteinsson et al. (2016) and hypocenters of micro-seismic events from Tim Greenfield et.al. (2019) do have undeniable contribution in aiding interpretation of results of this study. Indications of upwelling of magmatic body was reported by Birhan et al. (2023) which is believed to reside 10km west of the current geothermal wells drilled by Tulu Moye Geothermal Operations Plc. The 3D density model divulges the presence of a high-density body elongated from WNW to ESE whose value is pronounced at the location indicated by Birhan et al. (2023).

The top and bottom depths of the clay cap, in addition to providing information on the depth of alteration above the interpreted geothermal reservoir, coincided with relatively higher magnetic susceptibility zone which is shallow, and its thickness attenuates off in zones away from the reservoir lateral extent.

The seismic hypocentres not only coincide with the low magnetic susceptibility region but also with relatively low-density anomaly zones.

There are also geological features which are represented by both susceptibility and density anomalies. The volcanoes (Berriccha, Bora, Jarablla, and Tulu Moye) are associated with relatively low magnetic susceptibility and high-density anomalies.

The susceptibility and density 3D anomalies show a kind of pattern on the respective model's top surface. These susceptibilities have an alternating high and low values which take NEN to SWS trend whereas the density values have WNW to SES orientation. The high-density body which elongates from Tulu Moye to Bora Volcanoes could have relation with placement of magmatic body to relatively shallow depths and may be responsible for initiating micro-seismic events over and around it. Though their alignment is not exact, there are alteration zones which assume WNW to SES trend restricted to SW part of the study area and dominated by presence of the micro-seismic events. The altered zone probably indicates fault structures along this direction and geothermal fluid got passage through to be manifested on surface and cause the visible alteration.

Taking the anomalies of density and susceptibility along with previous study results, it could be possible to estimate the possible reservoir volume in the study area. Low susceptibility and density anomalies coincide with dense micro-seismic events, all the micro seismic events occur below the lower clay cap depth, clay cap thickness is considerably high over low susceptibility anomalies and attenuates away, and presence of aligned alteration zones indicate the presence of favorable conditions for a geothermal reservoir. Thus, taking these pieces of information together, this study suggests the presence of a geothermal reservoir in the southwestern part of the study area with an estimated volume of 9464 km^3. This estimate is based on the current available data from the area and the reservoir model which is the first of its kind in the history of geothermal investigation results in the study area. Therefore, a lot of work needs to be done to refine this result and come up with better geothermal reservoir models.

CHAPTER 7

7.1. Conclusion and Recommendations

7.1.1. Conclusion

The investigation results indicated a possible presence of a geothermal system with complete geothermal components. The role of the applied methods, ground gravity and ground magnetics data, and the applied processing method are important in identifying vital anomaly signature which are reflected by the anomalies of the two signals to understand the underlying ground condition and relate them with geothermal resource. In addition to this the data processing method aided the study to relate existing geological features, volcanoes, faults, etc., and take the maps obtained do represent the area. The 2D residual gravity and residual magnetic intensity maps, for instance, are well correlated with geological features and ground truth. So, the 2D maps presented in this study are used in the 3D processing to obtain density and magnetic susceptibility models which represent the area. So, the study could estimate the possible extent of a geothermal reservoir which has 9464 volumes**.**

7.1.2. Recommendation

This study uses existing data sets which do not have uniform data distribution and areal extent. The data processing was compelled to diminish the size of the gravity areal coverage into the size of magnetics data coverage area through re-griding process. This is a must to undergo joint 3D inversion of the two data sets. The current models of density and magnetics susceptibility are, therefore, results obtained as a result of interpolation and extrapolation. So, more data needs to be acquired to improve the data density and distribution. This generally increase the quality of map and model generation and interpretation of anomalies in 3D.

REFERENCES

Albino, F. et. al, (2020) Magmatic Processes in the East African Rift System: Insights From a 2015–2020 Sentinel-1 InSAR Survey

Ayalew, D., and Abebe, B. 2021. Geological report on the Gnaro-Salen area of the TMGO project

G. Wadge et al, (2016). Historical Volcanism and the State of Stress in the East African Rift System

Hjálmar, E. et al., 2016. Resistivity Study of Tulu Moye Geothermal Prospect, Ethiopia

Kazmin, V and **Seife**, M B. 1978. Geology and development of the Nazret Area, Northern Ethiopian Rift. Note No. 100 Ethiopian Institute of Geological Surveys.

Doetsch, J., et al, (2012) Constraining 3-D electrical resistance tomography with GPR reflection data for improved aquifer characterization.

Engidawerk, A. et. al, (2015) Characterization of Quaternary Extensional Structures: Tulu Moye Geothermal Prospect, Ethiopia

Kendall, J.M., Stuart, G.W., Ebinger, C.J., Bastow, I.D. and **Keir, D.** 2005. Magma assisted rifting in Ethiopia. Nature 433, 146-148.

Laury, R. L. and **Albritton, C. C.** 1975. Geology of Middle Stone Age archaeological sites in the main Ethiopian rift valley. Geological Society of America Bulletin, 86(7), 999-1011.

Lloyd, E.F. 1977. Geological Factors influencing geothermal exploration in the Langano region, Ethiopia, NHZ Geological Survey, Rotorua, New Zealand, unpublished report 73 pg.

Mamo, T, et al., 2016. Tulu Moye Geothermal Prospect, Surface Exploration: Geology report

Mamo, T. 2000. Report on the Geology and Surface Hydrothermal Alteration around Tulu Moye-Gedemsa Area, Main Ethiopian Rift, Geothermal Division, Ethiopian Geological Surveys, Addis Ababa, Ethiopia.

Mamo, T. 2001. Surface Hydrothermal Alteration in the Tulu Moye Area, Lakes District Rift, Ethiopia´´, Kyushu University, Japan.

Pizzi, A., Coltorti, M., Abebe, B., Disperati, L., Sacchi, G., & Salvini, R., 2006. The Wonji fault belt (Main Ethiopian Rift): structural and geomorphological constraints and GPS monitoring. Geological Society, London, Special Publications, 259(1), 191-207.

Meyer, W., Pilger, A., Rosler, A. and Stets, J. 1975. Tectonic evolution of the northern part of the Main Ethiopian Rift in Southern Ethiopia. In: Piler, A., Rosler, A. (Eds). Afar Depression of Ethiopia Sweizerbart, Stuttgart, pp.352-362.

Miller, H.G. and Singh, V. (1994) Potential Field Tilt a New Concept for Location of Potential Field Sources. Journal of

Mohr, P. A. 1967. Major volcano-tectonic lineament in the Ethiopian rift system. Nature, 213, 664-665.

Mohr, P.A. 1971. Ethiopian Rifts and Plateaus, some volcanic petrochemical differences **J. Geophys. Res**. 76(8), 1967-1984.

Tim Greenfield et al., 2019. Low-frequency Earth quack beneath Tulu Moye Volcano, Ethiopia, reveal fluid pulses from shallow magma chamber.

Temesgen Y., et. Al. 2016. Environmental Baseline Study Report for Tulu Moye Geothermal Project

Vozoff, K, et al, (1975) Joint Inversion of Geophysical Data